




Universitetet
i Stavanger

FACULTY OF SCIENCE AND TECHNOLOGY

MASTER'S THESIS

Study programme / specialization: Petroleum Engineering / Natural Gas Engineering	Spring semester, 2017 Open
Author: Ivan Murzin	 (signature of author)
Programme coordinator: Supervisor: Co-supervisor:	Prof. Aly Anis Hamouda Prof. Aly Anis Hamouda Rockey Abhishek
Title of master's thesis: Transport behavior of nanoparticles (NP) in Berea sandstone rock and the determining the EOR potential	
Credits: 30	
Keywords: Silica Nanoparticles Zeta potential Deionized water Synthetic sea water Static adsorption Adsorption / retention Berea sandstone Scanning Electron Microscope Ion tracking Enhanced Oil Recovery	Number of pages: 95 + supplemental material/other: 5 Stavanger, 15/06/2017 date/year

TOPIC

Transport behavior of nanoparticles (NP) in Berea sandstone rock
and the determining the EOR potential

Written by: **Ivan Murzin**

Supervised by: **Prof. Aly Anis Hamouda**

Co-supervised by: **Rockey Abhishek**

MSc Thesis

Natural Gas Engineering

Department of Petroleum Engineering

Faculty of Science and Technology

The University of Stavanger

Norway

2017

The University of Stavanger

June 2017

Abstract

Utilization of silica nanofluid is a promising technology for the petroleum industry. Specific interest is focused on potential application of nanoparticles (NP) for enhanced oil recovery (EOR). NP interactions in the porous media include the processes of reversible and irreversible adsorption / retention, interaction with rock minerals and fluids.

The first part of this work focused on characterizing and studying the NP at elevated salinity and temperature. To investigate the interaction of silica NP with minerals, the next stage of the project addressed the static adsorption of NP on three minerals: quartz, kaolinite, calcite in deionized water and high salinity conditions (synthetic sea water, SSW). Thereafter, single phase core flood experiments were conducted with Berea sandstone at ambient temperature to address transport behavior of silica NP, evaluate dynamic adsorption / retention and study their interactions with rock surfaces. Scanning electron microscopy (SEM) was performed to visualize the adsorption of silica NP on Berea sandstone. Finally, primary recovery floods at elevated temperature with two brine types (low salinity water and SSW) followed by secondary recovery with injection of nanofluid were conducted.

Characterization of nanofluids showed that the silica NP were stable at elevated temperature and salinity. Static adsorption experiments showed that NP have higher affinity for adsorption on calcite followed by quartz and kaolinite. It was also observed that adsorption process was enhanced by salinity. Dynamic adsorption of NP in Berea sandstone investigated by single phase core floods showed significant irreversible adsorption / retention of NP and associated increase in sweep efficiency. SEM imaging also showed preferential adsorption of silica NP on quartz mineral. It was also observed that silica NP were well distributed on the rock surface. Finally, oil recovery experiments performed with nanofluid indicated the potential of using silica NP for EOR. It was observed that injection of nanofluid suppresses the mineral reactions in Berea sandstone responsible for raising pH and potassium release. The injection of nanofluid also suppresses the dissolution of cementing mineral calcite. Preparation of nanofluid in SSW enhanced the retention of NP in Berea sandstone.

Acknowledgement

First of all, I would like to gratefully acknowledge my supervisor, Professor Aly Anis Hamouda for his support and dedicated involvement in every step throughout the work. It was an honor for me to be a part of his research team and under his supervision I learned a lot.

Besides, I owe my deepest gratitude to PhD candidate Rockey Abhishek who made an enormous contribution to this Master's Thesis as my co-supervisor. Without his persistent guidance this project would hardly have been completed.

I also want to thank Krzysztof Ignacy Nowicki for his generous assistance in the laboratory work.

I would like to show my greatest appreciation to my fellow students Amr Abde Monaem Ayoub and Ole Morten Isdahl for creation of good working environment and inspiring discussions on the subject. Their cooperation and support have been essential during this period.

Also, I must express my very profound gratitude to Sofya Ugryumova for providing me with unfailing support and continuous encouragement.

Furthermore, it is a pleasure for me to thank Mona Wetrhus Minde for her invaluable assistance with collection and interpretation of images from Scanning Electron Microscope.

Special thanks to Lutz Andreas Eichacker for making it possible to use "ZetaSizer Nano ZSP" equipment in this project.

Last but not the least, I would like to express my gratitude to the University of Stavanger and the Department of Petroleum Engineering for this brilliant opportunity to be a part of a big UiS family.

Ivan Murzin

Table of Contents

Abstract	v
Acknowledgement.....	vii
Table of Contents	ix
List of Figures	xi
List of Tables.....	xiv
List of Abbreviations.....	xv
1 Introduction	1
2 Literature survey	2
2.1 Mechanism of nanofluid spreading on solids	2
2.2 Nanofluid applications in low salinity and alkaline flooding.....	5
2.2.1 Nanofluid application in low salinity water flooding.....	5
2.2.2 Nanofluid application in alkaline flooding.....	6
2.3 Theoretical and experimental approaches to evaluate NP adsorption.....	8
2.4 Enhanced oil recovery tests with nanofluids	10
3 Theoretical introduction	12
3.1 Silica nanoparticles.....	12
3.2 Mechanisms of nanoparticles adsorption on rock surface.....	12
3.3 Zeta-potential.....	12
4 Methodology	14
4.1 Experimental materials and fluids	15
4.1.1 Deionized water.....	15
4.1.2 Nanofluid.....	15
4.1.3 Brines	16
4.1.4 Lithium chloride	16
4.1.5 Model oil	17
4.1.6 Mineral powders.....	17
4.1.7 Porous media	18
4.2 Laboratory equipment.....	19
4.2.1 “S220 SevenCompact™ pH/ion meter”	19
4.2.2 “Reax Top Vortex Mixer”	19
4.2.3 “Rotator Stuart SB-3”.....	20
4.2.4 Balances	20
4.2.5 Magnetic stirrer “VWR VMS-C10”.....	21

4.2.6	“Centrifuge 5804”	22
4.2.7	Vacuum saturation setup	22
4.2.8	Equipment for flooding cores.....	23
4.2.9	“AcoustoSizer II-M system”	25
4.2.10	“Zetasizer Nano ZSP”	26
4.2.11	“UV – 1700 spectrophotometer”	26
4.2.12	Ion Chromatograph “Dionex Ics-5000+ DP”.....	27
4.2.13	Scanning Electron Microscope “Supra 35VP FE-SEM”	28
4.3	Nanofluid characterization procedure	30
4.4	Procedure of zeta-potential measurements on mineral powder.....	30
4.5	Static adsorption experiment procedure	30
4.6	Core flood experiments procedures	34
4.6.1	Overview of core flood experiments.....	35
4.6.2	Description of NP transport behavior experiment.....	36
4.6.3	Description of EOR experiment.....	38
5	Results and Discussion.....	40
5.1	Nanofluid characterization	40
5.2	Zeta-potential measurements on mineral powders	41
5.3	Static adsorption experiments in DIW.....	42
5.4	Static adsorption experiments in SSW	46
5.5	Experiments on the transport behavior of NP	49
5.5.1	Core flood with “Berea 001”	49
5.5.2	Core flood with “Berea 002”.....	52
5.5.3	Core flood with “Berea 003”	59
5.5.4	Core flood with “Berea 004”.....	61
5.5.5	SEM imaging of Berea core and effluent.....	65
5.6	Enhanced oil recovery (EOR) experiments.....	67
5.6.1	Core floods with “Berea 005”	67
5.6.2	Core floods with “Berea 006”	74
6	Conclusions	78
7	References	79
	Appendix A.....	81

List of Figures

Figure 2.1 – Experimental setup and particle structuring in a wedge film [6].....	3
Figure 2.2 – Pressure profile and spreading coefficient as a function of film thickness [6].....	3
Figure 2.3 – Oil–solid displacement mechanism driven by structural forces [7]	4
Figure 2.4 – Results comparison of imbibition experiments [7].....	4
Figure 2.5 – Zeta potential of the beads and amount of particle release at different pH [15].....	7
Figure 2.6 – Oil recovery performance with various nanofluid concentrations [22].....	10
Figure 2.7 – Contact angle measurements of aqueous phase on quartz plate [24]	11
Figure 3.1 – Diagram of zeta-potential and slipping plane [30]	13
Figure 3.2 – Evaluation of dispersion stability [32].....	13
Figure 4.1 – “Milli-Q® Integral 5 Water Purification System”	15
Figure 4.2 – Nanofluid “NYACOL DP9711”	15
Figure 4.3 – Filtering setup for preparation of brines	16
Figure 4.4 – Container with Lithium Chloride for analysis	17
Figure 4.5 – A bottle of n-Decane for analysis	17
Figure 4.6 – Containers with mineral powders: Quartz, Kaolinite and Calcite	17
Figure 4.7 – Berea sandstone cylindrical cores in laboratory oven	18
Figure 4.8 – “S220 SevenCompact™ pH/ion meter”	19
Figure 4.9 – “Reax Top Vortex Mixer”	19
Figure 4.10 – “Rotator Stuart SB-3”	20
Figure 4.11 – Precision balance “Mettler PM 4600”	20
Figure 4.12 – Analytical balance “MS104-S”	21
Figure 4.13 – Magnetic stirrer “VWR VMS-C10”	21
Figure 4.14 – “Centrifuge 5804”	22
Figure 4.15 – Vacuum saturation setup.....	22
Figure 4.16 – Experimental core flooding setup	23
Figure 4.17 – Disassembled core holder	24
Figure 4.18 – Instruments and materials for wrapping the core.....	24
Figure 4.19 – Autosampler “GX-271 Liquid handler” with glass vials.....	25
Figure 4.20 – “AcoustoSizer II-M system”.....	25
Figure 4.21 – “Zetasizer Nano ZSP” [38].....	26
Figure 4.22 – “UV – 1700 spectrophotometer”	27
Figure 4.23 – Rectangular quartz cuvettes for “UV – 1700 spectrophotometer”	27
Figure 4.24 – Ion Chromatograph “Dionex Ics-5000+ DP”	28
Figure 4.25 – “GX-271 Liquid handler”	28
Figure 4.26 – Scanning Electron Microscope “Supra 35VP FE-SEM”	29

Figure 4.27 – “Emitech K550 automatic sputter coater”	29
Figure 4.28 – The process of zeta-potential measurement for mineral powder	30
Figure 4.29 – Calibration line for “DP9711” nanofluid prepared in DIW	32
Figure 4.30 – Core inside core holder ready for experiment	34
Figure 4.31 – Schematic diagram of NP transport experiment setup.....	36
Figure 4.32 – Effluent samples prepared for IC analysis	37
Figure 4.33 – Berea sandstone rock sample prepared for SEM imaging	38
Figure 4.34 – Equipment for core aging	39
Figure 5.1 – Size distributions for 1g/l nanofluid in DIW, LSW and SSW	40
Figure 5.2 – SEM image of nanofluid “DP9711”	41
Figure 5.3 – Specific adsorption of NP on minerals in DIW	43
Figure 5.4 – Combination of specific adsorption curves for minerals in DIW	44
Figure 5.5 – Specific adsorption of NP on minerals in DIW (original and reduced concentrations)	45
Figure 5.6 – Combination of specific adsorption curves for minerals in DIW with reduced concentration	46
Figure 5.7 – Calibration line for “DP9711” nanofluid prepared in SSW	46
Figure 5.8 – Specific adsorption of NP on minerals in SSW	48
Figure 5.9 – Combination of specific adsorption curves on minerals in SSW	48
Figure 5.10 – Comparison of specific adsorption of NP on minerals in DIW and SSW	49
Figure 5.11 – Injection sequence for “Berea 001”	49
Figure 5.12 – pH values for Berea 001	50
Figure 5.13 – ΔP vs PV injected for “Berea 001”	50
Figure 5.14 – Absorbance measurements for “Berea 001” effluent samples.....	51
Figure 5.15 – Calculated NP concentration for “Berea 001” effluent samples.....	52
Figure 5.16 – Injection sequence for “Berea 002”	52
Figure 5.17 – pH values for “Berea 002”	53
Figure 5.18 – ΔP vs PV injected for “Berea 002”	53
Figure 5.19 – Absorbance and pH values for “Berea 002”	54
Figure 5.20 – Comparison of absorbance values after dilution with DIW and “pre – flush bank” for “Berea 002”	55
Figure 5.21 – Adjusted values of absorbance after dilution with “pre – flush bank” for “Berea 002”	55
Figure 5.22 – Adjusted and corrected absorbance curve for post – flush samples of “Berea 002”	56
Figure 5.23 – Calibration line for DP + 0.1M LiCl (DIW as a reference).....	56
Figure 5.24 – NP concentration vs PV produced for “Berea 002”	58
Figure 5.25 – Li^+ ion and NP concentrations in effluent from “Berea 002” experiment.....	59
Figure 5.26 – Injection sequence for “Berea 003”	59

Figure 5.27 – pH values for “Berea 003”	60
Figure 5.28 – ΔP vs PV injected for “Berea 003”	60
Figure 5.29 – Li^+ ion concentration in effluent and pH values for “Berea 003”	61
Figure 5.30 – Injection sequence for “Berea 004”	61
Figure 5.31 – pH values for “Berea 004”	62
Figure 5.32 – Comparison of pH readings for “Berea 002” and “Berea 004”	62
Figure 5.33 – ΔP vs PV injected for “Berea 004”	63
Figure 5.34 – Absorbance and pH values for “Berea 004”	64
Figure 5.35 – Comparison of absorbance readings for “Berea 002” and “Berea 004”	64
Figure 5.36 – SEM image of Berea sandstone rock sample.....	65
Figure 5.37 – SEM image of Kaolinite mineral in Berea sandstone.....	65
Figure 5.38 – SEM image of Berea sandstone rock sample pretreated with nanofluid	66
Figure 5.39 – SEM image and spot analysis of turbid effluent produced during the core flood with “Berea 003”	66
Figure 5.40 – Injection sequence for oil recovery flood with “Berea 005”	67
Figure 5.41 – EOR experiment with “Berea 005”: Inlet pressure and ΔP vs PV injected.....	68
Figure 5.42 – EOR experiment with “Berea 005”: Cumulative oil recovery and pH vs PV injected.....	68
Figure 5.43 – EOR experiment with “Berea 005”: Absorbance curve and pH vs PV injected	69
Figure 5.44 – EOR experiment with “Berea 005”: Absorbance curve for nanofluid injection stages	69
Figure 5.45 – Calibration line for “DP9711” nanofluid prepared in LSW	70
Figure 5.46 – EOR experiment with “Berea 005”: NP concentration vs. PV injected	70
Figure 5.47 – K^+ ion concentration in effluent and pH values for “Berea 005”	72
Figure 5.48 – Mg^{2+} ion concentration in effluent and pH values for “Berea 005”	72
Figure 5.49 – Ca^{2+} ion concentration in effluent and pH values for “Berea 005”	73
Figure 5.50 – Injection sequence for oil recovery flood with “Berea 006”	74
Figure 5.51 – EOR experiment with “Berea 006”: Inlet pressure and ΔP vs PV injected.....	74
Figure 5.52 – EOR experiment with “Berea 006”: Cumulative oil recovery and pH vs PV injected.....	75
Figure 5.53 – EOR experiment with “Berea 006”: Absorbance curve and pH vs PV injected	75
Figure 5.54 – EOR experiment with “Berea 006”: Absorbance curve for nanofluid injection and post-flush stages	76
Figure 5.55 – EOR experiment with “Berea 006”: NP concentration vs PV injected	76

List of Tables

Table 4.1 – Brines composition [34]	16
Table 4.2 – Surface area of mineral powders [36]	18
Table 4.3 – Mineral analysis of the Berea sandstone [34]	18
Table 4.4 – Properties of Berea sandstone cores	18
Table 4.5 – Samples for static adsorption experiment in DIW	31
Table 4.6 – Baseline correction samples for static adsorption experiment in DIW	33
Table 4.7 – Samples for concentration sensitivity adsorption experiment in DIW	33
Table 4.8 – Baseline correction samples for concentration sensitivity adsorption experiment in DIW	34
Table 4.9 – Core flood experiments overview	35
Table 5.1 – Particle size and zeta-potential measurements for nanofluid samples	40
Table 5.2 – Zeta-potential measurements of mineral powder suspensions in DIW	42
Table 5.3 – Absorbance readings for nanofluid samples in DIW	42
Table 5.4 – Absorbance readings for mineral baseline correction samples in DIW	43
Table 5.5 – Measurements for concentration sensitivity adsorption experiment in DIW	44
Table 5.6 – Absorbance readings of baseline correction samples for concentration sensitivity experiment in DIW	45
Table 5.7 – Absorbance readings for nanofluid samples in SSW	47
Table 5.8 – Absorbance readings for mineral baseline correction samples in SSW	47
Table 5.9 – NP mass balance calculations for "Berea 002"	57
Table 5.10 – NP mass balance calculations for "Berea 005"	71
Table 5.11 – NP mass balance calculations for "Berea 006"	77

List of Abbreviations

Abs – Absorbance

DIW – Deionized water

DP – Nanofluid “DP 9711”

EOR – Enhanced oil recovery

IC – Ion chromatography

IFT – Interfacial tension

LSW – Low salinity water

NP – Nanoparticles

PDI – Polydispersity index

PV – Pore volume

SEM – Scanning electron microscopy

SSW – Synthetic sea water

S_{wirr} – Irreducible water saturation

UV – Spectrophotometer “UV – 1700”

ZP – Zeta-potential

1 Introduction

Nanotechnology is a comparatively new field of science that has a wide range of applications in different disciplines. In the past decade, this research direction has actively been utilized to solve the various problems faced by the petroleum industry. Many researchers have investigated the potential role of nanotechnology to solve different challenges connected to oil and gas exploration, production and processing. Kong et al. [1] discussed the potential use of nanoparticles (NP) in petroleum industry and one of the promising applications that NP can offer is enhanced oil recovery (EOR).

NP are designed with a purpose of altering the specific properties of the rock that can lead to better oil displacement. A certain type of nanoparticles can cause wettability alteration of the formation towards more water-wet, which could be used to reduce residual oil [2].

Silica NP are considered as appropriate candidates for these applications because they are not expensive to produce, environmentally friendly and have a good ability to be modified by chemical methods [3]. The key processes here are interactions of nanofluid with other fluids (water / oil phase) and rock grains, which can be connected with retention or adsorption of NP on mineral surface. Understanding and describing of these procedures are of higher importance for identifying better parameters and properties of nanofluids to utilize them in EOR techniques.

This Master's Thesis aimed at studying adsorption behavior of silica NP on mineral surfaces, investigating their transport behavior in Berea sandstone and potential application for EOR. The project was performed to address the interaction of the silica NP dispersion with different fluids and with Berea sandstone formation, describing the factors that affect NP performance in reducing the residual oil in reservoirs.

For achieving these goals, static adsorption experiments were conducted to investigate adsorption behavior of the NP on three minerals: quartz, kaolinite and calcite. After that, single-phase core flood experiments with silica nanofluid were performed to determine the reversible and irreversible adsorption / retention of NP inside Berea formation. Finally, the Berea sandstone cores were flooded with model oil, brines and silica nanofluid to evaluate the potential of NP to affect oil recovery.

2 Literature survey

Nanotechnology is a new science direction which makes it possible to provide new solutions to old challenges. For petroleum industry, these unique approaches have potential in different applications. Since it is becoming more and more difficult to explore new hydrocarbon reservoirs, research groups worldwide are mainly focused on investigation of advanced technologies to increase recovery from oil and gas fields which are in production. One of the most promising directions of nanotechnology in petroleum industry is application of nanoparticles for enhanced oil recovery (EOR).

Nanomaterials with a size range from 1 to 100 nm show unique behavior in porous media because of specific properties which are found interesting from petroleum engineering point of view and can be considered to enhance extraction of hydrocarbons. These properties of nanoparticles comprise their extremely high specific surface area, thermal properties, high potential to alter the wettability of the reservoir formations, modify rock surface charges and associated influence on the rheological properties of suspensions [4].

Nanoparticles have other potential use in petroleum industry: formation damage mitigation, surfactant, low salinity or alkaline flooding and well treatment after hydrofracturing in unconventional reservoirs. The main EOR mechanisms of nanoparticles: wettability alteration, interfacial tension reduction, disjoining pressure, emulsification and pore channels plugging [2].

Due to specific chemical and electrical properties and tiny size of NP, they can reduce the double layer force between the rock grains and fines by changing the corresponding zeta potentials of fine particles or rock grains which helps to keep the integrity of the rock without detachment of fines [5].

Many researchers conducted studies on nanoparticles and the role they play in enhanced oil recovery. One can find plenty of experimental and theoretical approaches investigating and concluding that various nanofluid applications have a positive effect on oil and gas extraction from the reservoir. In this literature survey, the focus has been made on theoretical introduction to the process of nanofluids spreading on solid surfaces based on experimental and analytical investigations made in Illinois Institute of Technology by Darsh T. Wasan and Alex D. Nikolov. Besides, investigations of nanoparticles application for petroleum industry carried out by three research groups: the University of Tehran (Danial Arab et al.), the University of Oklahoma (Bin Yuan et al.) and Norwegian University of Science and Technology (Ole Torsæter et al.) are considered here.

2.1 Mechanism of nanofluid spreading on solids

The concepts of spreading and adhesion are well-established for simple liquids. Nevertheless, these concepts are not applicable to nanofluids. Spreading and adhesion behavior of NPs on solid surfaces can yield materials with desirable structural and optical properties, and it also can be applied for enhanced oil recovery [6].

The main goal of Darsh Wasan and Alex Nikolov investigation [6] was to reveal the effects of the structural disjoining pressure and the particle structure formation on the spreading of colloidal fluids on solid surfaces. They showed that when a gas bubble or oil/liquid drop in aqueous nanofluid dispersion touches a smooth, horizontal hydrophilic solid surface, there occurs a microscopic transition between the meniscus and the liquid film. Reflected-light digital video microscopy was utilized to directly observe the particle-structuring phenomenon in the liquid film-meniscus region (Figure 2.1).

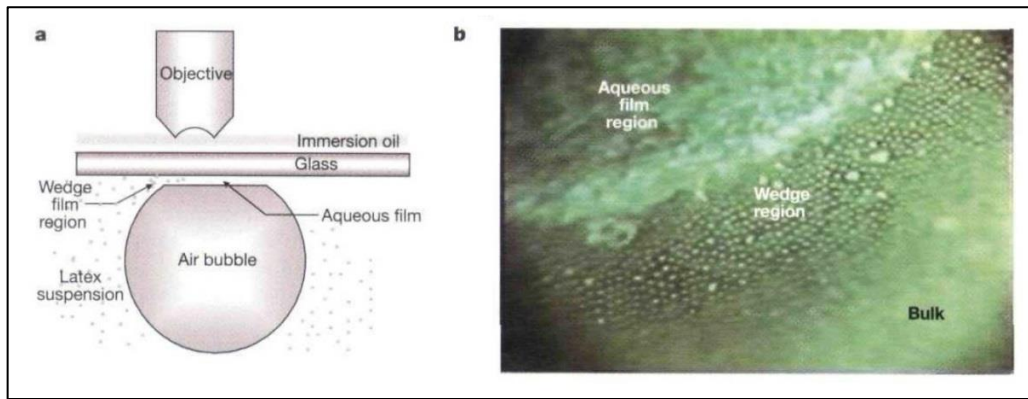


Figure 2.1 – Experimental setup and particle structuring in a wedge film [6]

The authors described the process of changing the nanofluid film thickness in the following steps:

- After the oil drop is present on a solid glass surface, three-phase contact region (liquid-solid-air) is formed;
- Forming and spreading of the pre-wetting aqueous film between the oil droplet and solid surface;
- Formation of small water lenses when the pre-wetted film covers the whole area;
- Thick aqueous film with a dimple causes the oil droplet separation from the glass surface.

The nanoparticle structuring phenomenon introduces a force normal to the interface in the wedge film, which is known as structural disjoining pressure. Disjoining pressure plot as a function of film thickness was obtained by using an analytical expression based on statistical mechanics while the spreading coefficient was estimated as a function of the number of particle layers in the wedge film. It was observed that the structural disjoining pressure is higher near the tip of the wedge than that in the bulk meniscus and its magnitude depends on polydispersity, the effective nanoparticle volume fraction, particle size and charge (Figure 2.2).

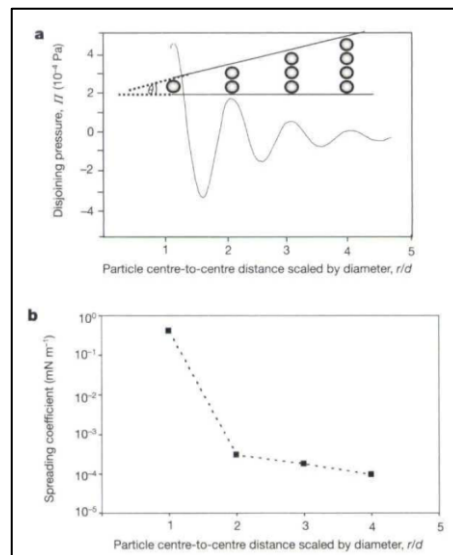


Figure 2.2 – Pressure profile and spreading coefficient as a function of film thickness [6]

Calculations made by Darsh Wasan and Alex Nikolov showed that the spreading coefficient increases with a decrease in film thickness, which is in turn determined by the number of particle layers inside the film. In addition, it was noticed that a significant change in the slope of the curve takes place at a wedge film thickness equal to twice the particle diameter and exactly at this film thickness there happens the change of the particle in-layer structure to an ordered structure. The results indicate that spreading of nanofluids on solids can be enhanced by the in-layer particle structuring.

Explanation for the detachment of an oil drop from the solid glass surface using a nanoparticles solution reported by authors is that with time the nanofluid concentration in the film increases, as nanoparticles diffuse more into the wedge film and interact with the surfaces of the film. At the same time the disjoining pressure increases dramatically at a wedge thickness of one nanoparticles layer. As a result of the pressure increase, the oil-solution interface spreads forward (Figure 2.3), and the nanoparticle solution spreads on the solid surface, detaching the oil drop.

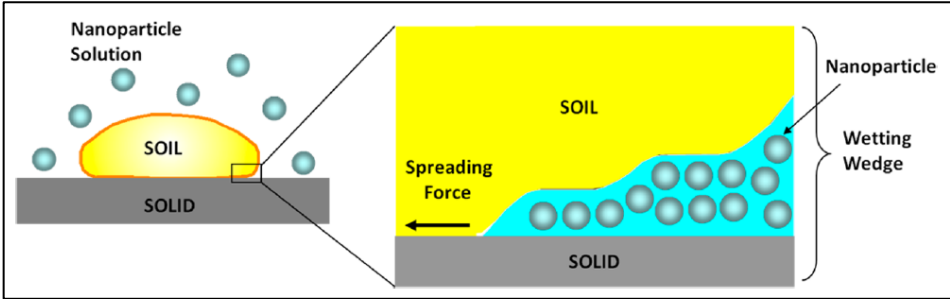


Figure 2.3 – Oil–solid displacement mechanism driven by structural forces [7]

The further investigation of Darsh Wasan, Alex Nikolov and Hua Zhang [7] demonstrated the importance of the nanoparticle formulation, contact angle, and the capillary pressure that influence dynamics of the contact lines between oil, solid and liquid film. A suitable combination of these factors favors detaching the oil drop from the solid surface by accelerated spreading of the nanofluid on this surface.

In order to observe the effect of nanoparticles on recovery the authors conducted also imbibition tests using a crude oil, a reservoir high salinity brine solution and nanofluid that displaces oil from water-wet Berea sandstone. Two types of nanofluids were used to displace crude oil from the rock samples: silica nanoparticle suspension and Illinois Institute of Technology (IIT) nanofluid. The Illinois Institute of Technology (IIT) nanofluid was specially created to cope with a high-salinity environment without aggregation.

According to experimental results, 50% crude oil can be extracted from Berea sandstone by using the IIT nanofluid, compared to 17% by the brine solution alone at a reservoir temperature of 55 °C. Since silica nanofluid is unstable in harsh saline environment its performance was compared with behavior of pH 9.7 deionized water. As a result, 55% of initial crude oil was recovered by this silica nanofluid, compared to only 2% in imbibition experiment with pH 9.7 deionized water at room temperature. Figure 2.4 shows the comparison of experimental results.

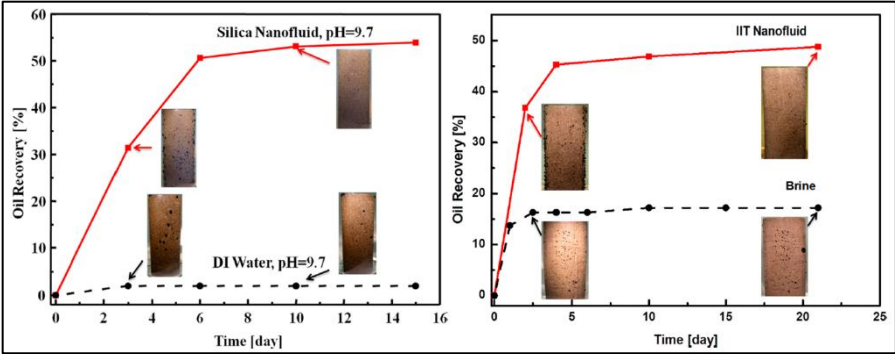


Figure 2.4 – Results comparison of imbibition experiments [7]

In their report Zhang et al. demonstrated that application of nanoliquids in imbibition tests led to significant increase in oil recovery from the reservoir rock compared to brine solution or deionized water with adjusted pH.

2.2 Nanofluid applications in low salinity and alkaline flooding

Low salinity water (LSW) flooding and alkaline flooding are considered as the two promising improved / enhanced oil recovery methods. However, these chemical conditions of high pH and low salinity are very unfavorable in terms of in-situ particles retention. As a matter of fact, this phenomenon is usually accompanied by fines migration and subsequent formation damage. The research group from University of Tehran carried out experiments in attempt to investigate the potential ability of nanofluids to avoid formation damage problem during low salinity water and alkaline flooding.

2.2.1 Nanofluid application in low salinity water flooding

Ultimate oil recovery is dominantly effected by the concentration of salts in water and when the salinity of the injected water is decreased the more oil can be produced from the reservoir according to Ashraf et al. [8], Hassenakam et al. [9]. During the low salinity water flooding the rock wettability alteration happens toward less oil wet (or more water wet). This phenomena is probably related to decreasing contact angles as the water salinity is lowered [10].

According to investigations made by D. Arab and P. Pourafshary [4] the main mechanism that can explain oil recovery improvement during LSW flooding is cation exchange with the rock surface. Ion concentration of low salinity water is lower than that of the rock, and there is a cation exchange between water and the rock surface. Eventually, the rock surface becomes more negatively charged and it decreases electrostatic attractive forces between crude oil and the rock, which helps to recover a greater volume of oil. However, it was a wettability alteration that was addressed by Berg et al. [11] as a major mechanism in improving oil recovery with LSW flooding.

When the salinity of the injected fluid drops below a certain value which is known as critical salt concentration (CSC) when zeta-potential decreases significantly and the resultant electron static forces between fine particles and the rock become more repulsive. Ionic strength of and pH of injected fluid are the major influencing factors for these forces and in case of low salinity flooding repulsive forces become prevailing and that causes dislodging and transport of small fine particles in a media [12]. This mobility of fines may lead to the pore blockage and eventually to formation damage and economically unfavorable rates of oil extraction. Applicably of LSW flooding is limited by a possible strong injectivity loss due to blockage of the rock pores.

From the other hand this blockage may lead to the opposite effect by plugging water swept zones in the rock and enhancing sweep efficiency. This can definitely favor oil recovery.

Therefore, formation damage should be controlled with lowering of the ionic strength during LSW flooding. There exists an optimum ionic strength window of water where operations can be carried out with allowing salinity of injected water to be low enough for desirable improvement of recovery but at the same time high enough to prevent fines detachment and migration in a porous media [13].

D. Arab and P. Pourafshary [4] investigated application of 5 types of nanofluid (γ -Al₂O₃, CuO, MgO, SiO₂, and ZnO) and thier potential for mitigating problems of low salinity flooding induced by fines migration in the cores. It was found out that when nanofluid is used to soak the core before LSW flooding expected formation damage can be reduced. By introducing nanoparticles the balance of forces inside the the porous media is changed which prevents the fine particles from detachment and migration. The best remedial effects were observed by using ZnO NP suspension in DIW. During flooding of LSW through the glass beads mimicing the core very high particle adsorption capabilities

were noticed when the beads were preliminary soaked with γ -Al₂O₃ nanofluid. Great improvements were observed also with application of CuO and SiO₂ NPs dispersed in LSW. Dispersion characteristics are better when these two types of nanofluids are prepared in LSW compared to distilled water, but this effect is not universal for all nanofluids. The surface charge of beads is altered with a presence of NP and thereby the adsorption of fine particles on glass surface is facilitated. Hence, with greater capability of nanofluid to change the charge of the beads into more positive values, the more potential of the glass beads to keep the suspended particles. LSW is considered as a very weak fluid in terms of changing the surface charge of the rock and that is why the detachment and migration of fines is enhanced during LSW flooding.

The following main conclusions have been made by D. Arab and P. Pourafshary based on results of LSW flooding experiments:

- 1 Flooding with LSW favors increase in ultimate oil recovery, but attention should be paid to possible formation damage;
- 2 Zeta-potential is a major parameter determining interactions between the rock surface and fine particles. Application of NP allows to alter zeta-potential;
- 3 Another important parameter affecting NP treatment efficiency is the ionic strength of NP dispersing fluid but it is not unified for all types of NP;
- 4 The surface properties of the glass beads are altered easier when NP are better dispersed;
- 5 Treating the surface with γ -Al₂O₃ NP allows to change the surface charge to very high values (up to 33.2 mV) that leads to 70 % mitigation of fine particles migration compared to the case without use of nanofluid. This type of nanoparticles out of 5 tested experimentally shows the highest potential for lowering severe permeability impairment in a porous media, so NP application can serve as a remedy for formation damage problems during LSW flooding.

2.2.2 Nanofluid application in alkaline flooding

Alkaline flooding is another technique that can be used to increase extraction of oil from the reservoir. Alkali is either used as a recovery agent during pre – flush slug, or as a mixture solution with polymers and surfactants. In conjunction with polymer, it becomes more viscous which helps to prevent fingering of injected water and therefore increase sweep efficiency [14]. As a major recovery agent injected alkali can create in-situ natural surfactant after reaction with oil. This surfactant also known as a petroleum soap can release trapped oil by reducing the interfacial tension [15].

From another point of view very high alkaline conditions are undesirable because at such environment scales or precipitates formation may occur. This can lead to the blockage of the rock pore throats thereby resulting in decline in productivity index [16].

Fine particles migration or clay swelling are another two possible consequences due to interactions of alkaline chemicals with clays which eventually can lead to severe formation damage. Besides, particles detachment and migration may be caused by the dominantly repulsive resultant surface forces between fines with a negative charge and medium surface. This happens when pH of injected fluids is higher than point of zero charge (PZC) [15].

In order to counteract this phenomena allowable pH level of injected fluid should be used. Among clays Kaolinite is considered as the most migrating one and impose a limitations on alkaline flooding. Therefore, an optimum pH range should be utilized than extremely high one in order to reach an optimum efficiency of the alkaline flooding process.

It should be noted that the chemistry of the solution play a very important role in the behavior of the fines and their migration. Experiments of Assef et al. [15] showed that the presence of divalent salts favors the tendency of fine particle to lodge on the glass bead surface rather than the presence of monovalent salts because divalent salts have greater capability to alter zeta-potential of the beads. Higher pH of the injected fluid implies alteration of the medium surface zeta-potential toward the more negative values and therefore this results in increase of double layer repulsion between particle fines and the medium. Assef et al. reported that zeta-potential measurements at different pH were conducted to investigate the effect of pH on the particles release (Figure 2.5).

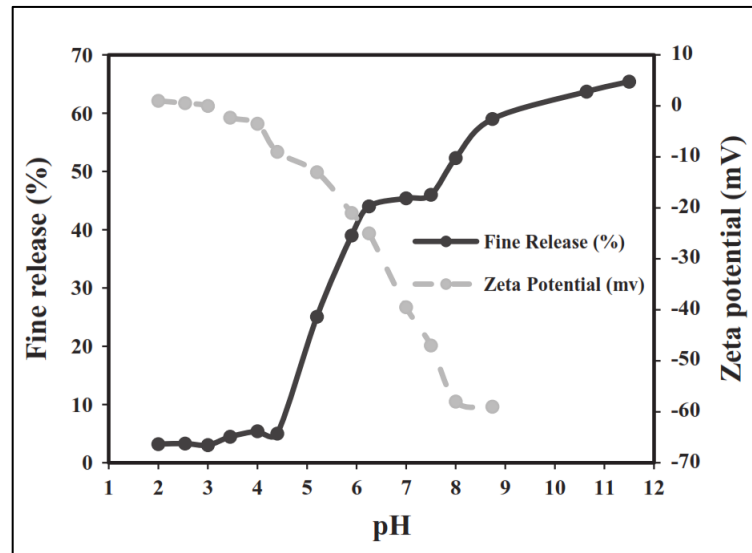


Figure 2.5 – Zeta potential of the beads and amount of particle release at different pH [15]

Experimental work of Assef et al. was aimed to test treatment of the media with MgO nanofluid to counteract aforementioned unfavorable conditions of alkali flooding. It was found that nanofluid pre – flush before LSW flooding can mitigate migration of colloidal particles and the presence of MgO NP can facilitate retention of the indigenous fines at quite harsh conditions for particle retention (very alkaline environment). Based on results of alkali flooding experiments, the following conclusions have been made [15]:

- 1) Zeta-potential of the medium surface can be shifted toward more positive values with application of MgO NP. Hence, negatively charged fine particles tend to be retained in extremely unfavorable (alkaline) conditions for retention of the particles ;
- 2) Both monovalent and divalent salts were present in the medium and MgO NP demonstrated reduction in fines migration.
- 3) Colloidal particles migration in a reservoir can be mitigated by using this technique. In addition, it was possible to modify the point of zero charge (PZC) from 3 up to 9 which allows to get distinguished benefits of alkali flooding process in a quite wide range of alkali conditions;
- 4) It was reported that in very alkaline environment the porous media preliminary treated with MgO NP allowed to retain close to 97% of the in-situ fines.

2.3 Theoretical and experimental approaches to evaluate NP adsorption

Another research group K. Wang et al. [17] presented core flood experiments on Berea sandstone together with theoretical investigations about dynamic adsorption / desorption of NP and associated possibilities for damage of formation. The main objectives of their investigations are:

- Conducting both mathematical and experimental investigations on dynamic adsorption / desorption during NP flow in the porous media and associated permeability impairment effects;
- Developing a mathematical model allowing to analyze and describe NP effectiveness in terms of control of fine particles migration in a one dimension porous media.

As was mentioned before, fines mobility can be lower with application of tiny NP with huge surface areas, because NP can help to alter the surface charge of rock surfaces and transported fines. It should be stressed that NP has insignificant effect on the pore – throat structures of the porous media due to their size dimensions and potential effect of small NP alone on formation permeability should be negligible. Nanofluids make it possible to retain more particles by modifying the balance between physicochemical forces (such as London-van der Waals, electric double layer, Born repulsive forces). Hence, interactions between NP and rock surfaces are dominated by these forces and Brownian motion [18].

The authors documented that at flooding stage of NSP (Nano-structure particles) injection pressure difference between inlet and outlet of the core sample raises rapidly. They attributed this pressure increase to adsorption and straining of NP that take place from the beginning of nanofluid injection. They stated the appearance of a multilayer adsorption in the core, which results in significant straining and decreasing of the pore-throat sizes. With increase of concentration of injected NP this effect escalates and pressure drop increases more rapidly and significantly. Post – flush period was characterized with gradual decrease of the pressure drop, indicating possible detachment of adsorbed NP caused. This reversible adsorption, occurring due to change of nanofluid environment at post - flush continues until steady – state conditions when no more straining or detachment of NP happens.

Transport behavior of NP with adsorption and desorption processes causes significant wettability alteration and affect permeability of the formation. Contact angle measurement performed by M. Maghzi et al. [19] demonstrated wettability alteration from oil-wet to water-wet occurring due to silica nanoparticles adsorption on the surface. Important condition to be fulfilled is adsorption of NP onto the surface and the results showed that adsorption can be intensified by increasing of the concentration of silica nanofluid concentration.

B. Yuan and K. Wang also reported the higher probability of NP retention in the core with increase of concentration of injected nanofluid. Besides, adsorption of NP leads to delay of breakthrough time of injected nanofluid. However, at high concentrations of nanofluid there is a risk of strong impairment of the core permeability [18].

All in all, the main contributions from NP injection to reducing the migration of fines and increasing retention of particles on the surfaces of the porous medium can be summarized in two important reactions: NP adsorption onto fines / surface of the grains and reduction the surface potential between fines and grains leading to enhanced fines retention.

Observation from core flooding experiments of B. Yuan and K. Wang [18] can be summarized with the following general conclusions:

- 1) With increase of NP injection concentration the maximum adsorption potential and subsequent reversible adsorption during post – flush also increases, with delaying of the nanofluid breakthrough;
- 2) With increase of NP concentration, the potential of the rock formation damage connected with adsorption and straining of NP also increases;
- 3) The pressure drop elevations are dominantly affected by straining behavior.

In order to evaluate theoretically the potential of NP to control migration of fines in one dimension permeable medium theoretical structure was developed by B. Yuan et al. [5] with derivation of semi-analytic solutions for two scenarios:

- Coinjection of NP with fine particles suspension in one dimension porous media.
- Preliminary soaking of the porous medium with nanofluid before fines injection.

The capability of the rock to capture fine particles with application of NP was also reported earlier by Huang et al. [20]. This observation was modeled in two steps:

- NP adsorption onto the fines / rock surface;
- Additional fines attachment.

With this model the total interaction energy between the grain surfaces and fine particles is described by Derjagin-Landau-Verwey-Overbeek (DLVO) theory. Besides, one dimension porous medium is presented as bundles of parallel pores (cylindrical tubes). Under assumption that the size of NP is extremely small compared to the sizes of fine particles and rock grain, the amount of NP adsorbed on surfaces is acquired by using Langmuir adsorption isotherm. As reported by Ahmadi et al. [21] the fines usually have less surface potential than rock grains which indicate stronger attractive forces between fines and NP than between the rock grains and NP. Adsorbed NP alter surface charge of fines attached to rock grains which results in increase of retention concentration of particles on rock surfaces. However, it was noted that there exists an optimal concentration of NP to modify the surface charges of fine particles by reaching the ultimate concentration of attachment. In case NP concentration is below this level there will be observed unattached particles in flowing fluids. In the opposite scenario at extremely high concentrations of nanofluid, some amount of NP is left unused in the system [5].

Developed analytical model allows to describe adsorption and straining behaviors of NP shows a good match with lab data. B. Yuan et al. formulated the following conclusions about their model:

- 1) The use of NP to control migration of fines was evaluated by semi-analytical solutions for three component flow (water, fine particles, NP) in one dimension porous medium;
- 2) Maximum attachment concentration of the fines on the grains can be enhanced by increase in adsorbed NP concentration;
- 3) A satisfactory fines migration control can be achieved even in case of NP injection at low concentrations;
- 4) According to the results acquired from testing two scenarios (coinjection of NP and preliminary saturation of the media with nanofluid) NP application showed reduction in fines migration by 36.91 % and 89.9 % respectively. Hence, precoating of the rock with NP is more effective than continuous injection in terms of fixing injected fine particles and preventing them from further migration.

2.4 Enhanced oil recovery tests with nanofluids

Significant research work related to nanoparticles transport behavior in porous media and applications of nanofluids in enhanced oil recovery (EOR) with investigation of possible working mechanisms has been made by researchers from Norwegian University of Science and Technology (NTNU).

In their work Hendraningrat et al. [22] investigated the potential of NP use in EOR by flooding with Berea sandstone cores with permeabilities from 9 to 400 mD. Mechanisms of NP structural disjoining pressure, lowering of interfacial tension (IFT) and altering the wettability were studied. For flooding the core they utilized a crude oil from the field in the North Sea and nanoliquid at three different concentrations (0.01, 0.05 and 0.1 wt. %). Lipophobic and hydrophilic nanoparticles (LHP) consisting mostly of silicon dioxide (SiO_2) were utilized in the study.

Lowering of IFT was observed when the nanofluid is introducing in the brine – oil system. Therefore some extra oil can be mobilized as the capillary number increases with IFT decrease. IFT is turned to be very sensitive to the concentration of NP as pH of nanofluid drops with concentration increase. Effect of pH on IFT in water – oil system was studied by J. Buckley and T. Fan [23].

Besides, during the core floods with Berea sandstone the research group from NTNU observed that high concentration of injected nanofluid results in NP retention which eventually increases the potential for permeability and porosity impairment [22].

Concerning to EOR potential increasing concentration of nanoparticles leads to higher displacement efficiency and give a slight increase in ultimate oil recovery. At the same time, additional recovery is greater in the cores with high permeability. No extra oil recovery was observed at nanofluid injection stage in rock samples with low and medium permeabilities and high NP concentration of 0.1 wt. % (Figure 2.6).

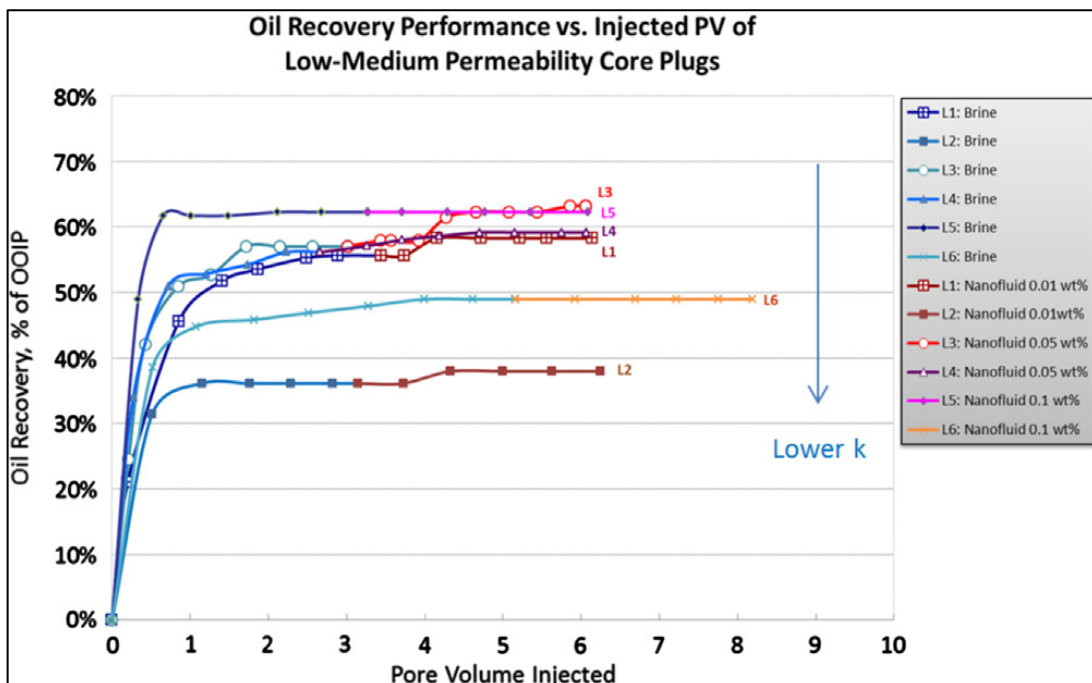


Figure 2.6 – Oil recovery performance with various nanofluid concentrations [22]

Therefore, the nanofluid concentration of 0.05 wt. % was considered as an optimum concentration corresponding to the highest recoveries in both the cores of various permeability.

The further survey of Hendraningrat et al. [24] was devoted to metal oxide nanoparticles and investigation of their potential to alter wettability of Berea sandstone cores. Additional focus was made on improving nanofluid stability against agglomeration because the major factor influencing the stability of suspension is surface area to volume ratio. Huge surface area of NP implies a great reactivity and better tendency for agglomeration. But practically NP should preserve their small size without aggregation to be able to flow through reservoir pore throats. Therefore, stability of nanofluids is a key parameter in NP application for EOR. The authors used three methods to evaluate the stability of NP: visual observation, surface area conductivity and particle size measurements. In order to maintain stability of the nanofluid 1 wt. % of polyvinylpyrrolidone (PVP) stabilizer has been utilized to provide stability of the NP suspension.

The relationship between metal oxide NP, wettability alteration and oil recovery has been investigated by using the cores with different wettabilities to figure out the most suitable condition for each type of NP. Figure 2.7 presents contact angle measurements at ambient conditions acquired by Hendraningrat et al. [24] for water-wet systems (left figure) and oil-wet systems (right figure).

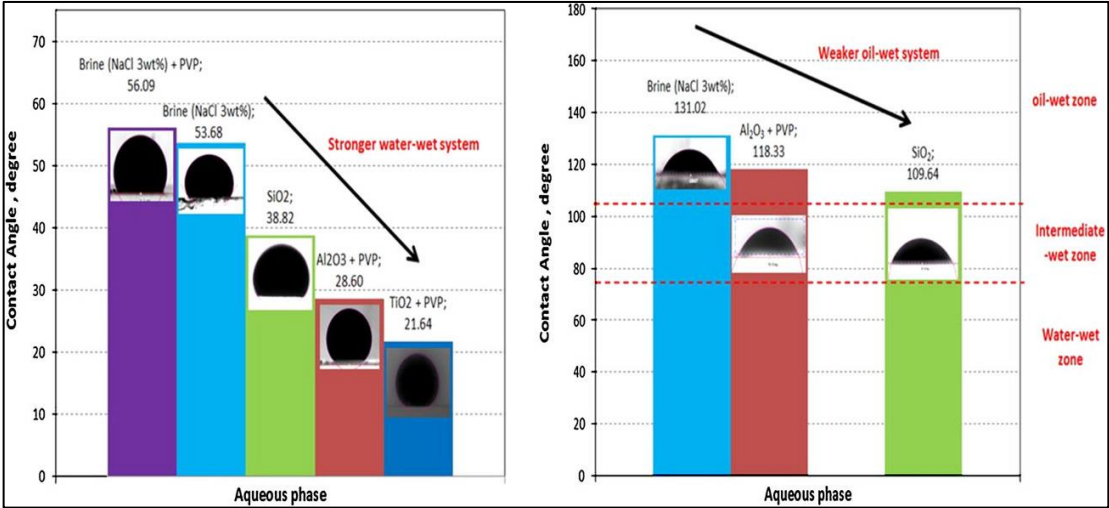


Figure 2.7 – Contact angle measurements of aqueous phase on quartz plate [24]

Application of the metal oxides NP has shown good results in changing of wettability of the cores from oil-wet to slightly water-wet. The same phenomenon was reported by Ehtesabi et al. [25] when the rock was treated with metal oxide TiO₂ NP. Hence, oil displacement mechanism can be affected by nanofluid application. However, these modification has not resulted in a significant increase in oil recovery.

The best potential in altering rock wettability from oil-wet to water-wet was found for TiO₂ metal oxide. This type of NP eventually showed better behavior in increasing of oil recovery that the rest NP used in the survey. However, silica dioxide NP demonstrated higher effectiveness in oil-wet systems as can be observed from Figure 2.7.

Metal oxide NP injection changed the surface charge and pH of the dispersion. With increasing concentration of metal oxide NP the surface charge increases whereas pH in the aqueous phase decreases. The values of pH play an important role in the efficiency of NP trapping. However, pH change as well as modification of the IFT are not the major factors in recovery improvement. Wettability alteration of the rock, in turn, is considered to become a more dominant key factor in recovery enhancement [4].

3 Theoretical introduction

3.1 Silica nanoparticles

Silicon dioxide (SiO₂) nanoparticles are spherical materials with poor conductivity for both heat and electrons that can be dispersed into various solutions.

Silica nanoparticles have been extensively investigated over the past decade for potential use in EOR applications. This specific interest for this type of nanoparticles is connected with the fact that silica nanoparticles are hydrophilic by nature and can easily be subjected to functionalization.

3.2 Mechanisms of nanoparticles adsorption on rock surface

Adsorption on grain surfaces of the rock can take place when nanoparticles are transported in a porous medium. Adsorption can be induced by the following physicochemical interactions [26]:

- Medium-particle collision;
- Static interaction between particle and rock surface;
- Hydrodynamic forces;
- Thermodynamic forces.

When a formation grain appears on the way on NP there can occur medium-particle collision that causes stagnant retention of nanoparticle on the surface of the rock grain.

Static interactions between NP and rock include double-layer repulsion and van der Waals attraction, according to developed Derjagin-Landau-Verwey-Overbeek (DLVO) theory.

According to Guzman et al. [27], van der Waals energy of interaction between NP and grain surface can be calculated as a function of the distance between surface and NP and particle size. Electrostatic double layer interaction, in turn, depends on the ionic strength of the surrounding fluid and surface potentials of both formation solid and NP. Low salinity of brine favors repulsion between NP and grain surfaces, while high salinity tends to shrink the double-layer.

Hydrodynamic forces that can contribute to detachment of the NP from a solid surface and required critical velocity of the fluid flow was investigated by Burdick et al. [28].

Langmuir adsorption is commonly used to describe adsorption caused by thermodynamic forces, regulated by various chemical potentials for a solute, moving between the aqueous phase and solid surface. Continuous injection of nanoparticles leads to their thermodynamic attraction to the rock surface, which changes in magnitude with time eventually reaches an equilibrium. This adsorption type is considered reversible. Desorption process can take place in the rock due to the sign change of thermodynamic force. For example, this can be expected during a post – flush period, when nanofluid injection is followed by injection of the aqueous phase without nanoparticles.

Therefore, it is considered that the key parameters influencing NP adsorption / desorption processes during their interaction with porous media are the surface properties of both the rock grains and nanoparticles, van der Waals attraction force, brine salinity and mineral composition of the rock [26].

3.3 Zeta-potential

Colloidal particles in a suspension have a certain electrical charge. This charge can be negative or positive, but its amount on particle surface can characterize many properties of the suspension. It should be stressed that there is a counterbalance between the charge of the particle surface and the

opposite sign charges (ions) in a solution around it which makes the suspension neutral in overall. The charge of the surrounding solution is less associated with the particle, but surface charge is usually considered to be attached to the particle [29].

Electrical charge of particles suspended in a liquid can be characterized by the zeta-potential, which shows a potential difference across solid and liquid phases. Zeta-potential is an electrostatic potential in a double layer between two phases from a position of slipping plane referred to a surrounding fluid away from the interface. Zeta-potential measured in millivolts (mV) is utilized to characterize double-layer properties, but it does not equal to Stern or electric surface potential (Figure 3.1) [30].

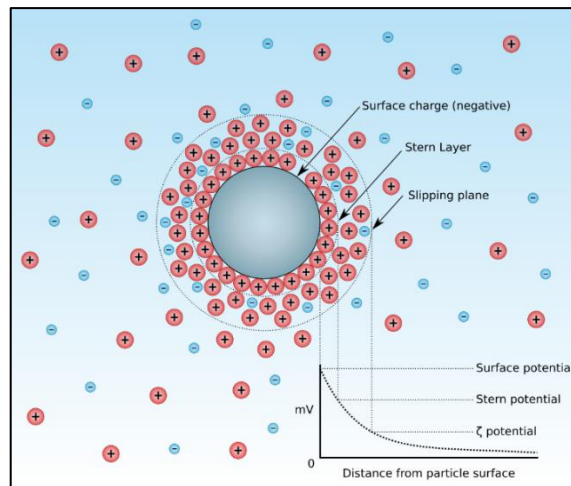


Figure 3.1 – Diagram of zeta-potential and slipping plane [30]

It is not possible to measure this parameter directly. Theoretical models or experimental estimations based on electrophoretic mobility are usually applied [31].

Practical use of zeta-potential is connected with many important industries, including nanotechnology which has a promising application for EOR techniques. Zeta-potential measurements can be used to acquire desired properties of the nanoparticles which will help to extract residual oil by interaction with reservoir formation.

Zeta-potential is considered as one of the key characteristics that affect stability of nanoparticle suspensions. With increase of zeta-potential suspended nanoparticles demonstrate good dispersability and therefore, better stability because electrostatic repulsion forces become stronger [32]. Typically, when zeta-potential becomes less negative than -15mV, there begins the process of nanoparticles agglomeration, and in case this value reaches zero, it is expected to observe their precipitation into a solid (Figure 3.2) [31].

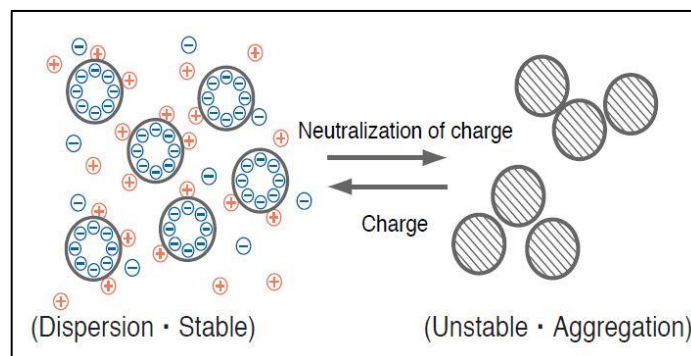


Figure 3.2 – Evaluation of dispersion stability [32]

4 Methodology

This chapter comprises a practical side of the investigation. It starts with a brief overview of all conducted experiments. Then all the fluids, chemicals, apparatus and experimental setups used during the work on this Master's thesis are listed and discussed. Finally, experimental procedures are described in detail.

The experimental part of the thesis starts from the characterization of nanofluid by determining a size and zeta-potential of nanoparticles, suspended in media of different salinity (DIW, LSW, SSW). Another test was conducted at three different temperatures (25, 50 and 80°C) to evaluate stability of the nanofluid (check for possible agglomeration tendency). Effect of suspension concentration on measured average size of nanoparticles was also considered.

Then zeta-potential and pH measurement were taken for quartz, kaolinite and crushed Berea sandstone core mineral powders suspended in DIW at different concentrations. Acquired data was important to evaluate possible attractive or repulsive tendencies between NP and mineral surfaces.

After that static adsorption experiments were developed to evaluate possible adsorption taking place on surfaces of individual minerals: quartz, kaolinite and calcite. Acquired specific adsorption values at different concentration ratios between minerals and nanoparticles prepared in DIW were compared to that of the samples prepared in SSW, so the salinity effect on adsorption of nanoparticles was examined.

Four core flood experiments ("Berea 001" – "Berea 004") were conducted by injecting deionized water and nanofluid slug at different concentrations to investigate a transport behavior of nanoparticles in sandstone rock. The pressure difference across the core was recorded, several characterization tests were run on effluents: pH of the samples, ion concentration to describe in detail interactions between the core and injected fluids. Besides, the absorbance of the samples was measured to get an idea about injected nanoparticles production / retention as well as fine particles behavior. Some effluent probe was chosen for scanning electron microscope (SEM) and chemical component analysis together with a sandstone core that was saturated with nanofluid for 24 hours.

Another set of core flood experiments ("Berea 005" – "Berea 006") was aimed to examine potential of nanofluid use in enhanced oil recovery by establishing irreducible water saturation in the core, aging it for at least 2 weeks and subsequent running of secondary imbibition flood with NP injection until all possible extraction of oil happened and residual oil saturation point was reached.

It should be stressed that all experiments were performed in accordance with safety regulations at the University of Stavanger. Assessment of possible risks connected with dangerous equipment and chemicals was carried out and submitted to the university department before laboratory work.

4.1 Experimental materials and fluids

4.1.1 Deionized water

Deionized water (DIW) was actively used for dilution of fluids, different samples preparation and core flood experiments. DIW was provided with “Milli-Q® Integral 5 Water Purification System” supplied by “Merck KGaA” (Figure 4.1). Properties of DIW were determined before experiments. Its density at ambient conditions was measured equal to 0.997 g/cm^3 and $\text{pH} = 6.54$.



Figure 4.1 – “Milli-Q® Integral 5 Water Purification System”

4.1.2 Nanofluid

Nanofluid suspension “DP9711” was produced by “NYACOL® Nano Technologies Inc.” (United States of America). It is a surface modified colloidal silica, which has a nominal particle size of 20 nm and is supplied in 1 liter bottles as a very concentrated fluid, approximately 3 wt % (Figure 4.2). For different experiments, it is usually diluted with DIW to get the required concentration. According to information from the manufacturer the nanofluid “DP9711” is stable against agglomeration in salt and brine solutions and has excellent stability over a wide range of pH [33].



Figure 4.2 – Nanofluid “NYACOL DP9711”

This modified silica nanofluid was tested at harsh conditions: temperature $+50 \text{ }^\circ\text{C}$ and elevated pressure up to 80 bars for 24 hours. As a result, no agglomeration observed, which indicated a very high level of fluid stability.

4.1.3 Brines

Two brine types were used in laboratory experiments – synthetic sea water (SSW) and low salinity water (LSW). They were prepared by dissolving different amounts of chemicals in deionized water and sequent stirring using magnetic bar. After salts dissolution an important step is filtering of the brine through a 0.22 μm filter by using filtering setup (Figure 4.3). This is required to remove undissolved impurities from the liquids before further storage in glass bottles and utilization in experiments. In their work A.A. Hamouda et al. [34] used the composition of brines presented in Table 4.1. The density of SSW at ambient conditions is 1.024 g/cm^3 .

Table 4.1 – Brines composition [34]

Ion name	SSW (mol/l)	LSW (mol/l)
HCO_3^-	0.002	0.00008
Cl^-	0.525	0.021
SO_4^{2-}	0.0240	0.00096
Mg^{2+}	0.045	0.0018
Ca^{2+}	0.013	0.00052
Na^+	0.450	0.018
K^+	0.010	0.0004
TDS (g/l)	33.39	1.3356
Ion strength (mol/l)	0.657	0.0263

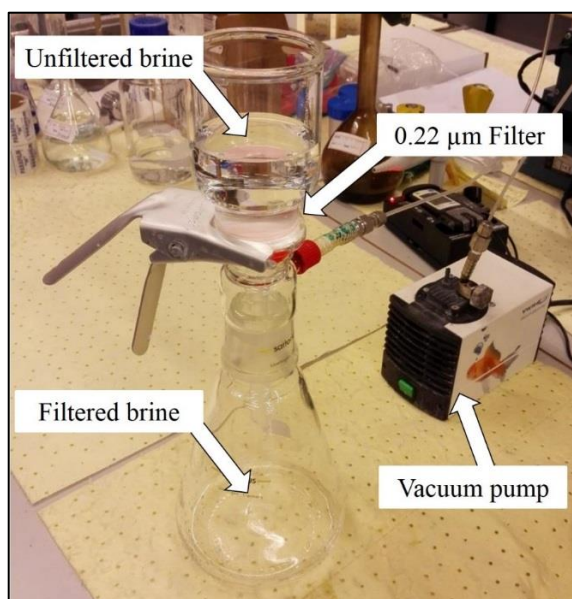


Figure 4.3 – Filtering setup for preparation of brines

4.1.4 Lithium chloride

Lithium chloride powder produced by “Merck KGaA” (Germany) is a trace on metal basis with purity > 99 % (Figure 4.4). It was used in experiments as a tracing material to be detected in effluent.



Figure 4.4 – Container with Lithium Chloride for analysis

4.1.5 Model oil

Normal-Decane (n-C₁₀) was supplied by “Chiron AS” (Norway). It has purity > 99% in high-performance liquid chromatography grade. According to A.A Hamouda, O.M. Valderhaug et al. [35], the density and viscosity of n-Decane at ambient conditions (pressure: 1 atm, temperature: 25 °C) are equal 0.73 g/cm³ and 0.920 cP respectively.



Figure 4.5 – A bottle of n-Decane for analysis

N,N-Dimethyldodecylamine (NN-DMDA) with structural formula CH₃(CH₂)₁₁N(CH₃)₂ supplied by “Fluka[®] Analytical” (Germany) was used to mimic amine in model oil by adding in concentration 0.01 mol/l. Hence, n-Decane + 0.01M NN-DMDA liquid was utilized as hydrocarbon phase in EOR experiments [34].

4.1.6 Mineral powders

Mineral powders of Quartz (SiO₂), Kaolinite (Al₂Si₂O₅(OH)₄) and Calcite (CaCO₃) were supplied by Fluka[®] Analytical” (Germany). These three types of minerals, are stored in a form of dry powder in plastic containers (Figure 4.6).



Figure 4.6 – Containers with mineral powders: Quartz, Kaolinite and Calcite

Surface areas of minerals presented in Table 4.2 were measured and calculated using BET equation from water adsorption isotherm by V.A. Tabrizy [36].

Table 4.2 – Surface area of mineral powders [36]

Mineral powder	BET surface area (m ² /g)
quartz	0.65
kaolinite	9.95
calcite	0.23

4.1.7 Porous media

Berea sandstone cylindrical cores to be used in flooding experiments are of the same type utilized in survey by A.A. Hamouda et al. [34]. The mineral analysis is presented in Table 4.3.

Table 4.3 – Mineral analysis of the Berea sandstone [34]

Mineral name	Chemical formula	Semi – quantitative (%)
quartz	SiO ₂	94
kaolinite	Al ₂ Si ₂ O ₅ (OH) ₄	1
muscovite	(K, Na) (Al, Mg, Fe) ₂ (Si ₃ ·Al, O ₁₀)O ₁₀ (F, OH) ₂	1
microline	KAlSi ₃ O ₈	1

The main properties of sandstone cores used in experiments are listed in Table 4.4.

Table 4.4 – Properties of Berea sandstone cores

Core type	Berea Sandstone
Length	8.95 ± 0.08 cm
Diameter	3.78 cm
Porosity	20.05 ± 0.76 %
Permeability	200 - 220 mD

Cores are stored in laboratory oven at 100 °C to keep them dry before use in experiments (Figure 4.7).



Figure 4.7 – Berea sandstone cylindrical cores in laboratory oven

4.2 Laboratory equipment

4.2.1 “S220 SevenCompact™ pH/ion meter”

“S220 SevenCompact™ pH/ion meter” was produced by “Mettler-Toledo International Inc.” (Figure 4.8) According to data sheet this machine is suited for measuring pH values from -2 to 20 in a wide range of temperatures (from -30 to +130 °C) with accuracy ± 0.002 . This machine was used to measure pH of prepared fluids and produced effluents during core flood experiments.

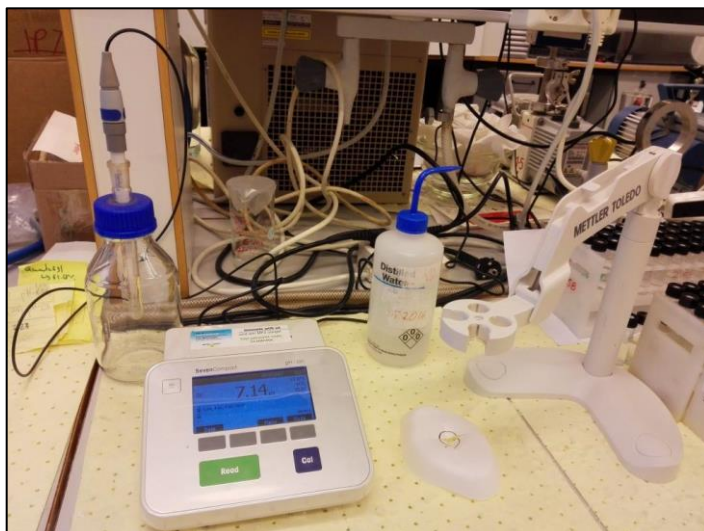


Figure 4.8 – “S220 SevenCompact™ pH/ion meter”

4.2.2 “Reax Top Vortex Mixer”

“Reax Top Vortex Mixer” was supplied by “Heidolph Instruments GmbH & Co.KG” (Germany). This machine allowing rotation speed from 0 to 2500 rpm was usually utilized to shake solutions and suspensions in plastic tubes as an important step in all cases of samples preparation (Figure 4.9).



Figure 4.9 – “Reax Top Vortex Mixer”

4.2.3 “Rotator Stuart SB-3”

“Rotator Stuart SB-3” with fully adjustable mixing angle and speed of rotation from 2 to 40 rpm was supplied by “Cole-Parmer” (United Kingdom). It was utilized for effective mixing and rotating prepared suspensions in plastic tubes (Figure 4.10).

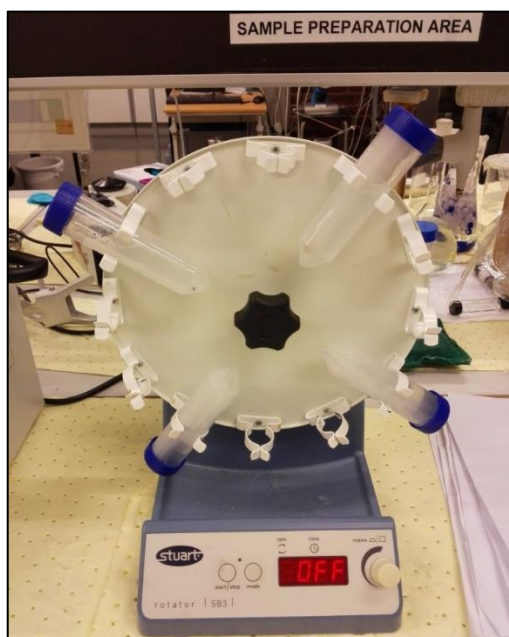


Figure 4.10 – “Rotator Stuart SB-3”

4.2.4 Balances

Precision balance “Mettler PM 4600” was supplied by “Mettler-Toledo International Inc.” It has an operational capacity from 0 to 4100 grams with a fine range of 0.01 g. It was used predominantly to measure the weight of cores before and after flooding experiments (Figure 4.11).



Figure 4.11 – Precision balance “Mettler PM 4600”

Analytical balance “MS104-S” was also supplied by “Mettler-Toledo International Inc.” (Switzerland). Maximum capacity of the balance is 120 g with readability 0.1 mg. It was widely used in experiment to weigh nanofluid, mineral powders and other chemicals. An analytical balance is presented in Figure 4.12.

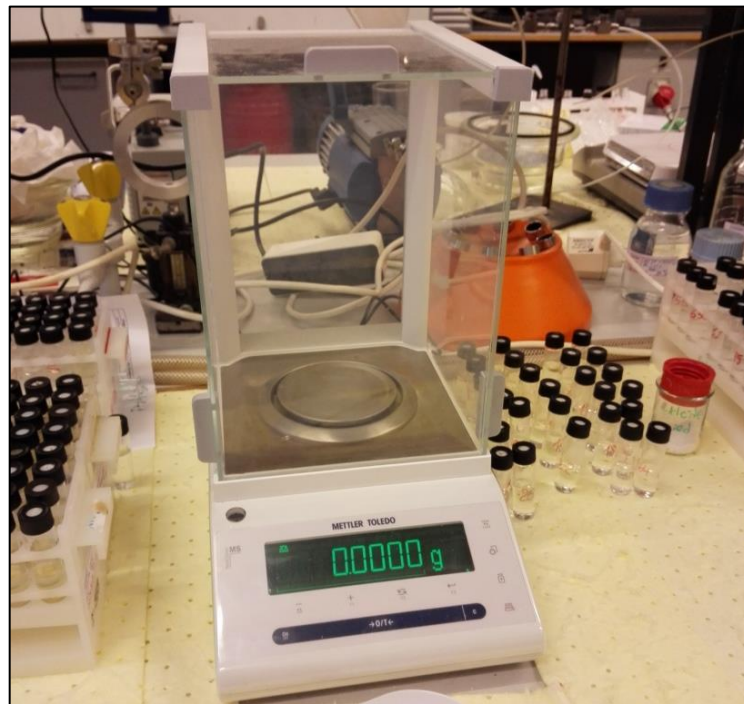


Figure 4.12 – Analytical balance “MS104-S”

4.2.5 Magnetic stirrer “VWR VMS-C10”

Magnetic stirrer “VWR VMS-C10” by “VWR International” was utilized for mixing fluids during the preparation of brines and other liquids to be used in experiments. Magnetic bar is put into the flask with fluid and then the flask is placed on the magnetic stirrer for proper mixing (Figure 4.13).



Figure 4.13 – Magnetic stirrer “VWR VMS-C10”

4.2.6 “Centrifuge 5804”

“Centrifuge 5804” was supplied by “Eppendorf AG” (United States of America). The machine has an operational spin range from 200 to 11 000 rpm and can hold up to 6 plastic sampling tubes simultaneously which is suitable for conducted experiments to separate mineral powder from pure fluid in samples. Centrifuge is presented in Figure 4.14.

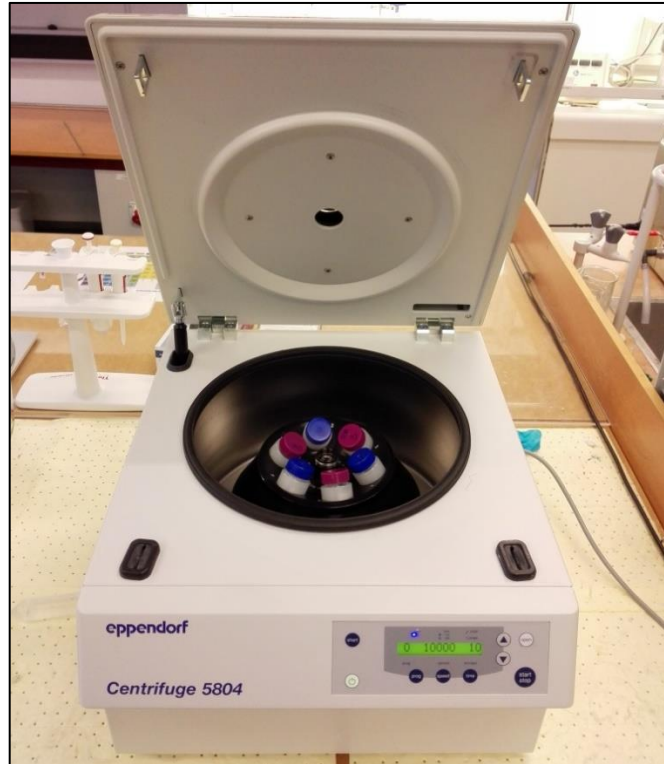


Figure 4.14 – “Centrifuge 5804”

4.2.7 Vacuum saturation setup

The setup that was used to saturate cores with required fluids under vacuum is shown in Figure 4.15.

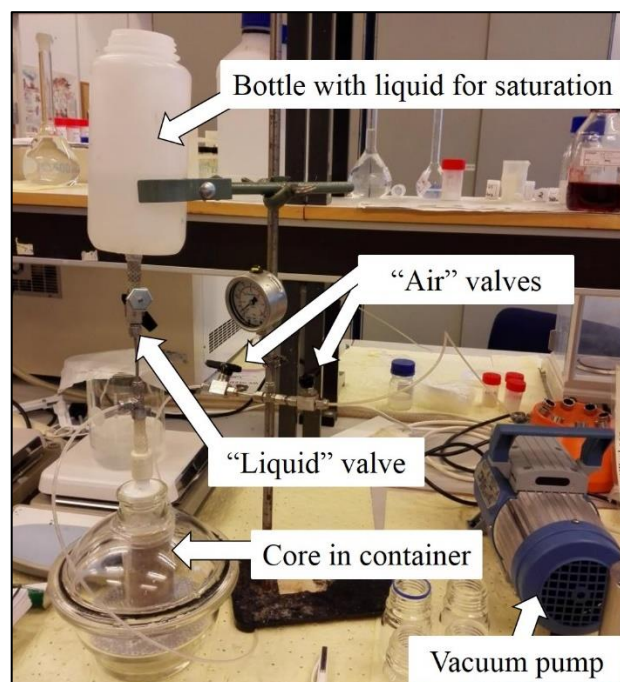


Figure 4.15 – Vacuum saturation setup

First, the core in a plastic container is placed inside a glass camera, and the air is sucked off from it by a vacuum pump for 30 minutes with closed “liquid” valve and opened “air” valves. Plastic bottle on the top is filled with fluid to be used for saturation. Then “air” valves are closed, the pump is turned off, and the “liquid” valve is opened slowly, allowing fluid from the plastic bottle to go inside the camera, fill the plastic container and saturate the core.

4.2.8 Equipment for flooding cores

Special experimental setup depicted in Figure 4.16 was used for core flood experiments. It consists of core holder; cylinders filled with required fluids for the flood; inlet, differential and confinement pressure gauges; injection and confinement pumps “Gilson 305”; sampling machine or burette to collect the effluent. Core holder and fluid cylinders are placed inside a laboratory oven capable to sustain a certain temperature during the experiment. The back pressure valve is also applied whenever necessary, and the back pressure is built by nitrogen that is stored in N₂ tank.

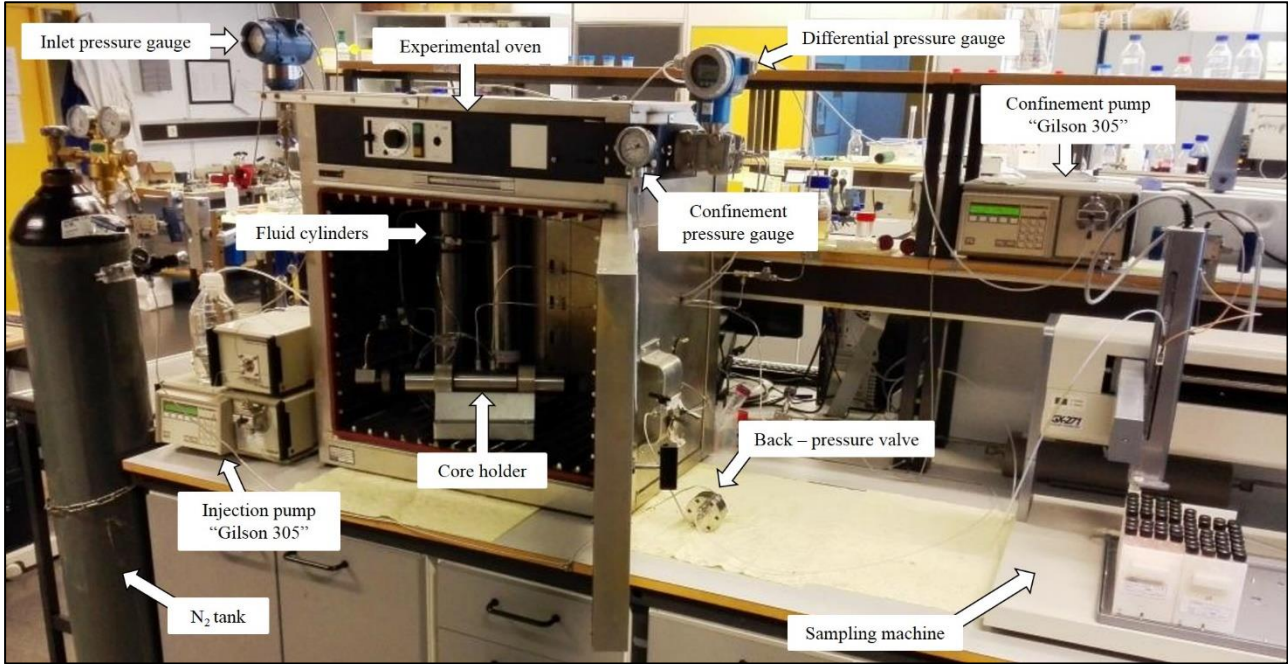


Figure 4.16 – Experimental core flooding setup

Individual parts of disassembled core holder are presented in Figure 4.17. Belt wrench is used to tighten and release locks of the core holder.

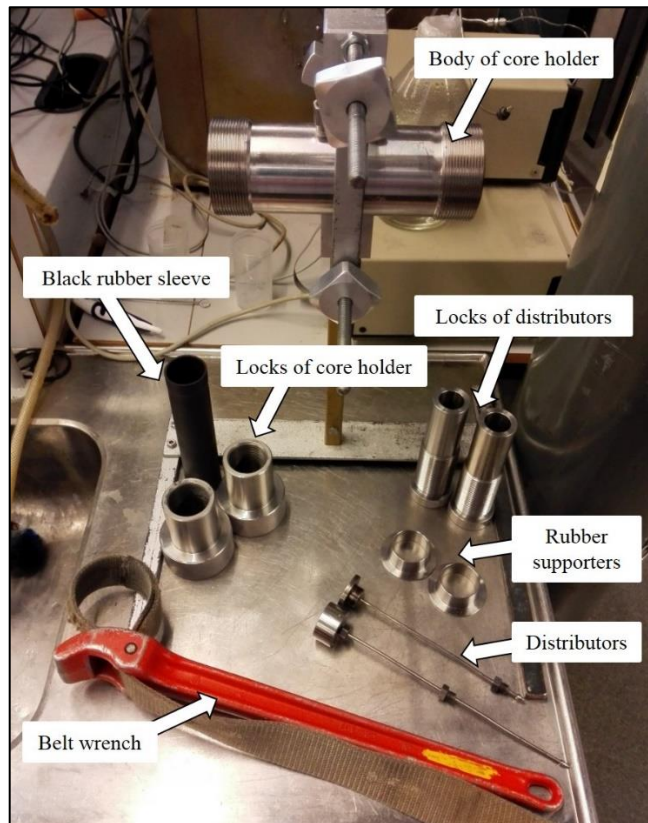


Figure 4.17 – Disassembled core holder

Before putting on a rubber sleeve and placing the core inside the core holder, it should be wrapped with teflon tape and plastic sleeve (Figure 4.18). Auxiliary instruments utilized in this process are cutter or scalpel, scissors, and a heat gun.

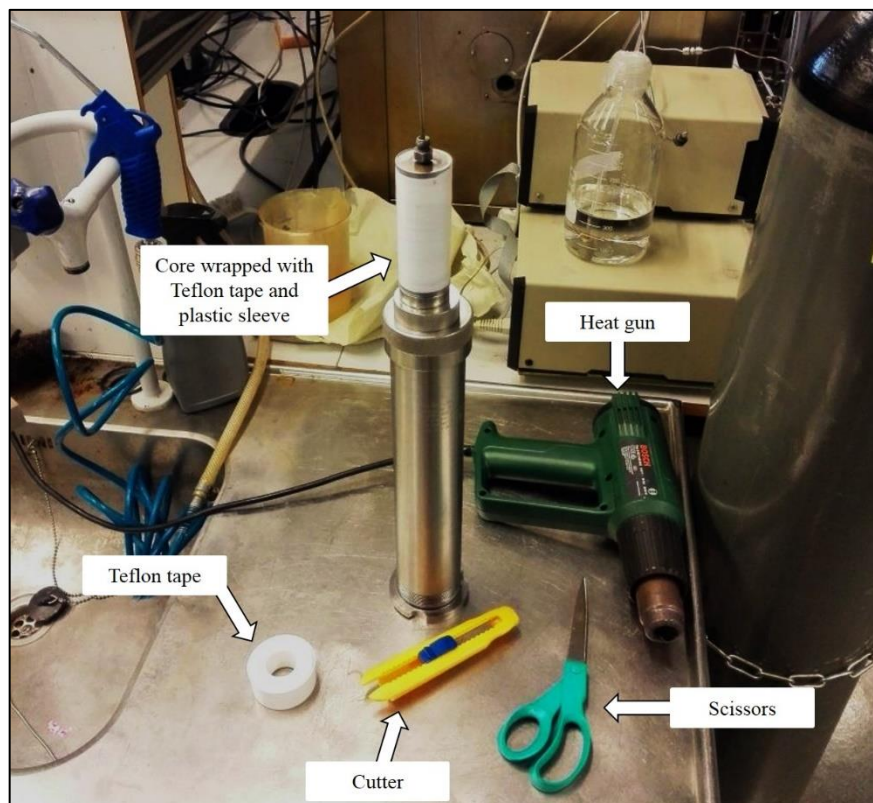


Figure 4.18 – Instruments and materials for wrapping the core

Autosampler “GX-271 Liquid handler” produced by “Gilson Inc.” (United States of America) serves for collecting effluents in glass vials (Figure 4.19).

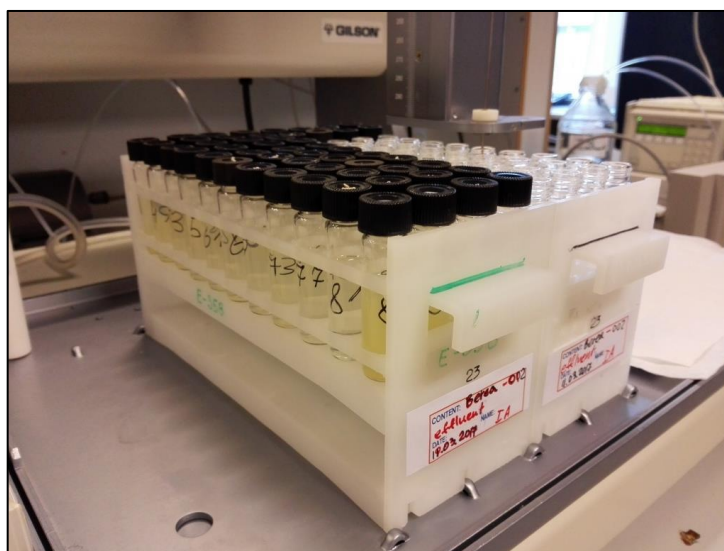


Figure 4.19 – Autosampler “GX-271 Liquid handler” with glass vials

4.2.9 “AcoustoSizer II-M system”

“AcoustoSizer II-M system” was supplied by “Colloidal Dynamics LLC” (United States of America). It allows measuring particle size distributions and zeta-potentials in both concentrated aqueous and non-aqueous suspensions. Electroacoustic and Attenuation Spectroscopy techniques are used to detect particle size in a range from 0.015 to 100 microns. Zeta-potential can be measured for concentrations from 1 to 40 volume % [37]. The apparatus is depicted in Figure 4.20.

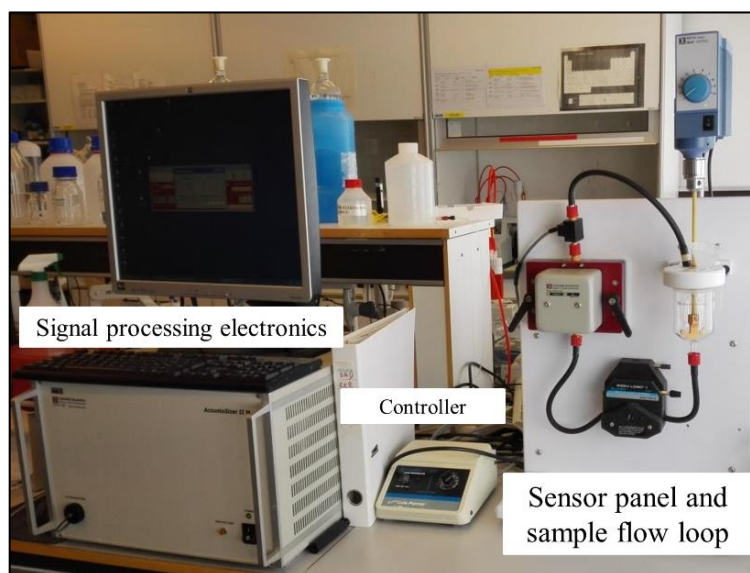


Figure 4.20 – “AcoustoSizer II-M system”

4.2.10 “Zetasizer Nano ZSP”

“Zetasizer Nano ZSP” by “Malvern Instruments Ltd” (United Kingdom) is shown in Figure 4.21.



Figure 4.21 – “Zetasizer Nano ZSP” [38]

This versatile instrument allows performing very quick, simple, repeatable and non-destructive nanoparticle characterization by a combination of measurement techniques of Dynamic Light Scattering (DLS) and Electrophoresis. DLS method is utilized to determine the size of NP by measuring the Brownian movement of particles in a solvent or suspension. After that, the Stokes-Einstein relationship is used to convert this diffusion speed into a size distribution. Micro-electrophoresis is implemented to determine the zeta-potential of dispersions being analyzed [39].

4.2.11 “UV – 1700 spectrophotometer”

“UV - 1700 spectrophotometer” was produced by “Shimadzu Corp.” (Japan). The work of the machine presented in Figure 4.22 is based on the following principle. The light beam is induced in this apparatus and the intensities of the light beam I_t and I_0 after it passes through two cells are measured. Equation 4.1 shows the transmittance or effectiveness in transmitting radiant energy [40].

$$T = \frac{I_t}{I_0}, \quad (4.1)$$

where T – transmittance;

I_t – intensity of the light beam after it passes through the cell with solvent;

I_0 – intensity of the light beam after it passes through the cell with solution in solvent.

However, the absorbance Abs is used more often for solution samples (Equation 4.2).

$$Abs = \text{Log}_{10} \frac{1}{T}, \quad (4.2)$$



Figure 4.22 – “UV – 1700 spectrophotometer”

During the analysis solution and solvent samples are kept in transparent rectangular quartz cuvettes manufactured especially for use in this apparatus. Cuvettes are presented in Figure 4.23.

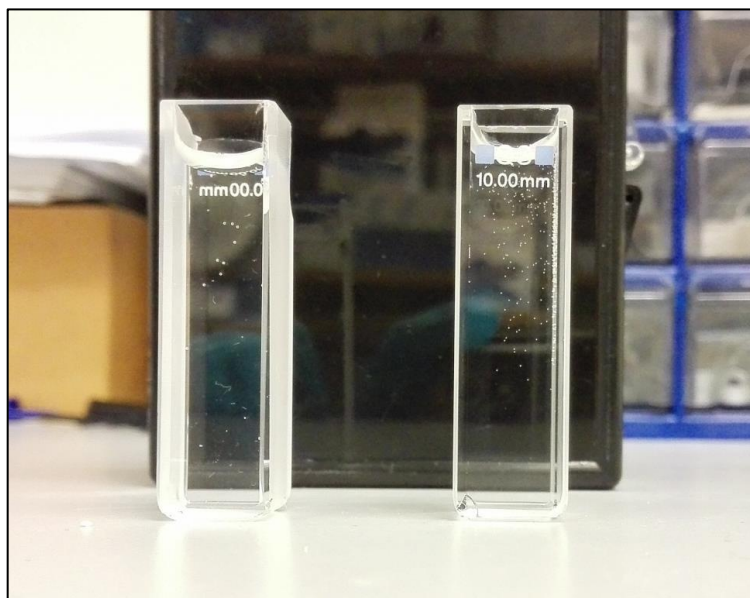


Figure 4.23 – Rectangular quartz cuvettes for “UV – 1700 spectrophotometer”

Spectrophotometer supports a wide wavelength range (from 190 to 1100 nm) and photometric range (Abs from -0.5 to $+3.0$). Besides, photometric accuracy and repeatability are ± 0.002 and ± 0.001 , respectively, at 0.5 Abs according to information provided by “Shimadzu Corporation” [41].

4.2.12 Ion Chromatograph “Dionex Ics-5000⁺ DP”

Ion Chromatograph “Dionex Ics-5000⁺ DP” was produced by “Thermo Fisher Scientific Inc.” (United States of America). The apparatus presented in Figure 4.24 was utilized to evaluate the concentration of ions in effluent samples from core flood experiments.



Figure 4.24 – Ion Chromatograph “Dionex Ics-5000+ DP”

Before analysis in IC – machine samples were diluted to required concentrations by using another equipment - “GX-271 Liquid handler” produced by “Gilson Inc.” (United States of America) which presented in Figure 4.25.

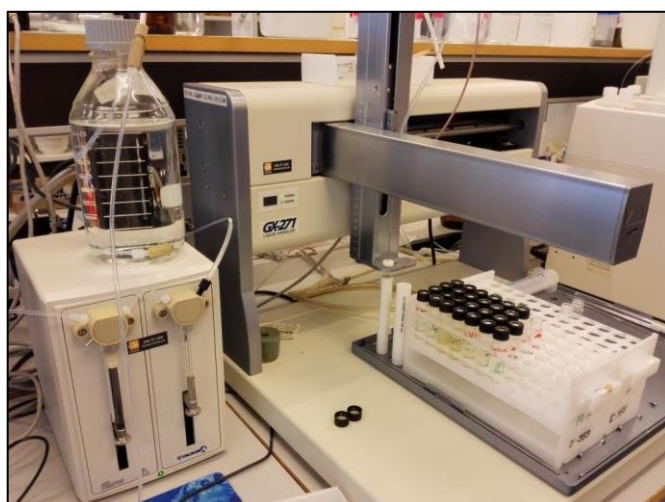


Figure 4.25 – “GX-271 Liquid handler”

4.2.13 Scanning Electron Microscope “Supra 35VP FE-SEM”

“Supra 35VP FE-SEM” supplied to the University of Stavanger by “Carl Zeiss” (Germany) was used in this project (Figure 4.26). The images of the samples are produced by the interaction of the beam of electrons with the surface of the sample. The machine can provide magnification up to 100 000 times which cannot be achieved by normal light microscope due to limitations in the wavelength of visual light. The sample is placed in a sample chamber under vacuum. Electron gun accelerates electrons to create a focused beam focused and adjusted by electromagnetic lenses to scan the sample. When electrons reach the sample, energy signals of different magnitude reflected or produced from the surface are eventually captured by various detectors. The speed of electrons depends on the acceleration voltage and the higher the voltage the further they can penetrate into the sample. Also, Energy-dispersive X-ray spectroscopy system is mounted in the SEM. This system allows performing analysis of the chemical composition on the semi-quantitative level of the area corresponding to a beam of 2 μm wide. [42].

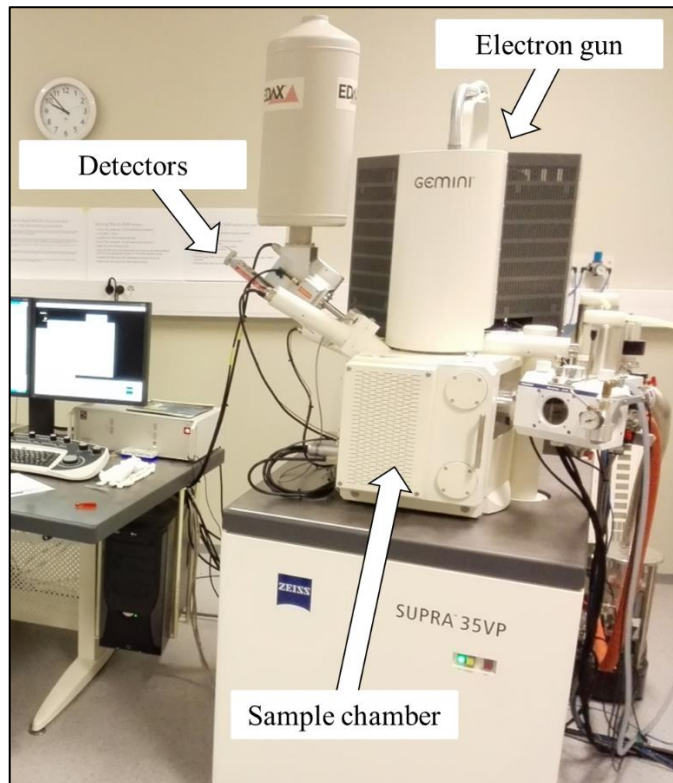


Figure 4.26 – Scanning Electron Microscope “Supra 35VP FE-SEM”

More than that before proceeding with SEM, samples have to be coated with some conductive material (palladium, gold or carbon) to avoid charging and provide a steady flux of electrons [42]. “Emitech K550 automatic sputter coater” supplied by “Emitech Ltd.” was used to coat the samples before analysis in SEM. The process of coating of the sample with thin palladium layer of is presented in Figure 4.27.

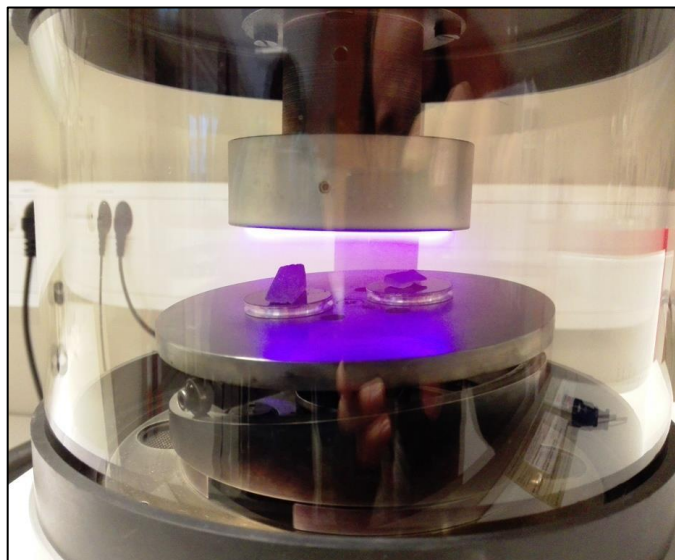


Figure 4.27 – “Emitech K550 automatic sputter coater”

A 25 mA current was used to reach the thickness of coating close to 20 nm and the cylindrical camera was filled with gas argon to stabilize the process and ensure even coating of the sample with palladium.

4.3 Nanofluid characterization procedure

Before conducting experiments with nanofluid, it is important to perform its characterization by determining the size range of dispersed nanoparticles and zeta-potential. “Zetasizer Nano ZSP” by “Malvern Instruments Ltd.” (United Kingdom) was used to conduct several tests on nanofluid “DP9711” supplied by “NYACOL® Nano Technologies Inc.” (United States of America).

At first, nanofluid was diluted in DIW at three different concentrations 1 g/l, 2 g/l, 4 g/l and the average size was determined giving an idea of concentration change influence. Then nanofluid samples at 1 g/l concentration were prepared in DIW, LSW and SSW and measured to evaluate the effect of salinity on nanoparticle size and zeta-potential readings. After that, the temperature test was conducted for samples of the same concentration 1 g/l diluted in DIW, LSW and SSW at three different temperatures 25, 50 and 80°C.

4.4 Procedure of zeta-potential measurements on mineral powder

“AcoustoSizer II-M Particle Size and Zeta Potential Analysis System” by “Colloidal Dynamics LLC” (United States of America) was used to measure zeta-potential of concentrated mineral powder suspensions in DIW. Three types of mineral powder were prepared at different concentrations in DIW for zeta-potential analysis: Quartz (SiO_2), Kaolinite $\text{Al}_2\text{Si}_2\text{O}_5(\text{OH})_4$ and Berea sandstone powder (crushed core). Samples were stirred for 20 minutes and values of pH were measured before the experiment. After pH value is taken for a certain powder suspension, it is placed inside transparent camera of the apparatus and then pump is activated to ensure continuous fluid circulation in a flow loop through an electroacoustic sensor which measures zeta-potential (Figure 4.28).

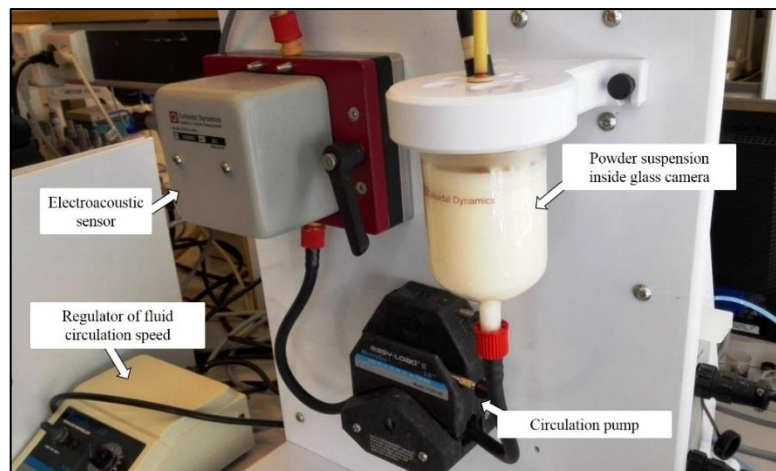


Figure 4.28 – The process of zeta-potential measurement for mineral powder

4.5 Static adsorption experiment procedure

This set of experiments was run to investigate nanoparticles adsorption behavior on mineral surfaces of quartz, kaolinite, and calcite mineral powders. The adsorption of nanofluid dispersed in DIW and SSW with the three types of minerals was investigated according to the following three steps:

- 1) a constant amount of each mineral (in grams) prepared in two different concentrations of nanofluid suspension (constant mass experiment);
- 2) different concentrations of minerals with maintaining equal surface area for all minerals prepared in two different concentrations of nanofluid suspension (constant surface area experiment);
- 3) a varying amount of mineral powders in different concentrations of nanofluid (extra points experiment).

The first set of tests was performed in DIW. Nanofluid “DP9711” was diluted in DIW at concentration 1g/l and was further used for samples preparation in plastic tubes. Table 4.5 shows the detailed information about concentrations of nanoparticles and mineral powders used for this experiment, 17 samples in total.

Table 4.5 – Samples for static adsorption experiment in DIW

NP concentration (g/l)	Mineral	Specific surface area (m ² /g)	Mineral amount (g)*	Surface area (m ²)	Mineral concentration (g/l)	Mineral/NP concentrations ratio
Constant mass samples						
1	Quartz	0.65	0.15	0.0975	5	5
0.5	Quartz	0.65	0.15	0.0975	5	10
1	Kaolinite	9.95	0.15	1.4925	5	5
0.5	Kaolinite	9.95	0.15	1.4925	5	10
1	Calcite	0.23	0.15	0.0345	5	5
0.5	Calcite	0.23	0.15	0.0345	5	10
Constant surface area samples						
1	Quartz	0.65	0.058	0.0375	1.923	1.923
0.5	Quartz	0.65	0.058	0.0375	1.923	3.846
1	Kaolinite	9.95	0.0038	0.0375	0.126	0.126
0.5	Kaolinite	9.95	0.0038	0.0375	0.126	0.251
1	Calcite	0.23	0.163	0.0375	5.435	5.435
0.5	Calcite	0.23	0.163	0.0375	5.435	10.870
Extra points samples						
1	Quartz	0.65	0.030	0.0195	1	1
1	Quartz	0.65	0.015	0.00975	0.5	0.5
1	Kaolinite	9.95	0.060	0.597	2	2
1	Calcite	0.23	0.090	0.0207	3	3
1	Calcite	0.23	0.030	0.0069	1	1

*Samples are prepared in plastic tubes and calculations are made for 30 ml of fluids

After the samples are prepared they are mixed intensively using vortex mixer and placed in the rotator for mixing at 30 rpm for 24 hours to facilitate mineral powder interaction with NP and establish a thermodynamic equilibrium in the sample. After that, the samples are retrieved from rotator and centrifuged at a speed of 10 000 rpm for 10 minutes. After centrifuging decanting is carried out to remove the most of the mineral particles from the suspension and supernatant is subjected to the second centrifuging step at 10 000 rpm for 10 minutes.

“UV-1700 spectrophotometer” by “Shimadzu Corp.” (Japan) was used to investigate adsorption of NP on minerals. Quantitative analysis of adsorption is based on “Lambert-Beer law” (Equation 4.3). It expresses a proportional relationship between the absorbance and sample concentration [40].

$$Abs = \varepsilon \cdot C \cdot L, \quad (4.3)$$

where *Abs* – absorbance;
ε – absorption coefficient;
C – sample concentration;
L – optical path length of the cell.

“Abs” value measured in the machine allows estimating the amount of NP adsorbed on mineral surfaces. The more absorbance reading - the more light is transmitted through the cuvette filled with a sample, and therefore the less NP is left in the sample without being adsorbed during rotation stage. Before taking readings in spectrophotometer, all the samples must be filtered through a micron filter 0.2 μm to get rid of residual mineral particles and impurities.

All measurements were taken at preliminarily determined parameters: DIW was used as a reference fluid, and working wavelength of the machine was set to 240 nm. The optimum wavelength for experiments was chosen according to the best possible sensitivity for concentration. Figure 4.29 demonstrates a calibration line - relation between absorbance values and sample concentration for “DP9711” nanofluid suspension in DIW. The closer the angle of this straight line to 45° the better sensitivity between absorbance and concentration. The closest to 45° angle was acquired with 240 nm wavelength.

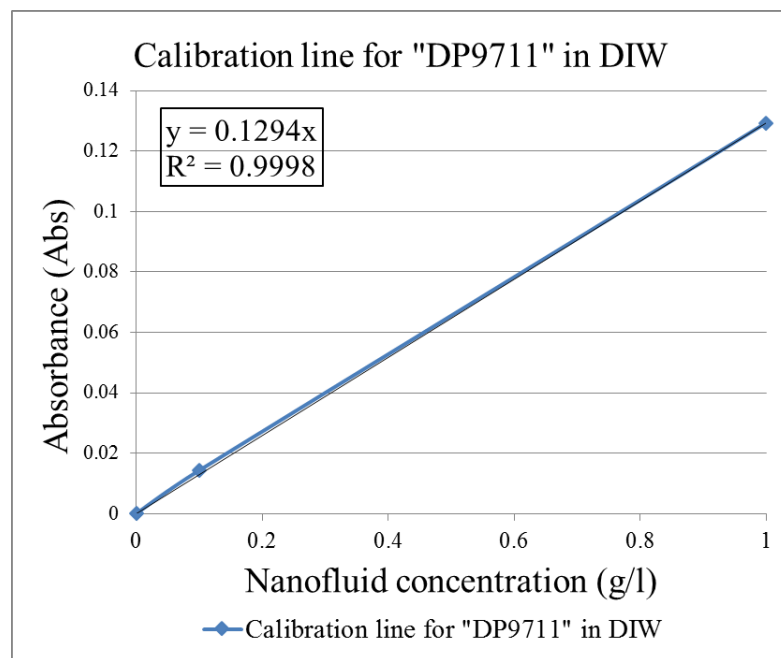


Figure 4.29 – Calibration line for “DP9711” nanofluid prepared in DIW

In order to build a calibration line in DIW nanofluid is prepared in three concentrations. Three samples then are vortexed, centrifuged in one step at 10 000 rpm for 10 minutes and analyzed in UV – machine to get Abs readings. When trend line is applied to the plot, its equation can be applied to calculate the concentration of NP in suspension from measured absorbance values.

In addition, a set of samples presented in Table 4.6 was used to take into account mineral effect on absorbance values, serving as a baseline correction for corresponding samples with the same amount of mineral powder applied.

Table 4.6 – Baseline correction samples for static adsorption experiment in DIW

Fluid	Mineral	Mineral amount (g)*	Mineral concentration (g/l)	Corresponding experiment
Baseline correction samples				
DIW	Quartz	0.15	5	Constant mass
DIW	Kaolinite	0.15	5	
DIW	Calcite	0.15	5	
DIW	Quartz	0.058	1.923	Constant surface area
DIW	Kaolinite	0.0038	0.126	
DIW	Calcite	0.163	5.435	
DIW	Quartz	0.030	1	Extra points
DIW	Quartz	0.015	0.5	
DIW	Kaolinite	0.060	2	
DIW	Calcite	0.090	3	
DIW	Calcite	0.030	1	

***Samples are prepared in plastic tubes and calculations are made for 30 ml of fluids**

The prepared samples were treated in the same way as the samples for calibration line build-up and used to acquire absorbance readings that are eventually subtracted from the Abs values of corresponding samples.

By applying a baseline correction to experimental absorbance readings and further using of a calibration line specific adsorption of nanoparticles (mg of NP adsorbed per m² of a mineral surface) is calculated.

In addition, a sensitivity experiment for NP and mineral concentrations was conducted in DIW when all concentrations were decreased ten times, but the mass of mineral per unit mass of NP was preserved. All the procedures and calculations were repeated as constant mass and constant surface area experiments from the previous case. Nanofluid with concentration 0.1 g/l was used and the samples were prepared according to Table 4.7 and Table 4.8.

Table 4.7 – Samples for concentration sensitivity adsorption experiment in DIW

NP concentration (g/l)	Mineral	Specific surface area (m ² /g)	Mineral amount (g)*	Surface area (m ²)	Mineral concentration (g/l)	Mineral/NP concentrations ratio
Constant mass samples						
0.1	Quartz	0.65	0.015	0.00975	0.5	5
0.05	Quartz	0.65	0.015	0.00975	0.5	10
0.1	Kaolinite	9.95	0.015	0.14925	0.5	5
0.05	Kaolinite	9.95	0.015	0.14925	0.5	10
0.1	Calcite	0.23	0.015	0.00345	0.5	5
0.05	Calcite	0.23	0.015	0.00345	0.5	10
Constant surface area samples						
0.1	Quartz	0.65	0.0058	0.00375	0.192	1.923
0.05	Quartz	0.65	0.0058	0.00375	0.192	3.846
0.1	Kaolinite	9.95	0.00038	0.00375	0.013	0.126
0.05	Kaolinite	9.95	0.00038	0.00375	0.013	0.251
0.1	Calcite	0.23	0.0163	0.00375	0.543	5.435
0.05	Calcite	0.23	0.0163	0.00375	0.543	10.870

***Samples are prepared in plastic tubes and calculations are made for 30 ml of fluids**

Table 4.8 – Baseline correction samples for concentration sensitivity adsorption experiment in DIW

Fluid	Mineral	Mineral amount (g)*	Mineral concentration (g/l)	Corresponding experiment
Baseline correction samples				
DIW	Quartz	0.015	5	Constant mass
DIW	Kaolinite	0.015	5	
DIW	Calcite	0.015	5	
DIW	Quartz	0.0058	1.923	Constant surface area
DIW	Kaolinite	0.00038	0.126	
DIW	Calcite	0.0163	5.435	

*Samples are prepared in plastic tubes and calculations are made for 30 ml of fluids

Finally, in accordance with aforementioned sample preparation and calculation procedures, the similar static adsorption experiment was carried out in SSW to investigate salinity influence on adsorption of NP on mineral surfaces.

4.6 Core flood experiments procedures

Core flood experiment starts from taking the core out from the laboratory oven to let it cool down in the air. Core dimensions (diameter, length) and “dry” weight are measured before the experiment. Then the core is saturated with required fluid in the vacuum saturation setup, and the “wet” weight is measured. Given the density of saturation fluid and the weight difference before and after saturation pore volume can be calculated according to Equation 4.4.

$$PV = \frac{W_{wet} - W_{dry}}{\rho_{s.f.}}, \quad (4.4)$$

where PV – pore volume (cm^3);

W_{wet} – core weight after saturation (g);

W_{dry} – core weight before saturation (g);

$\rho_{s.f.}$ – density of saturation fluid (g/cm^3).

Pore volume is required to calculate pump injection rate according to the planned experiment. After the core is wrapped with a teflon tape, plastic sleeve and rubber sleeve and put inside a core holder, it is ready for flooding. (Figure 4.30).

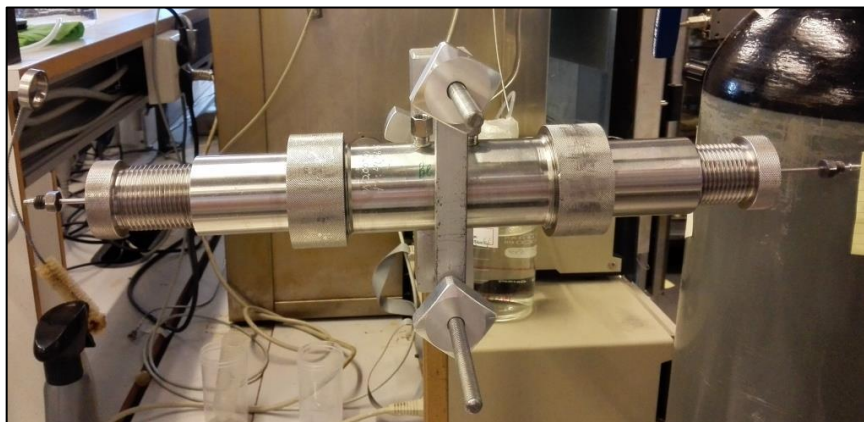


Figure 4.30 – Core inside core holder ready for experiment

Injection fluids are prepared according to planned injection sequence, placed in cylinders and connection lines of an experimental core flooding setup are cleaned and filled with the first fluid to be injected into the core.

When the setup is cleaned, the core holder is connected to it, and the flood can be started. Sampling can be carried out by auto sampling machine or manually with a burette, depending on the type of experiment.

4.6.1 Overview of core flood experiments

Several flood experiments were performed using Berea sandstone cores with almost equal dimensions. All core floods can be classified into two groups:

- Investigation of a transport behavior of NP in porous media;
- Enhanced oil recovery (EOR) experiment.

All NP transport behavior experiments were conducted at ambient temperature (about +25 °C), with back – pressure of around 10 bar and confinement pressure of 30 bar. The cores were saturated 100 % with DIW before the floods. Nanofluid suspensions were prepared at different concentrations with adding LiCl as a tracing element.

EOR experiment comprised three main stages:

- drainage flood;
- core aging in laboratory oven;
- primary and secondary oil recovery floods;

Drainage flood was carried out at ambient temperature (about +25 °C) but without using of a back-pressure. Model oil (n-Decane + 0.01M NN-DMDA) was utilized at this experiment stage. The core was initially saturated with brine. The main purpose here was establishing of irreducible water saturation S_{wirr} in a sandstone core.

Aging of the core was performed at 50°C replicating a temperature in a reservoir;

Brines (LSW, SSW) and nanofluids prepared in LSW and SSW were used in oil recovery core floods, performed at 70 °C temperature and 10 bars back-pressure to mimic reservoir conditions. The detailed list of experiments is presented in Table 4.9.

Table 4.9 – Core flood experiments overview

Core name	Length (cm)	Diameter (cm)	Pore volume (ml)	Porosity (%)	Flooding fluids sequence [injected volume]	Injection rate (PV/day)	Back pressure (bar)
NP transport behavior in porous media experiments							
“Berea 001”	9.0	3.78	20.73	20.53	1) Pre – Flush DIW [5 PV] 2) 4 g/l DP + 0.5M LiCl in DIW (pH = 5.29) [0.5 PV] 3) Post –Flush DIW [5 PV]	10	10
“Berea 002”	9.0	3.78	23.12	22.89	1) Pre – Flush DIW [6.25 PV] 2) 2 g/l DP + 0.1M LiCl in DIW (pH = 5.14) [0.5 PV] 3) Post – Flush DIW [13.5 PV]	10	10
“Berea 003”	9.0	3.78	20.75	20.54	1) Pre – Flush DIW [6.5 PV] 2) 1 g/l DP + 0.1M LiCl in DIW (pH = 6.01) [1.5 PV] 3) Post – Flush DIW [18 PV]	10	10
“Berea 004”	9.0	3.78	20.84	20.63	1) Pre – Flush DIW [6 PV] 2) DIW+0.1M LiCl+90µl 0.1M HCl (pH=5.05) [0.5PV] 3) Post – Flush DIW [18.5 PV]	10	10

Core name	Length (cm)	Diameter (cm)	Pore volume (ml)	Porosity (%)	Flooding fluids sequence [injected volume]	Injection rate (PV/day)	Back pressure (bar)
EOR experiments							
"Berea 005"	9.0	3.78	20.46	20.26	1) Drainage n - Decane + 0.01M NN-DMDA [50 PV]	1) 0.7-170	1) No
					2) Primary recovery LSW [8 PV] 3) Secondary recovery 1 g/l DP in LSW [8 PV]	2) 4, 16 3) 4, 16	2) 10 3) 10
"Berea 006"	9.0	3.78	20.6	20.40	1) Drainage n - Decane + 0.01M NN-DMDA [30 PV]	1) 0.7-150	1) No
					2) Primary recovery SSW [8 PV] 3) Secondary recovery 1 g/l DP in LSW [8 PV] 4) Post - Flush SSW [8 PV]	2) 4, 16 3) 4, 16 4) 16	2) 10 3) 10 4) 10

4.6.2 Description of NP transport behavior experiment

Single phase core floods from "Berea 001" to "Berea 004" were conducted to investigate transport behavior of NP in sandstone rock. DIW was used as an injection fluid at Pre - Flush and Post - Flush stages and each core was also saturated with DIW before flooding. Schematic diagram of the NP transport experiment setup is presented in Figure 4.31.

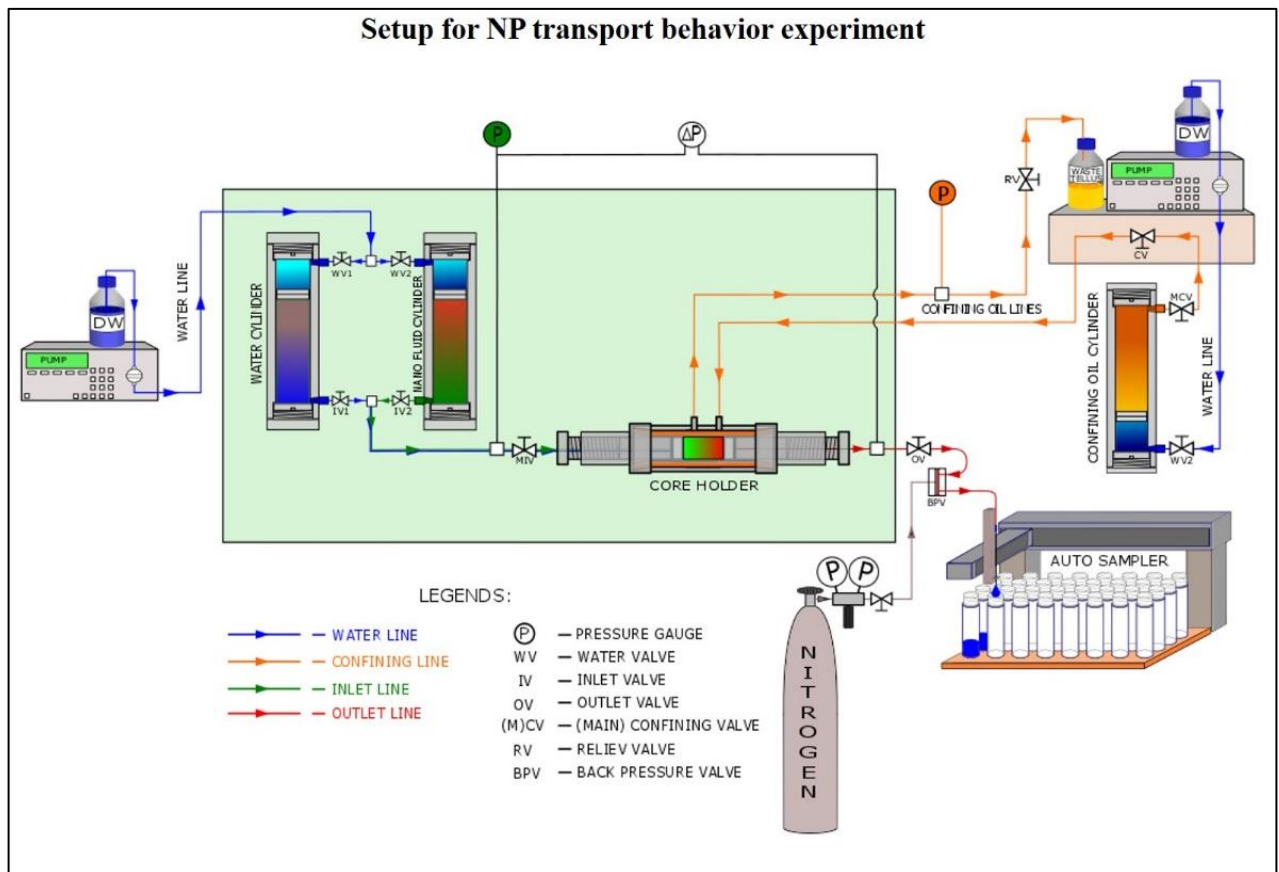


Figure 4.31 – Schematic diagram of NP transport experiment setup

Pressure difference across the core was recorded for all core flood experiments by using software "LabView™ 2012". The effluent was collected by auto sampler in glass vials where each four vials represented one pore volume of the core.

Effluent characterization (pH and ABS)

First of all, after a certain flood was finished, pH readings were taken for effluent samples by using “S220 SevenCompact™ pH/ion meter”. Before measurements, the apparatus was calibrated by buffer standard liquids with known pH. Measured values were averaged within each produced pore volume and plotted.

Then, another analysis was run on effluents. “UV-1700 spectrophotometer” was used to measure absorbance values for produced samples, which were chosen for investigation according to the acquired pH plot. The procedure samples treatment and measurements was very close to that of the static adsorption experiment. DIW was used as a reference fluid; samples were centrifuged @ 10 000 rpm for 10 min, filtered through a 0.2 µm micron filter and analyzed with a wavelength of 240 nm. For effluent of “Berea 0001” readings were taken without dilution, whereas in experiments “Berea 002” and “Berea 004” the samples were diluted in a ratio 1:1 with DIW before measurements.

Ion chromatography (IC analysis)

One of the most important analyses of the core flood experiment is an exchange and interaction of ions. Ion Chromatograph “Dionex Ics-5000+ DP” by “Thermo Scientific” was used to evaluate the presence of different ions in effluents. Core flood samples to be examined in apparatus were chosen according to pH readings, and before analysis, they were diluted in a ratio 1:500 with DIW by using “GX-271 Liquid handler” supplied by “Gilson Inc.” After dilution samples were collected and stored in small plastic vials (Figure 4.32) which were eventually put inside the IC – machine. SSW was used as a reference fluid to calculate concentrations of cations and anions in the samples.

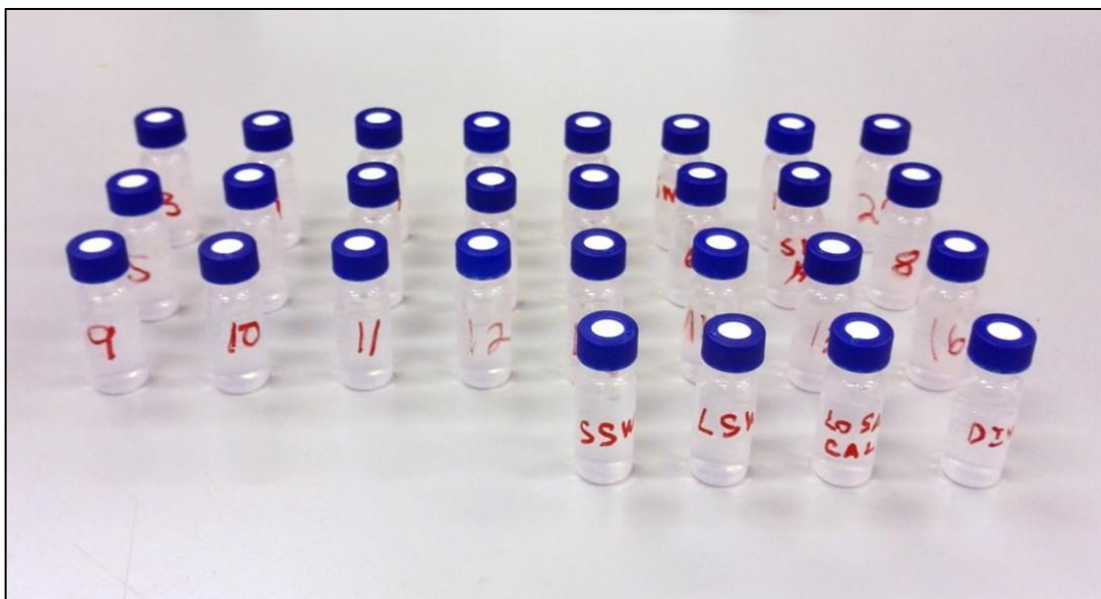


Figure 4.32 – Effluent samples prepared for IC analysis

SEM imaging of Berea sandstone core

A small Berea sandstone core was taken out from the laboratory oven and saturated in vacuum saturation setup with 1 g/l nanofluid prepared in DIW. It was kept submerged in nanofluid for 24 hours to allow NP interact with the rock surfaces, reaching a thermodynamic equilibrium. After that, the core was dried in vacuum and prepared for analysis in SEM. The core was cracked into pieces, and before investigation, one piece of it was coated with palladium (Figure 4.33).

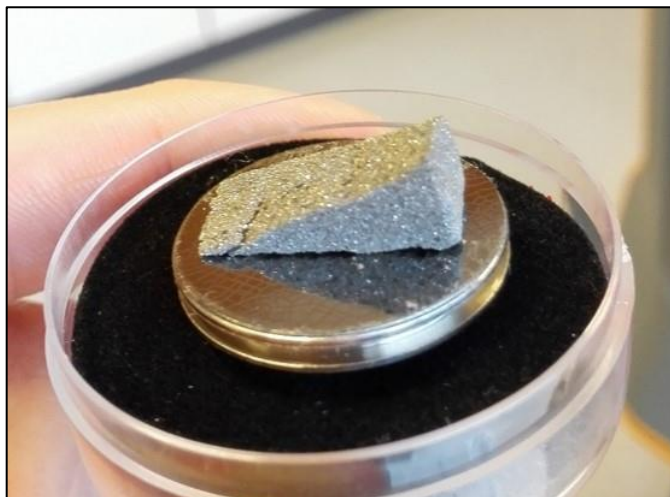


Figure 4.33 – Berea sandstone rock sample prepared for SEM imaging

SEM imaging of “Berea 003” effluent

Effluent sample from “Berea 003” core flood was prepared for SEM analysis by drying in vacuum and coating with palladium. The sample was subjected to chemical component analysis with X-ray spectroscopy system mounted in SEM at the University of Stavanger.

4.6.3 Description of EOR experiment

A Core flood experiments from “Berea 005” to “Berea 007” were conducted to investigate a potential use of NP in enhanced oil recovery (EOR). Both drainage and oil recovery floods were run in the same type of experimental setup which was used for NP transport behavior experiments, but instead of using autosampler, the effluent solution was collected in a burette and samples were taken manually.

The experiment started from a drainage core flood. Berea sandstone core was saturated 100% with SSW and flooded with a model oil (n-Decane + 0.01M NN-DMDA) until all the possible water production happened and irreducible water saturation in the core was established. Pump injection rate varied starting from extremely low (0.01 ml/min) up to high rates (2-3 ml/min). Produced oil was periodically removed from the top of the burette with a syringe while water accumulated on the bottom.

After irreducible water saturation was determined, the core was retrieved from the core holder, weighed and prepared for aging. Two plastic balls were put on the bottom of an aging cell and the core was placed on the top of them. Then the cell was filled with the same fluid that was used for drainage flooding (n-Decane + 0.01M NN-DMDA) and locked from the upper side with applying of a rubber O-ring for better sealing. Finally, the cell is marked according to the name of the core and placed inside a small laboratory oven. All aforementioned equipment involved in core aging procedures in presented in Figure 4.34.

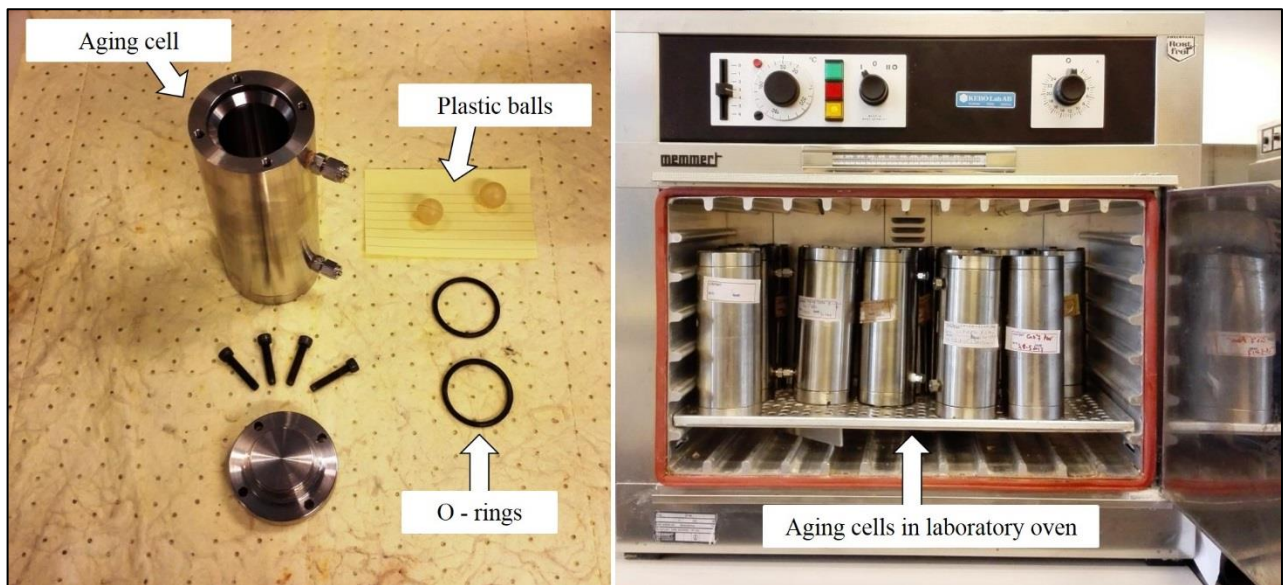


Figure 4.34 – Equipment for core aging

At last, oil recovery flood was conducted after the aging process was finished. Oil was displaced from the core by various injection fluids. SSW and LSW, as well as nanofluids prepared in brines, were utilized. Flood was run until the ultimate recovery was reached and residual oil saturation in the core was established.

Inlet pressure and the pressure difference between inlet and outlet of the core was recorded by using software “LabView™ 2012”. Cumulative oil produced was estimated by the volume of oil column in the burette. Water accumulated on the bottom was manually collected for further analysis in glass vials, where one vial represented a quarter of the core PV produced.

Effluent characterization (pH and ABS)

Readings of pH were taken with “S220 SevenCompact™ pH/ion meter” for every effluent sample at once after water was produced and collected in glass vials.

Absorbance values were acquired for the effluent samples by using “UV - 1700 spectrophotometer”.

Ion chromatography (IC analysis)

Ion Chromatograph “Dionex Ics-5000+ DP” by “Thermo Scientific” was used to investigate the ion concentration profiles for effluent samples. Before analysis, EOR core flood samples were diluted in a ratio 1:1000 with DIW by using “GX-271 Liquid handler”.

5 Results and Discussion

This chapter of the Master's thesis comprises all the results of conducted experiments in the form of tables and plots with detailed interpretation and elaborate discussions.

5.1 Nanofluid characterization

The first experimental step was a characterization of the nanofluid “DP9711” by determining the size of dispersed NP and zeta-potential of the fluid. Table 5.1 presents the results of particle size and zeta-potential measurements for all prepared samples.

Table 5.1 – Particle size and zeta-potential measurements for nanofluid samples

Concentration (g/l)	Dispersing fluid	Temperature, T (°C)	Average size, z-avg (nm)	PDI	Zeta-potential, ZP (mV)	pH
1	DIW	25	37.52	0.090	-30.73	5.92
2	DIW	25	36.95	0.077	N/A	N/A
4	DIW	25	35.29	0.106	N/A	N/A
1	DIW	50	38.57	0.078	N/A	N/A
1	DIW	80	39.40	0.083	N/A	N/A
1	LSW	25	37.91	0.067	-12.13	7.21
1	LSW	50	38.18	0.056	N/A	N/A
1	LSW	80	38.70	0.045	N/A	N/A
1	SSW	25	56.35	0.105	-6.40	8.17
1	SSW	50	57.54	0.110	N/A	N/A
1	SSW	80	88.11	0.104	N/A	N/A

As we can see from Table 5.1, the particle diameter of 1 g/l nanofluid in DIW was averaged to 37.52 nm. Measurements for higher concentrations were also successful. At 4 g/l concentration average diameter of NP was determined as 35.29 nm, so with increasing concentration of NP in suspension slight decrease in average size readings was observed.

Ionic strength change (DIW – LSW – SSW) demonstrated enlargement in measured average diameter of nanoparticles. It increased, for example, from 37.52 nm for 1 g/l nanofluid in DIW, to 37.91 nm in LSW and noticeably up to 56.35 nm in SSW at a constant temperature of 25° C. Particle size distribution intensity plot for these samples is presented in Figure 5.1.

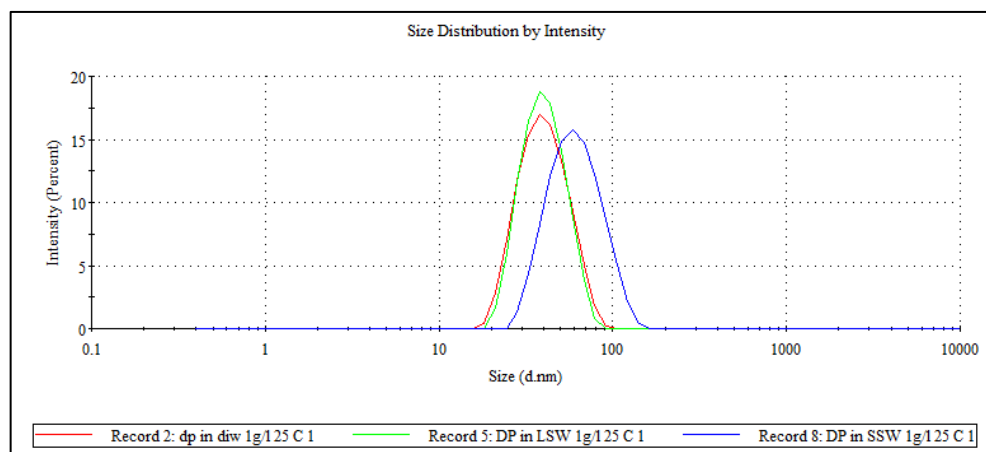


Figure 5.1 – Size distributions for 1g/l nanofluid in DIW, LSW and SSW

According to the results for 1 g/l DP in DIW sample, the temperature rise led to insignificant increase of average NP size up to 38.57 nm at 50°C and 39.40 nm at 80°C. Small elevation was observed also for nanofluid prepared in LSW (from 37.91 at 25° C to 38.70 at 80° C). The highest effect of temperature increase was noticed for nanofluid sample in SSW since NP average diameter readings changed from 56.35 nm at 25°C up to 88.11 nm at 80°C.

Zeta-potential measurements showed the following tendency: with an increase of salinity zeta-potential values move toward zero, becoming less negative. So, zeta-potential for 1 g/l DP in DIW is equal to -30.73 mV but for SSW this value changes to -6.40 mV. Salinity increase causes reduction of the zeta-potential because the presence of ions in SSW leads to shrinking of the double layer. Besides, salinity rise is reflected in an increase of measured pH values.

Acquired results show that temperature variations do not lead to NP aggregation and indicate a good stability of nanofluid prepared in DIW, LSW, and SSW. Harsh conditions (high salinity and temperature) affect NP size readings but particles are still characterized by nanoscale. It should be noted that polydispersity index (PDI) for all the samples measured was not higher than 0.11 and these values met the criteria specified in ISO standards 13321:1996E and ISO 22412:2008 which indicates that samples were suitable for use in dynamic light scattering measurements [39].

Nanofluid “DP9711” was also used for imaging with scanning electron microscope. Acquired image of 1 g/l DP prepared in DIW and dried under vacuum is presented in Figure 5.2.

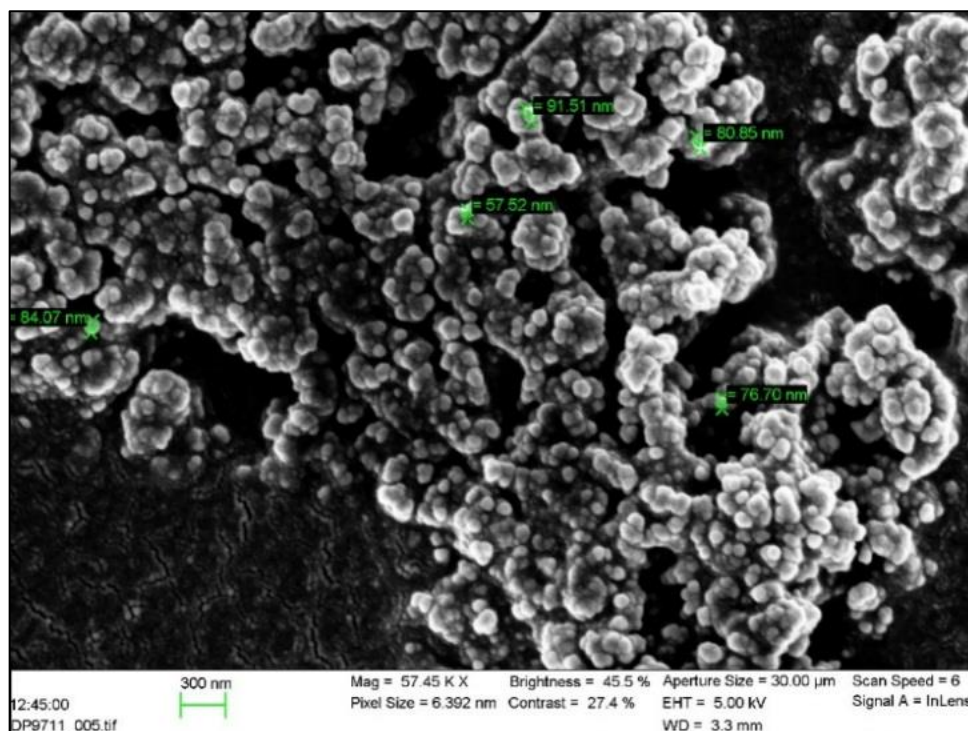


Figure 5.2 – SEM image of nanofluid “DP9711”

As we can see from Figure 5.2 the sizes of NP being analyzed are less than 100 nm. It can be observed that some NP formed clusters, but this happened because of the process of drying of the sample before analysis with SEM.

5.2 Zeta-potential measurements on mineral powders

Zeta-potential test was carried out for three types of mineral powder suspended in DIW. The list of samples and corresponding experimental results are presented in Table 5.2.

Table 5.2 – Zeta-potential measurements of mineral powder suspensions in DIW

Sample	Zeta-potential (mV)	pH
Berea (10 g/l) in DIW	-29.53	9.99
Quartz (10 g/l) in DIW	-14.67	6.18
Quartz (20 g/l) in DIW	-15.77	6.68
Kaolinite (10 g/l) in DIW	-15.89	6.92
Kaolinite (20 g/l) in DIW	-16.66	7.31

Table 5.2 shows that zeta-potential is negative for all the samples. Berea powder suspension at 10 g/l concentration in DIW has the most negative value that equals to -29.53 mV. Quartz and kaolinite have close values at 10 g/l concentration in DIW (-14.67 mv and -15.89 mV respectively). When the concentration of quartz and kaolinite minerals is doubled, the measured values become slightly more negative. Besides, zeta-potential for kaolinite samples is slightly more negative than that for quartz at both powder concentrations.

So, zeta-potential was determined as strongly negative both at 10 g/l and 20 g/l mineral concentrations. At the same time, it was shown during nanofluid characterization in the previous section that zeta-potential of nanofluid suspension is also negative even in high salinity environment (up to -6.40 mV for 1 g/l NP concentration).

5.3 Static adsorption experiments in DIW

Adsorption behavior of NP on mineral surfaces was investigated in this set of experiments. Measured absorbance readings for nanofluid and mineral samples in DIW are presented in Table 5.3.

Table 5.3 – Absorbance readings for nanofluid samples in DIW

Sample	Absorbance (Abs)
Constant mass samples	
1 g/l in DIW + 0.15 g of Quartz	0.1265
0.5 g/l in DIW + 0.15 g of Quartz	0.0652
1 g/l in DIW + 0.15 g of Kaolinite	0.1155
0.5 g/l in DIW + 0.15 g of Kaolinite	0.0607
1 g/l in DIW + 0.15 g of Calcite	0.0895
0.5 g/l in DIW + 0.15 g of Calcite	0.0481
Constant surface area samples	
1 g/l in DIW + 0.058 g of Quartz	0.1198
0.5 g/l in DIW + 0.058 g of Quartz	0.0695
1 g/l in DIW + 0.0038 g of Kaolinite	0.1317
0.5 g/l in DIW + 0.0038 g of Kaolinite	0.0702
1 g/l in DIW + 0.163 g of Calcite	0.1190
0.5 g/l in DIW + 0.163 g of Calcite	0.0593
Extra points samples	
1 g/l in DIW + 0.015 g of Quartz	0.1312
0.5 g/l in DIW + 0.03 g of Quartz	0.1287
1 g/l in DIW + 0.06 g of Kaolinite	0.1233
1 g/l in DIW + 0.03 g of Calcite	0.0922
0.5 g/l in DIW + 0.09 g of Calcite	0.0919

Absorbance values for mineral baseline correction samples in DIW are presented in Table 5.4.

Table 5.4 – Absorbance readings for mineral baseline correction samples in DIW

Sample	Absorbance (Abs)
Baseline correction samples (constant mass)	
DIW + 0.15 g of Quartz	0.0049
DIW + 0.15 g of Kaolinite	0.0057
DIW + 0.15 g of Calcite	0.0035
Baseline correction samples (constant surface area)	
DIW + 0.058 g of Quartz	0.0067
DIW + 0.0038 g of Kaolinite	0.0057
DIW + 0.163 g of Calcite	0.0055
Baseline correction samples (extra points)	
DIW + 0.015 g of Quartz	0.0005
DIW + 0.03 g of Quartz	0.0022
DIW + 0.06 g of Kaolinite	0.0026
DIW + 0.03 g of Calcite	0.0021
DIW + 0.09 g of Calcite	0.0025

Specific adsorption of nanoparticles (mg of NP /m² of mineral) on each mineral powder was calculated for all samples by using a calibration line (Figure 3.29) and absorbance readings. The results were plotted against the mass of mineral per unit mass of NP (Figure 5.3).

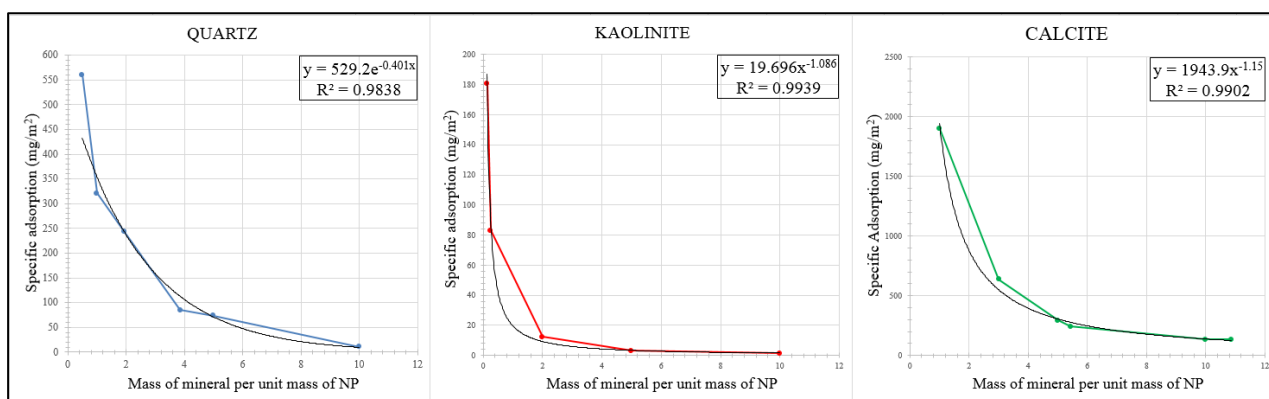


Figure 5.3 – Specific adsorption of NP on minerals in DIW

As we can see from Figure 5.3, the same behavior is observed for all three minerals. After applying trendlines to calculated values, it was observed that for kaolinite and calcite powder the specific adsorption variation depending on concentrations ratio between mineral and nanoparticles show a good match with a trendline of power type, whereas the specific adsorption for quartz mineral follows the exponential trend. It is clear that in all three cases specific adsorption increases when the mass of mineral per unit mass of NP decreases. Since specific adsorption values are quite different in magnitude, these three plots were combined and presented in Figure 5.4 for better comparison.

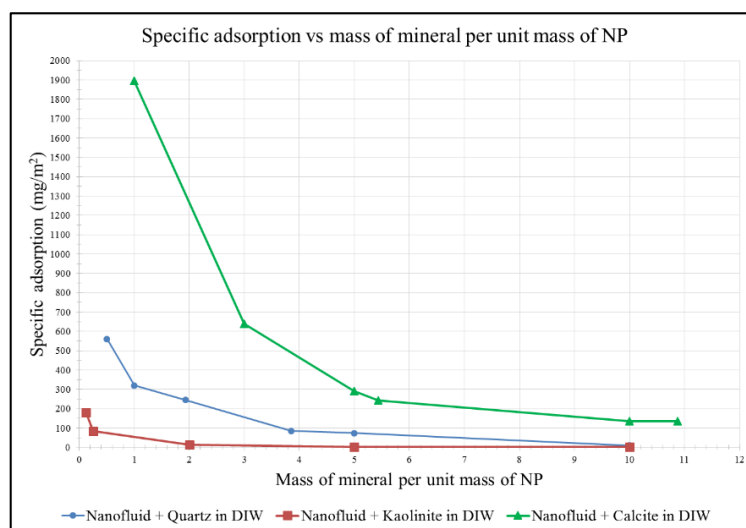


Figure 5.4 – Combination of specific adsorption curves for minerals in DIW

Figure 5.4 demonstrates the difference between specific adsorption of NP measured and calculated for different minerals. The highest specific adsorption is observed for calcite mineral powder, while kaolinite demonstrates the weakest tendency for adsorption of NP. The decrease in the surface area of mineral most likely favors NP adsorption. The importance of specific surface area and its influence on NP retention was observed by Caldelas, Murphy et al. [43].

More than that, measured zeta-potentials for quartz and kaolinite powders in DIW are negative, and zeta-potential of nanofluid prepared in DIW is strongly negative, which may indicate that repulsion forces most likely influence adsorption on these two minerals.

As a sensitivity test for NP and mineral concentrations, another run of the experiment was carried out but this time all concentrations were decreased ten times, and the mass of mineral per unit mass of NP was preserved. Samples with ten times reduced concentrations were used for absorbance measurements using “UV-1700 spectrophotometer” but it was possible to repeat only constant mass and constant surface area steps of the experiment due to reduced sensitivity of the machine at very low concentrations. Measured absorbance readings are presented in Table 5.5.

Table 5.5 – Measurements for concentration sensitivity adsorption experiment in DIW

Sample	Absorbance (Abs)
Constant mass samples	
0.1 g/l in DIW + 0.015 g of Quartz	0.0165
0.05 g/l in DIW + 0.015 g of Quartz	0.0089
0.1 g/l in DIW + 0.015 g of Kaolinite	0.0148
0.05 g/l in DIW + 0.015 g of Kaolinite	0.0088
0.1 g/l in DIW + 0.015 g of Calcite	0.0129
0.05 g/l in DIW + 0.015 g of Calcite	0.0076
Constant surface area samples	
0.1 g/l in DIW + 0.0058 g of Quartz	0.0160
0.05 g/l in DIW + 0.0058 g of Quartz	0.0090
0.1 g/l in DIW + 0.00038 g of Kaolinite	0.0149
0.05 g/l in DIW + 0.00038 g of Kaolinite	0.0089
0.1 g/l in DIW + 0.0163 g of Calcite	0.0106
0.05 g/l in DIW + 0.0163 g of Calcite	0.0069

Absorbance readings for corresponding baseline correction samples in DIW are shown in Table 5.6.

Table 5.6 – Absorbance readings of baseline correction samples for concentration sensitivity experiment in DIW

Sample	Absorbance (Abs)
Baseline correction samples (constant mass)	
DIW + 0.015 g of Quartz	0.0010
DIW + 0.015 g of Kaolinite	0.0011
DIW + 0.015 g of Calcite	0.0016
Baseline correction samples (constant surface area)	
DIW + 0.0058 g of Quartz	0.0010
DIW + 0.00038 g of Kaolinite	0.0011
DIW + 0.0163 g of Calcite	0.0016

Specific adsorption of nanoparticles (mg of NP /m² of mineral) on each mineral powder was calculated for all samples by using a calibration line and absorbance readings. The results were plotted against the mass of mineral per unit mass of NP together with the previous results (Figure 5.5).

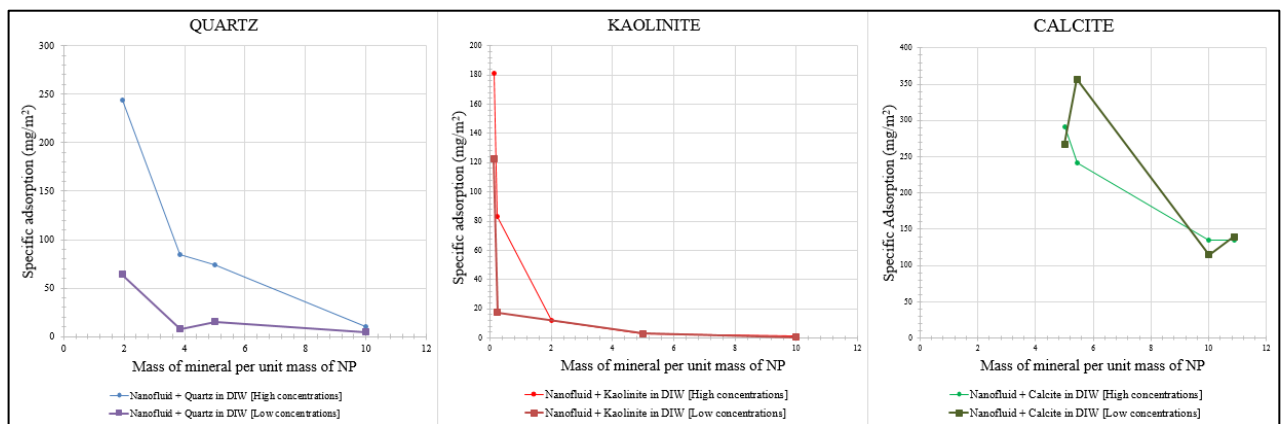


Figure 5.5 – Specific adsorption of NP on minerals in DIW (original and reduced concentrations)

Quartz shows a decrease in specific adsorption at proportionally reduced mineral and NP concentrations. It is noted that quartz powder more sensitive to concentrations change and the difference between two experiments becomes higher as the mass of mineral per unit mass of NP decreases. This is also true for kaolinite mineral – specific adsorption values decreased especially at lower mineral to NP concentrations ratio. As for calcite powder, the huge difference in specific adsorption is not observed in the plot. Probably the difference would be distinguishable at very low ratios of mineral to NP concentrations, but such small values cannot be measured by the apparatus used. The expected tendencies may be examined only by combining plots and applying trendlines to them so that we could observe similar behaviors of the specific adsorption curves as in the former experiment (Figure 5.6).

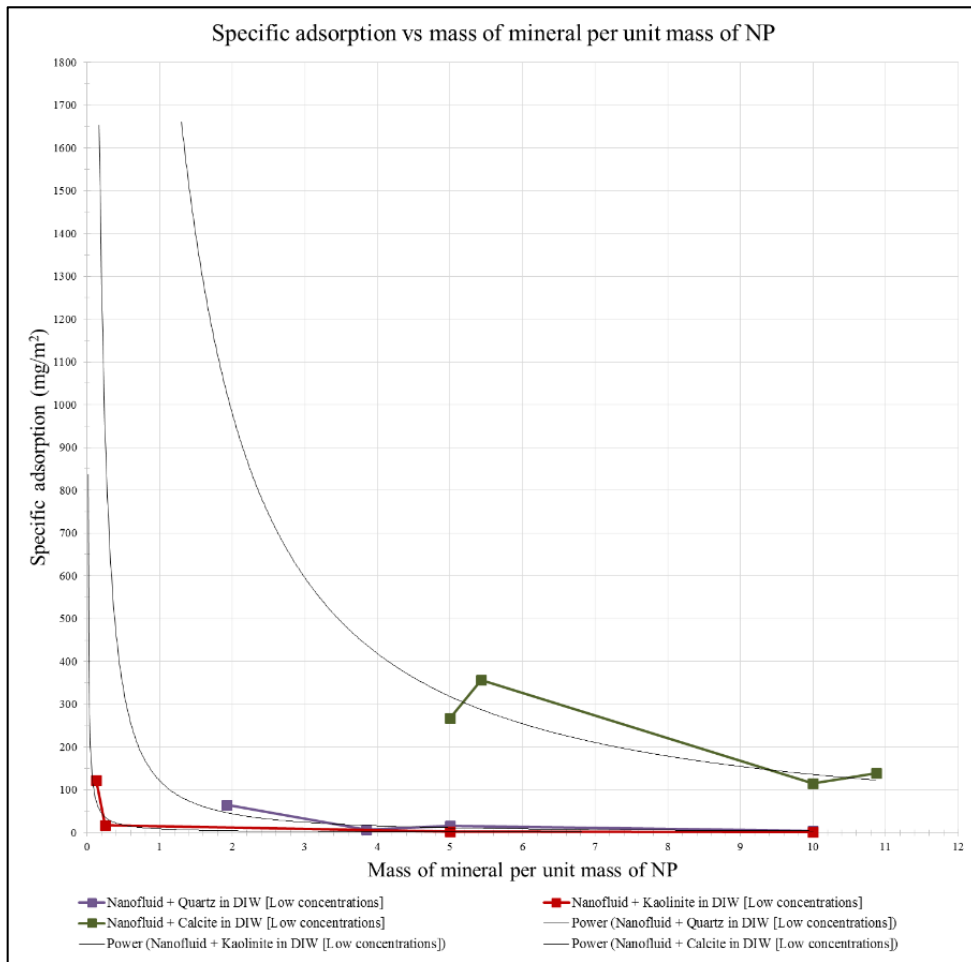


Figure 5.6 – Combination of specific adsorption curves for minerals in DIW with reduced concentration

5.4 Static adsorption experiments in SSW

To investigate the effect of high salinity when NP adsorb on the mineral surface, synthetic sea water (SSW) was used in a repetition run of the static adsorption experiment. The experiment implied replication of the previous experiment (at higher NP concentration), but the differences are that “DP9711” nanofluid was prepared at concentration 1 g/l in SSW and SSW was utilized as a reference fluid in absorbance measurements. Calibration line was built for nanofluid in SSW (Figure 5.7).

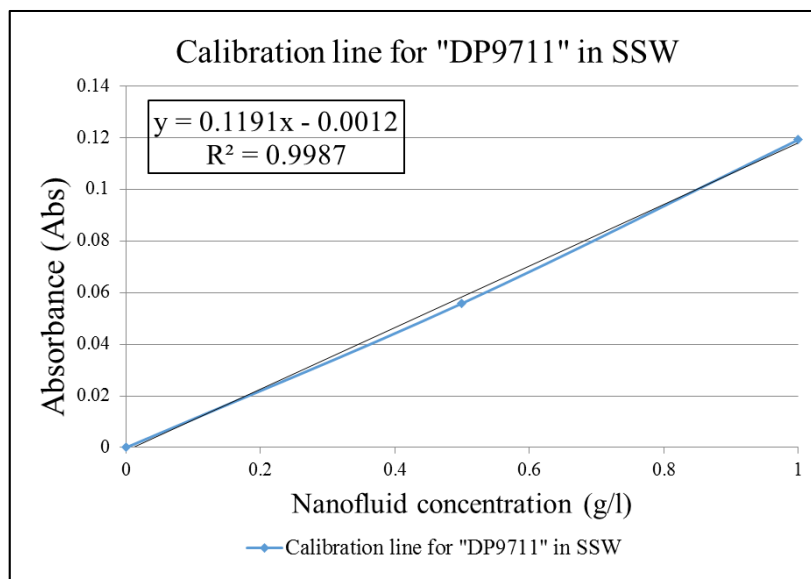


Figure 5.7 – Calibration line for “DP9711” nanofluid prepared in SSW

Table 5.7 and Table 5.8 contain the results of the absorbance measurements for nanofluid and baseline correction samples prepared in SSW.

Table 5.7 – Absorbance readings for nanofluid samples in SSW

Sample	Absorbance (Abs)
Constant mass samples	
1 g/l in SSW + 0.15 g of Quartz	0.0802
0.5 g/l in SSW + 0.15 g of Quartz	0.0433
1 g/l in SSW + 0.15 g of Kaolinite	0.0784
0.5 g/l in SSW + 0.15 g of Kaolinite	0.0386
1 g/l in SSW + 0.15 g of Calcite	0.0867
0.5 g/l in SSW + 0.15 g of Calcite	0.0474
Constant surface area samples	
1 g/l in SSW + 0.058 g of Quartz	0.0811
0.5 g/l in SSW + 0.058 g of Quartz	0.0376
1 g/l in SSW + 0.0038 g of Kaolinite	0.0669
0.5 g/l in SSW + 0.0038 g of Kaolinite	0.0263
1 g/l in SSW + 0.163 g of Calcite	0.074
0.5 g/l in SSW + 0.163 g of Calcite	0.0328
Extra points samples	
1 g/l in SSW + 0.015 g of Quartz	0.0758
0.5 g/l in SSW + 0.03 g of Quartz	0.0800
1 g/l in SSW + 0.06 g of Kaolinite	0.0715
1 g/l in SSW + 0.03 g of Calcite	0.0815
0.5 g/l in SSW + 0.09 g of Calcite	0.0820

Table 5.8 – Absorbance readings for mineral baseline correction samples in SSW

Sample	Absorbance (Abs)
Baseline correction samples (constant mass)	
SSW + 0.15 g of Quartz	0.0186
SSW + 0.15 g of Kaolinite	0.0143
SSW + 0.15 g of Calcite	0.0156
Baseline correction samples (constant surface area)	
SSW + 0.058 g of Quartz	0.0077
SSW + 0.0038 g of Kaolinite	0.0057
SSW + 0.163 g of Calcite	0.0115
Baseline correction samples (extra points)	
SSW + 0.015 g of Quartz	0.0134
SSW + 0.03 g of Quartz	0.0171
SSW + 0.06 g of Kaolinite	0.0178
SSW + 0.03 g of Calcite	0.0120
SSW + 0.09 g of Calcite	0.0150

Specific adsorption of nanoparticles (mg of NP /m² of mineral) on each mineral powder was calculated for all samples by using absorbance readings and calibration line for nanofluid prepared in SSW. The results were plotted against the mass of mineral per unit mass of NP with applying trendlines (Figure 5.8).

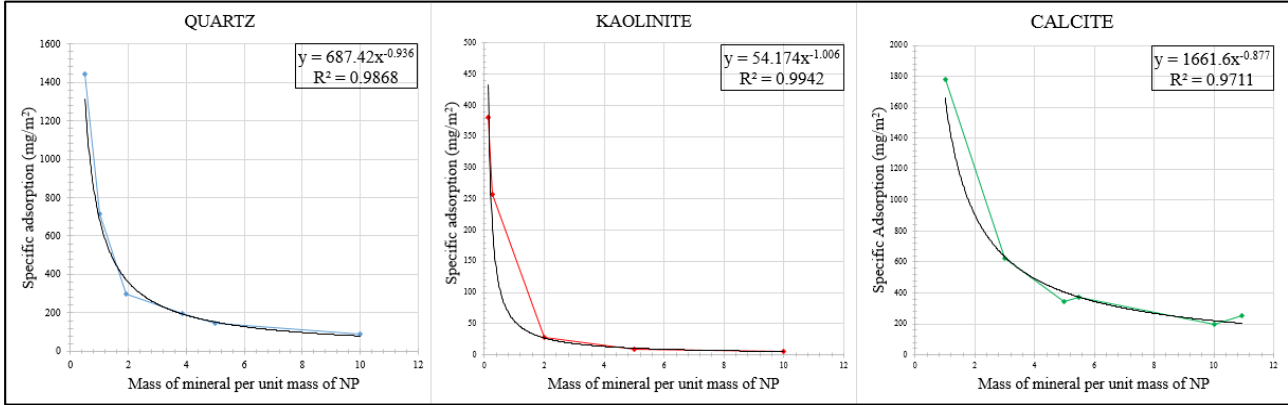


Figure 5.8 – Specific adsorption of NP on minerals in SSW

The combination of NP adsorption curves for three minerals in SSW is presented in Figure 5.9.

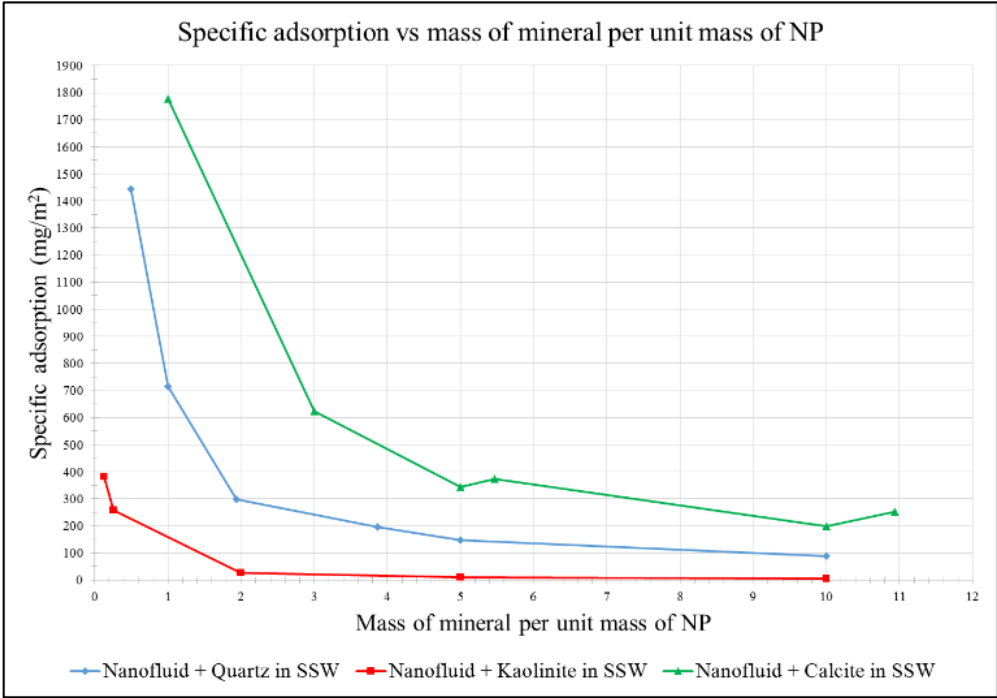


Figure 5.9 – Combination of specific adsorption curves on minerals in SSW

As we can see from Figure 5.9 the tendencies observed in experiment with DIW are preserved in SSW experiment. Calcite mineral shows the highest adsorption, kaolinite demonstrates very poor adsorption potential. Specific adsorption in quartz, in turn, is expected to have intermediate values between calcite and kaolinite powders. This preferential behavior of NP towards quartz mineral as compared to kaolinite is of specific interest. Previous work performed in our lab looked at the relative adsorption of unmodified silica on quartz and kaolinite and found the same preferential behavior. This was confirmed by both static adsorption experiment and analysis with SEM. SEM imaging carried out during this study also confirmed similar behavior for this more stable silica nanofluid (“DP 9711”).

The differences in specific adsorption for three minerals in DIW and SSW were compared and comparison plots are presented in Figure 5.10.

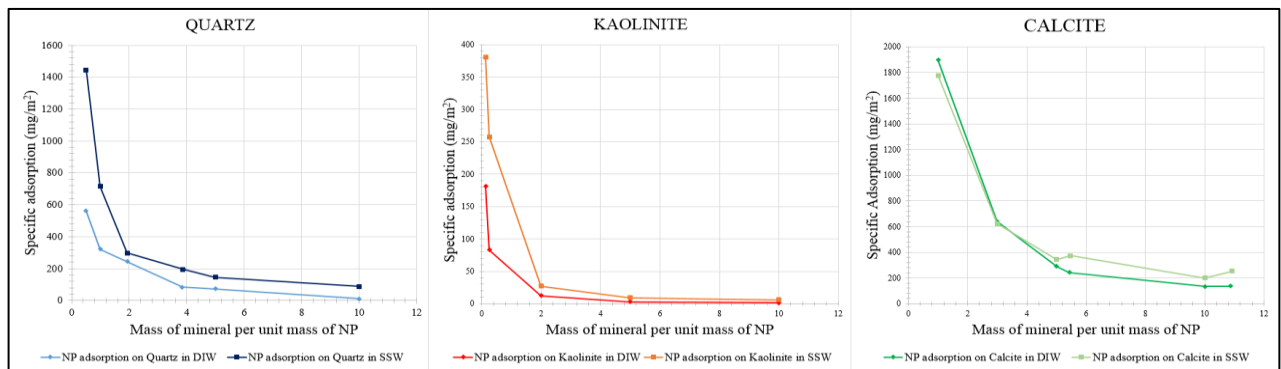


Figure 5.10 – Comparison of specific adsorption of NP on minerals in DIW and SSW

It is clear from the plot above that increased salinity favors specific adsorption of nanoparticles on quartz and kaolinite minerals. More than that, the less the ratio between the mass of mineral and unit mass of NP the greater the specific adsorption value in SSW. It was documented by Caldelas and Murphy et al. that increasing the salinity of the medium has a great influence on adsorption of nanoparticles [43]. They showed that lowered repulsion between NP in more saline environment may enhance attraction between NP and mineral surfaces. This is in agreement with our investigations which show that zeta-potential is definitely becomes less negative when salinity is increased, favoring attraction forces. That may explain higher specific adsorption values observed in high salinity static adsorption experiment compared to experiment in DIW.

For calcite powder, the similar behavior is not observed at small mineral to NP ratios, but for ratios more than 5, SSW experiment demonstrates an increase in specific adsorption.

5.5 Experiments on the transport behavior of NP in porous medium

5.5.1 Core flood with “Berea 001”

Core flood experiment was conducted with sandstone core “Berea 001” at injection rate 10 pore volumes per day (pump injection rate 0.15 ml / min). Deionized water (DIW) was injected during the pre - flush period of 5 PV. After that a nanofluid slug with tracing chemical (4 g/l DP + 0.5M LiCl in DIW, where DP stands for nanofluid “DP 9711”) was introduced in total volume of 0.5 PV. The slug was followed by the post - flush with DIW for 5 PV. Injection stages are shown in Figure 5.11.

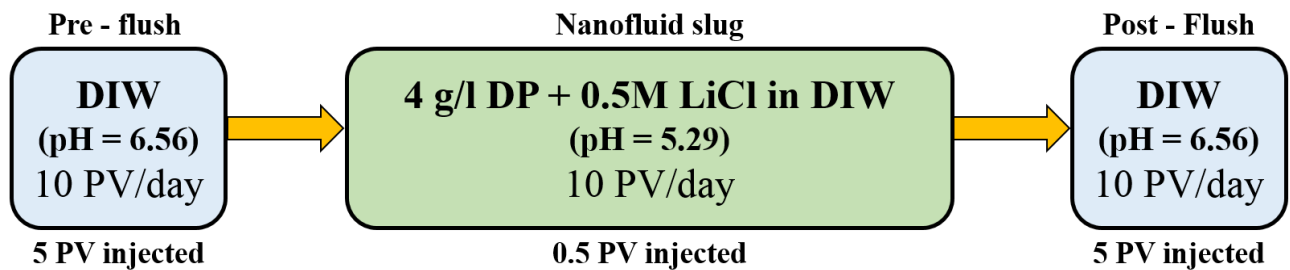


Figure 5.11 – Injection sequence for “Berea 001”

Values of pH for effluent samples were plotted against PV produced. Results were averaged within each PV and presented in Figure 5.12.

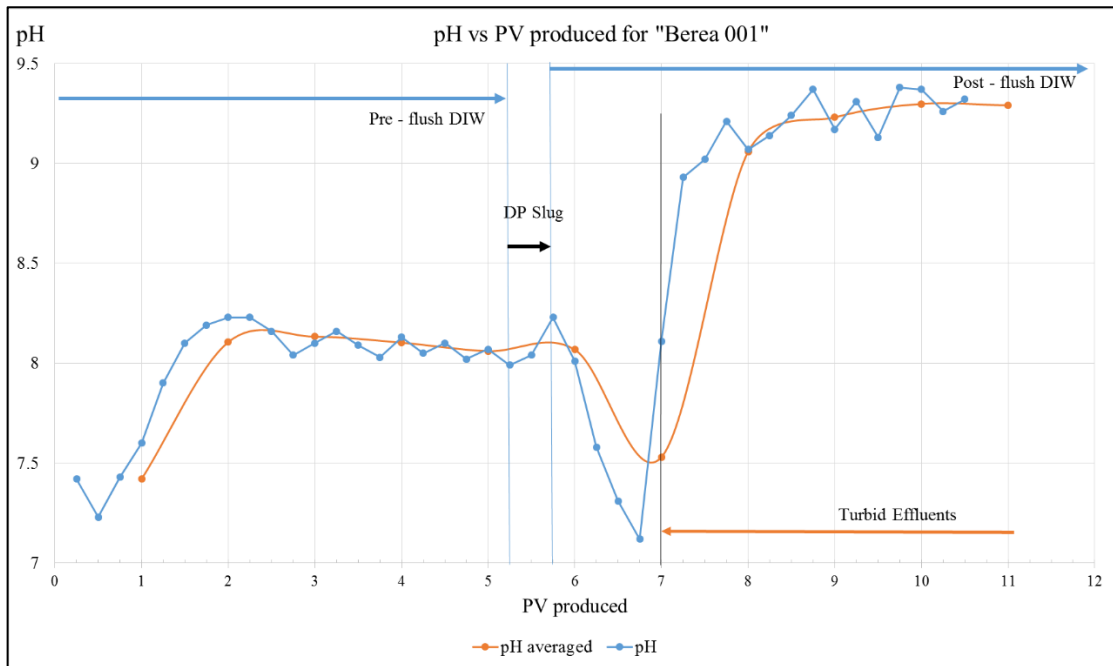


Figure 5.12 – pH values for Berea 001

From Figure 5.12 we can observe comparatively constant pH values around 8.2 during the pre-flush period (PV 2 – PV 5 produced), but 1 PV after DP slug injection (PV 6.25 produced) there is a rapid decrease in pH down to 7.3. After one more PV is produced (PV 7) we can see a huge increase in pH up to 9.3. Exactly at this time, turbid fluid starts to appear in the effluent which may be connected with an enormous production of kaolinite mineral, which was confirmed by SEM imaging.

Figure 5.13 shows recorded pressure drop between inlet and outlet of the core at all flooding steps.

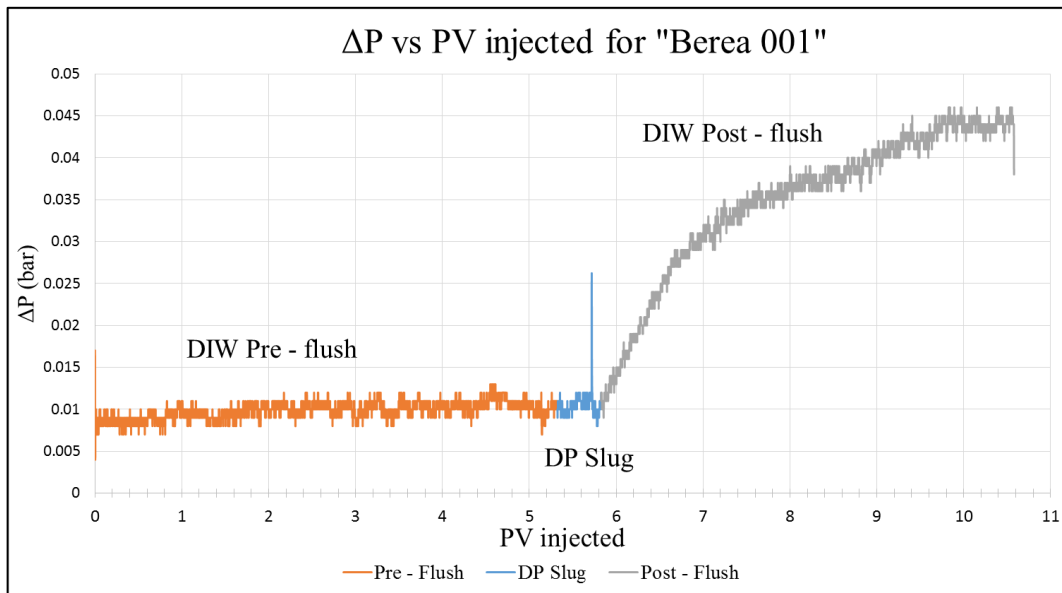


Figure 5.13 – ΔP vs PV injected for "Berea 001"

As we can see from Figure 5.13, pressure difference between inlet and outlet of the core remains constant within the range of 0.007 – 0.013 bars during pre – flush and DP injection stages. After the post – flush period is started there occurs a gradual pressure increase up to 0.045 bars as the more amount of deionized water injected into the core. Pressure difference increase may indicate blockage of the rock pore throats by dissolved and mobilized fines since the production of turbid effluent with a large amount of mineral particles (kaolinite) is observed at post – flush period.

Absorbance measurements were taken for “Berea 001” effluents from DP slug and post – flush stages without any dilution of the samples. The detailed procedure of absorbance measurements was discussed in the previous chapter. The results were plotted against PV produced (Figure 5.14).

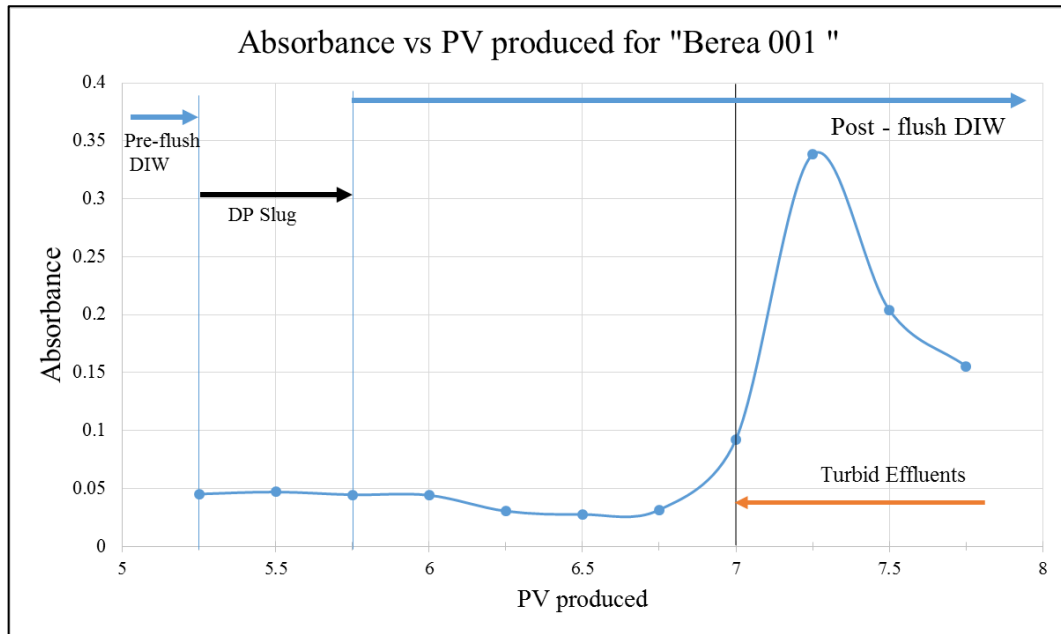


Figure 5.14 – Absorbance measurements for “Berea 001” effluent samples

During DP slug injection stage absorbance values are very close to 0.05 units. Half PV later there can be seen an insignificant decrease and starting from PV 7 when the production of turbid fluid started the measured absorbance rapidly increases having the highest value of 0.3383 at PV 7.25 and starts to decrease again.

Measured values of absorbance were utilized further in an attempt to evaluate the amount of nanoparticles present in effluent samples. Calibration line was built by preparing the nanofluid used for flood at different concentrations in DIW and further applied to calculate NP concentration. Absorbance values measured for the nanofluid slug stage were assumed to be a universal baseline for all later measured points because it is natural to expect some delay in production of NP from the beginning of nanofluid injection to the core. Taking into consideration this assumption, calculated NP concentration can be plotted as shown in Figure 5.15.

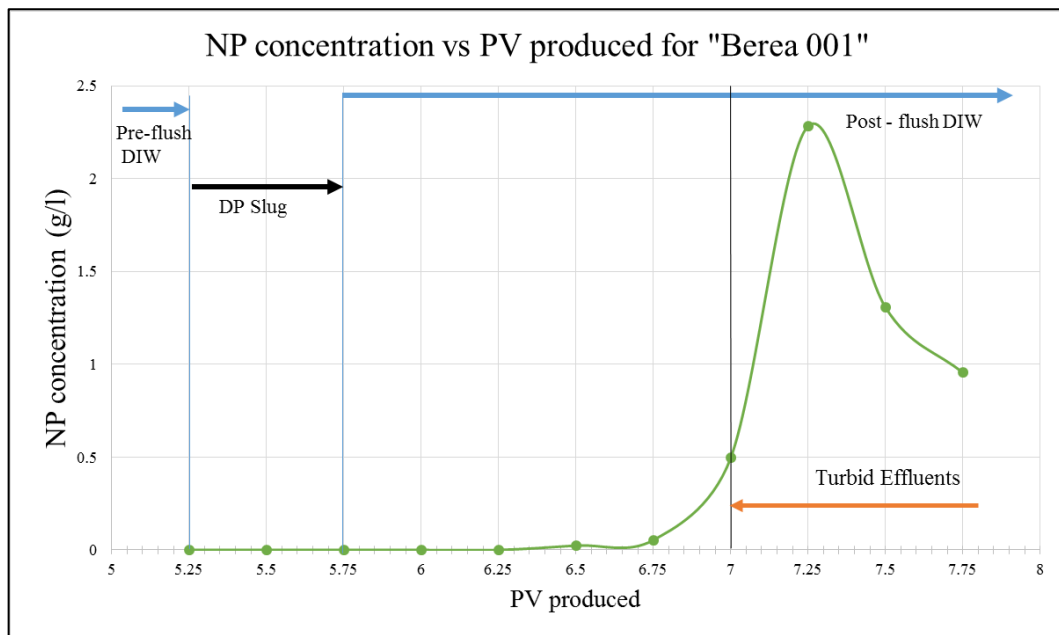


Figure 5.15 – Calculated NP concentration for “Berea 001” effluent samples

Figure 5.15 shows that calculated values are obviously too high and unlikely represent only NP produced from the core. Hence, it was found out that plotted nanoparticles concentration curve probably does not reflect the real NP concentration due to the presence of fine particles in the effluent, small enough to go through the 0.2 μm micron filter and affect absorbance measurements. We can also conclude that this contribution is not linear with time which makes it incorrect to apply a single baseline correction for the whole core flood samples. Starting from PV 6.25 we possibly began producing injected nanofluid but at the same time minerals presence in samples may change, especially after the PV 7 where fines were observed in the effluent.

5.5.2 Core flood with “Berea 002”

In order to confirm that production of turbid effluent was not accidental in the previous experiment, “Berea 002” core flood was conducted as a repetition of “Berea 001” at the same injection rate of 10 pore volumes per day (pump injection rate 0.16 ml / min), confinement pressure of 30 bar and back-pressure close to 10 bar but the concentrations of nanofluid and tracing chemical were reduced.

Deionized water was injected during the pre-flush period of 6.25 PV. Then a nanofluid slug with lower NP concentration and tracing chemical (2 g/l DP + 0.1M LiCl in DIW) was introduced in a total volume of 0.5 PV. The slug was followed by the post - flush with DIW injection for 13.5 PV. Stages of injection are presented in Figure 5.16.

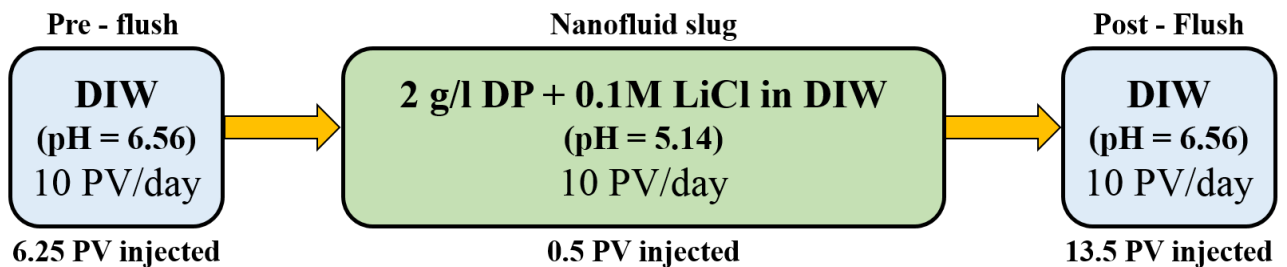


Figure 5.16 – Injection sequence for “Berea 002”

Effluent pH values were measured, averaged within each produced PV and presented in Figure 5.17.

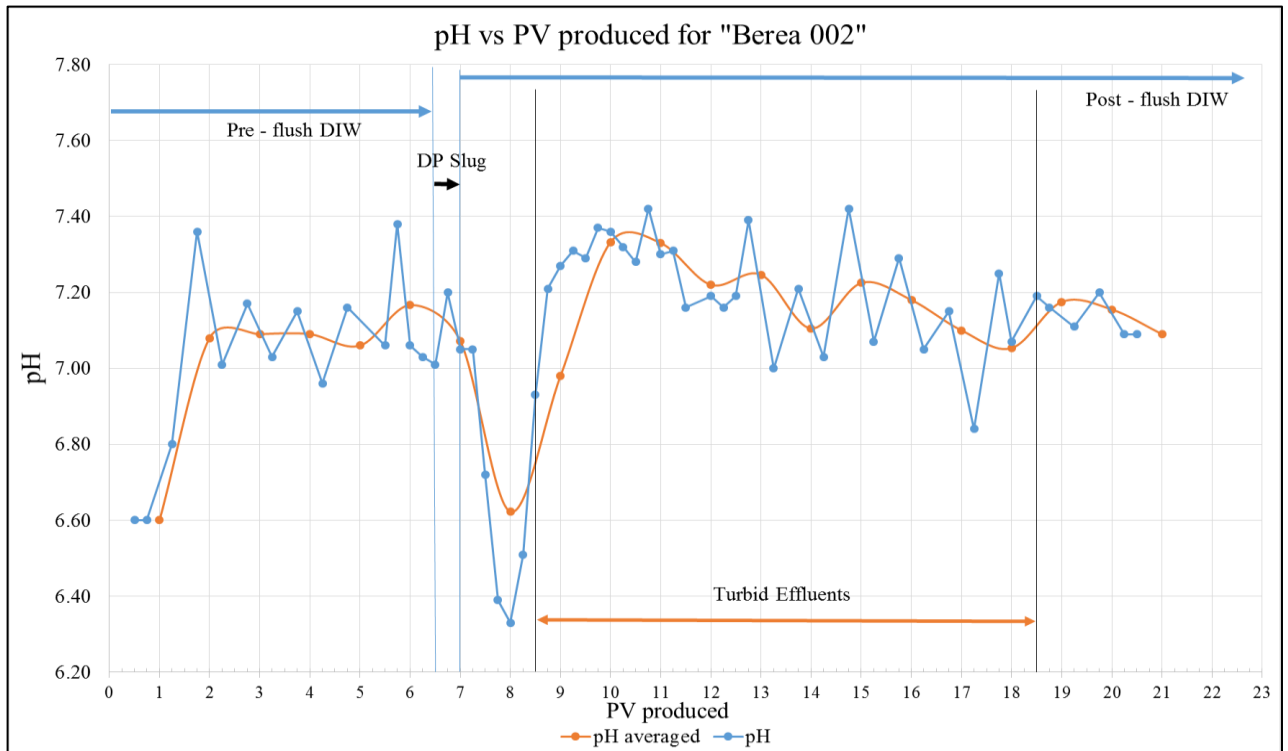


Figure 5.17 – pH values for “Berea 002”

The same production of turbid effluent was observed for “Berea 002” effluents 1.5 PV after switching to post – flush flooding stage. It is reflected in Figure 5.17 by pH increase up to 7.42 compared to relatively constant values during pre – flush period (7.13 in average for PV 2 – PV 6). It may be an indication that produced fine particles (kaolinite) contribute to the pH increase. The same behavior as in “Berea 001” can be noted at the period after the nanofluid slug injection, i.e. a quick decrease of pH (6.33 for the lowest point).

Pressure difference across the core was recorded at all experiment stages. Figure 5.18 demonstrates ΔP readings plotted against PV injected.

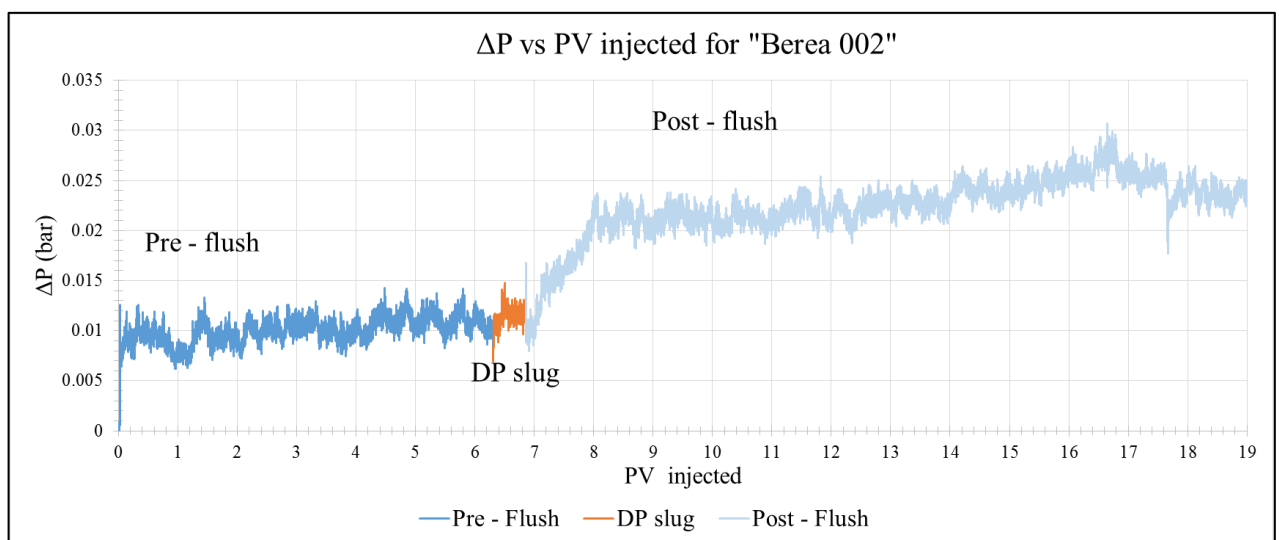


Figure 5.18 – ΔP vs PV injected for “Berea 002”

As in the previous experiment, pre – flush and nanofluid slug injection stages can be characterized by a relatively constant differential pressure, but when nanofluid is injected in the amount of 0.5 PV, there is an obvious rise in ΔP values for the whole post – flush period. The increase in pressure drop across the core indicates an increase in sweep efficiency, which is expected to help in oil recovery.

The effluent of “Berea 002” core flood was used in an attempt to find NP concentration in the produced fluid. For this purpose representative samples from each flooding stage were chosen, diluted 1:1 with DIW and measured in “UV-1700 spectrophotometer”. Acquired values of absorbance for these samples are presented in Figure 5.19 together with pH readings against PV produced.

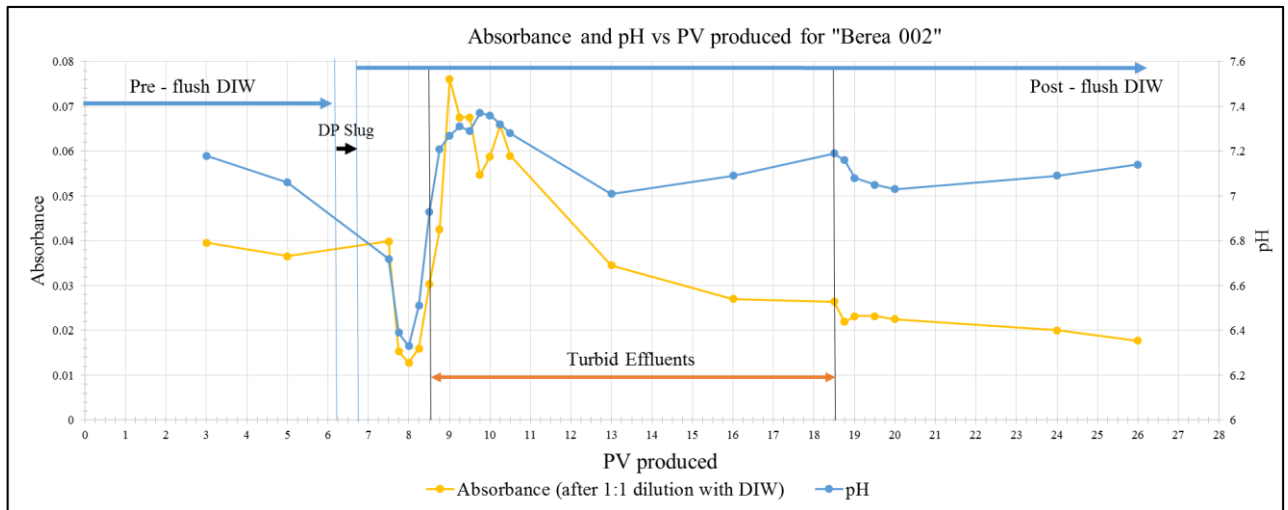


Figure 5.19 – Absorbance and pH values for “Berea 002”

From Figure 5.19 we can see that measured absorbance is relatively constant during the pre – flush period and equals to around 0.04. Then the nanofluid is injected and this has a great effect on absorbance values. Approximately one PV after the end of NP slug we observe a quick decline down to 0.0128 at PV 8 followed by a rapid increase up to 0.0760 at PV 9 and further gradual decline at later post – flush period. The second distinctive peak of 0.0658 appears at PV 10.2. Rock fine particles are noticed in effluent since PV 8.5 and stop being observed after PV 18.5, and their presence influences absorbance values and makes it difficult to estimate the amount of NP produced.

This experiment replicates the situation observed in “Berea 001” experiment showing that due to fines contribution to absorbance values it is difficult to find a universal baseline correction applicable for all flooding periods. For example, we can see from Figure 5.19 that absorbance values for pre – flush period and late post-flush differ, which may indicate decreasing contribution by rock fine particles present in the effluent.

As a try to account for the varying presence of fine particles in effluent samples and calculate the concentration of NP in effluent the method described below was followed. First of all, a “pre – flush bank” was created by mixing samples from the pre – flush period in one plastic tube. Then each measured previously post – flush sample from PV 8 to PV 20 was diluted in 1:1 ratio with fluid from the “bank”. This is aimed to equally increase the contribution of fines to absorbance readings at post – flush stage, establishing an artificial baseline for those points that equals by magnitude to absorbance values of pre – flush period. Figure 5.20 demonstrates a comparison between previously measured absorbance values and corresponding readings for samples diluted with the “bank”.

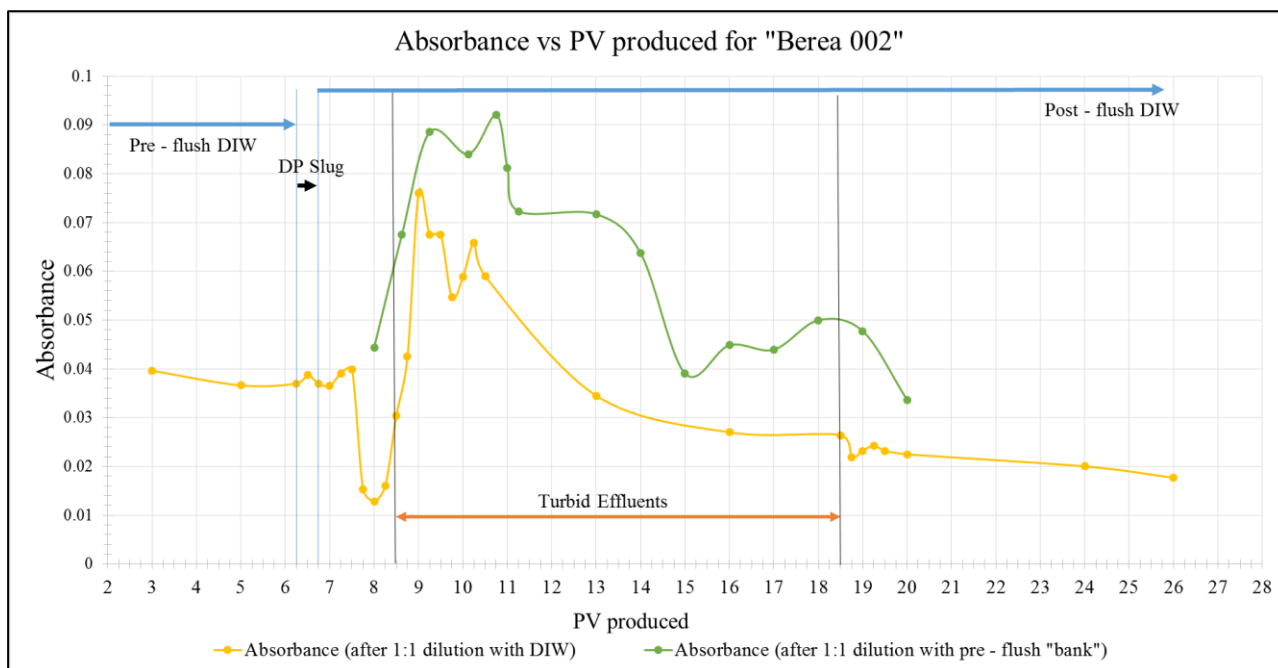


Figure 5.20 – Comparison of absorbance values after dilution with DIW and “pre – flush bank” for “Berea 002”

As we can see from Figure 5.20, the double-peak behavior in a new absorbance curve was preserved but at the same time, some deviations from the original trend appeared in flood period from PV 11 to PV 20. Taking into account the initial readings for the post - flush stage, acquired for samples diluted 1:1 with DIW, the correction to be made was matching the new absorbance curve with the original trend by ignoring points with enormously “high” values (PV 13, PV 14, and PV 16 – PV 19). Figure 5.21 show adjusted absorbance values for samples diluted 1:1 with “pre – flush bank” along with initial readings for samples diluted 1:1 with DIW.

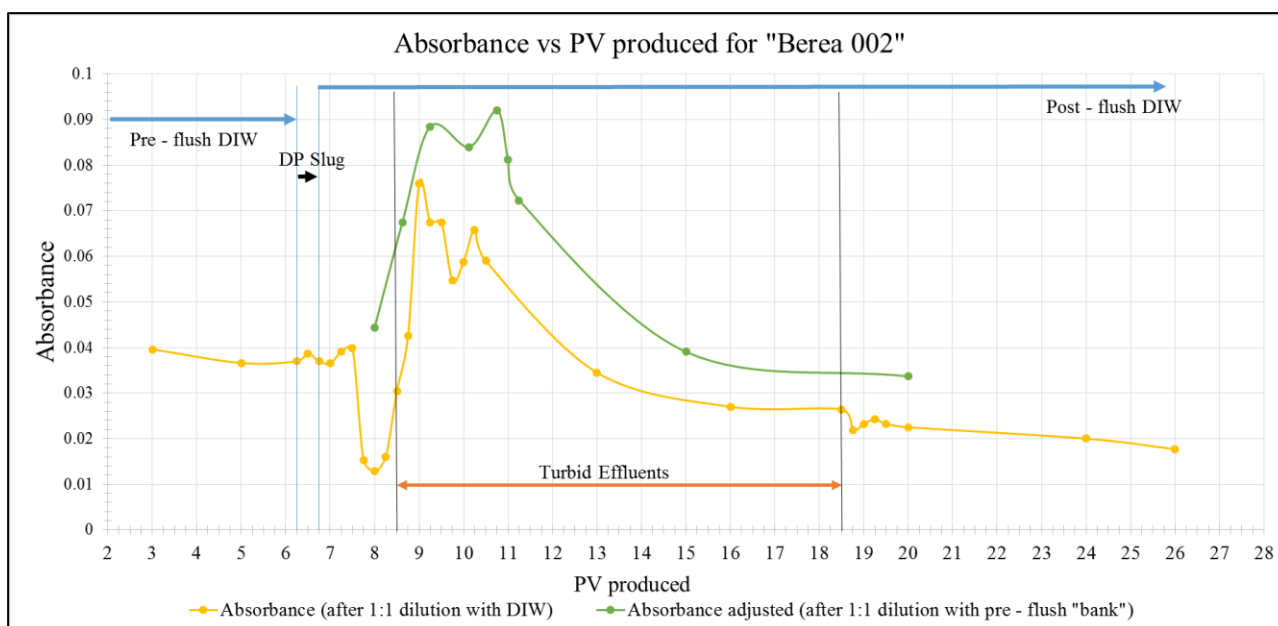


Figure 5.21 – Adjusted values of absorbance after dilution with “pre – flush bank” for “Berea 002”

In addition, after averaging absorbance readings for pre – flush stage, a baseline correction value of 0.03805 was applied by its subtraction from all measured points for samples diluted 1:1 with the “bank”. Absorbance value at PV 20 is appeared to be less than the baseline, so it was taken as zero. Figure 5.22 presents a plot with absorbance values for those points after a unified baseline correction was introduced. This curve was used for calculations of NP concentration in effluent.

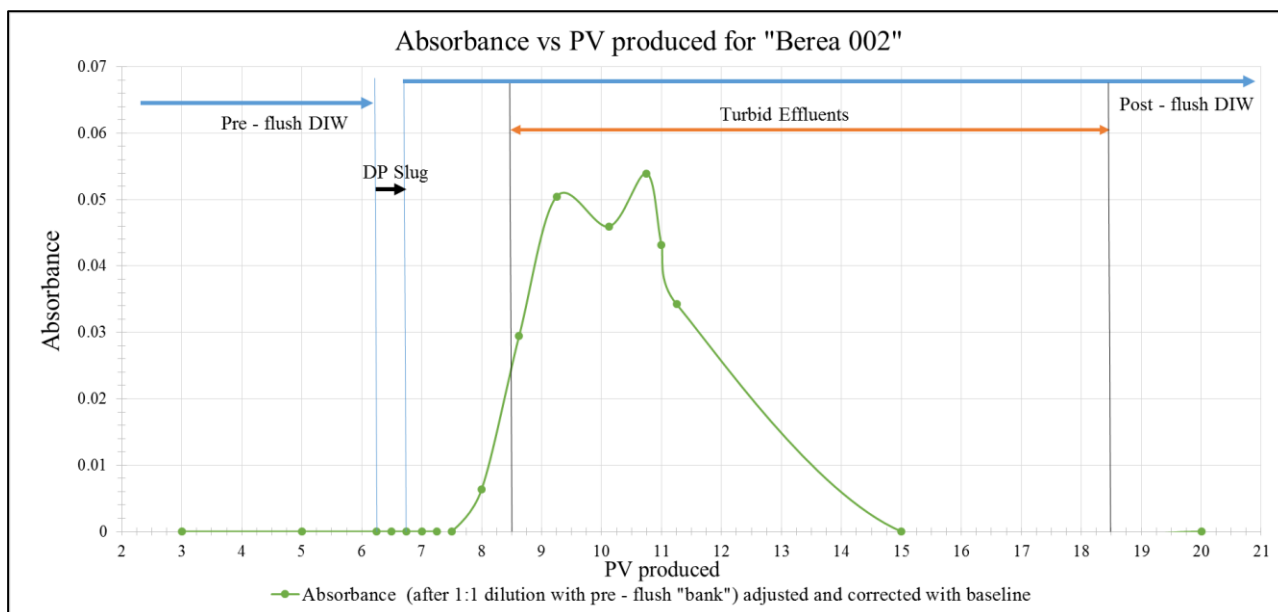


Figure 5.22 – Adjusted and corrected absorbance curve for post – flush samples of “Berea 002”

In order to calculate the amount of NP from absorbance values, calibration line was built by preparing nanofluid with tracer DP + 0.1M LiCl used for flood at three concentrations: 2 g/l, 1 g/l and 0.66 g/l and measuring in “UV-1700 spectrophotometer” with DIW as a reference (Figure 5.23). After that trendline equation was extracted from the plot and then mass balance calculations are carried out for “Berea 002” to estimate the amount of NP adsorbed / retained in the rock and the amount of nanoparticles produced in effluent.

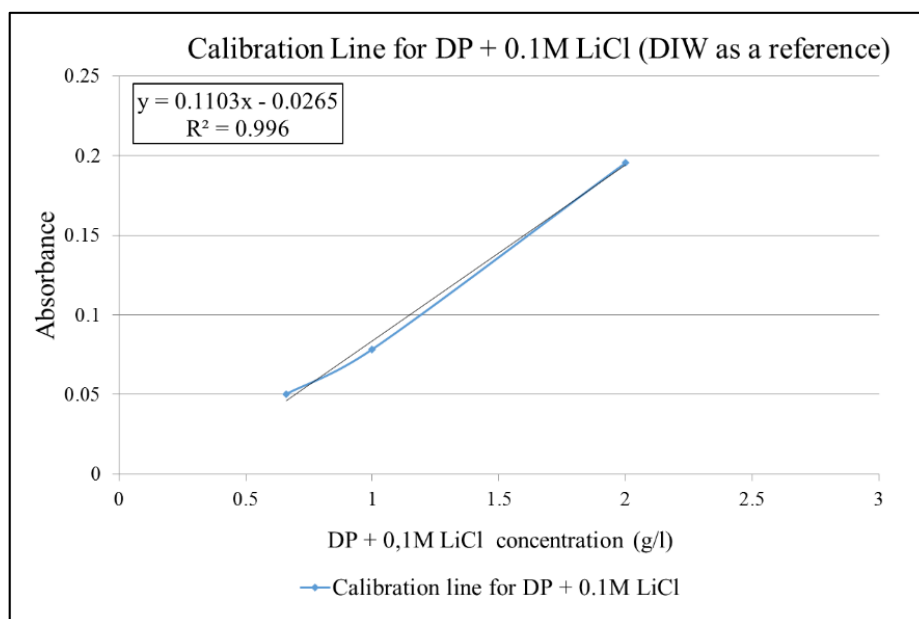


Figure 5.23 – Calibration line for DP + 0.1M LiCl (DIW as a reference)

Mass balance calculations were based on absorbance readings of samples and calibration line for injected nanofluid. The results are presented in Table 5.9.

Table 5.9 – NP mass balance calculations for "Berea 002"

PV produced	Absorbance	Absorbance after correction with baseline	NP concentration (g/l)	Sample volume (l)	NP amount (g)
3	0.03805	0	0	0.0025	0
5	0.03805	0	0	0.0025	0
6.25	0.03805	0	0	0.0025	0
6.5	0.03805	0	0	0.0025	0
6.75	0.03805	0	0	0.0025	0
7	0.03805	0	0	0.0025	0
7.25	0.03805	0	0	0.0025	0
7.5	0.03805	0	0	0.0025	0
8	0.0444	0.00635	0.2978	0.0025	0.00074
8.625	0.0675	0.02945	0.5073	0.0025	0.00127
9.25	0.0885	0.05045	0.6976	0.0025	0.00174
10.125	0.0840	0.04595	0.6568	0.0025	0.00164
10.75	0.0920	0.05395	0.7294	0.0025	0.00182
11	0.0812	0.04315	0.6315	0.0025	0.00158
11.25	0.0723	0.03425	0.5508	0.0025	0.00138
15	0.03805	0	0	0.0025	0
20	0.03805	0	0	0.0025	0
PRODUCED NP amount (g)					0.01018
INJECTED NP amount (g)					0.02312
Percent of NP produced (%)					44.0
Percent of NP adsorbed / retained (%)					56.0

Initial amount of NP injected in grams was calculated from known nanofluid concentration 2g/l multiplied by 0.5 PV of the core (slug volume). Total amount of NP produced was calculated by multiplication of NP concentration, acquired from calibration line and absorbance values (corrected with baseline) and corresponding volume of effluent samples. It was assumed that concentration of NP in the certain PV (formed by a mixture of samples) was generalized and representative for the whole produced effluent volume within this PV. Figure 5.24 shows a NP concentration plotted against PV produced.

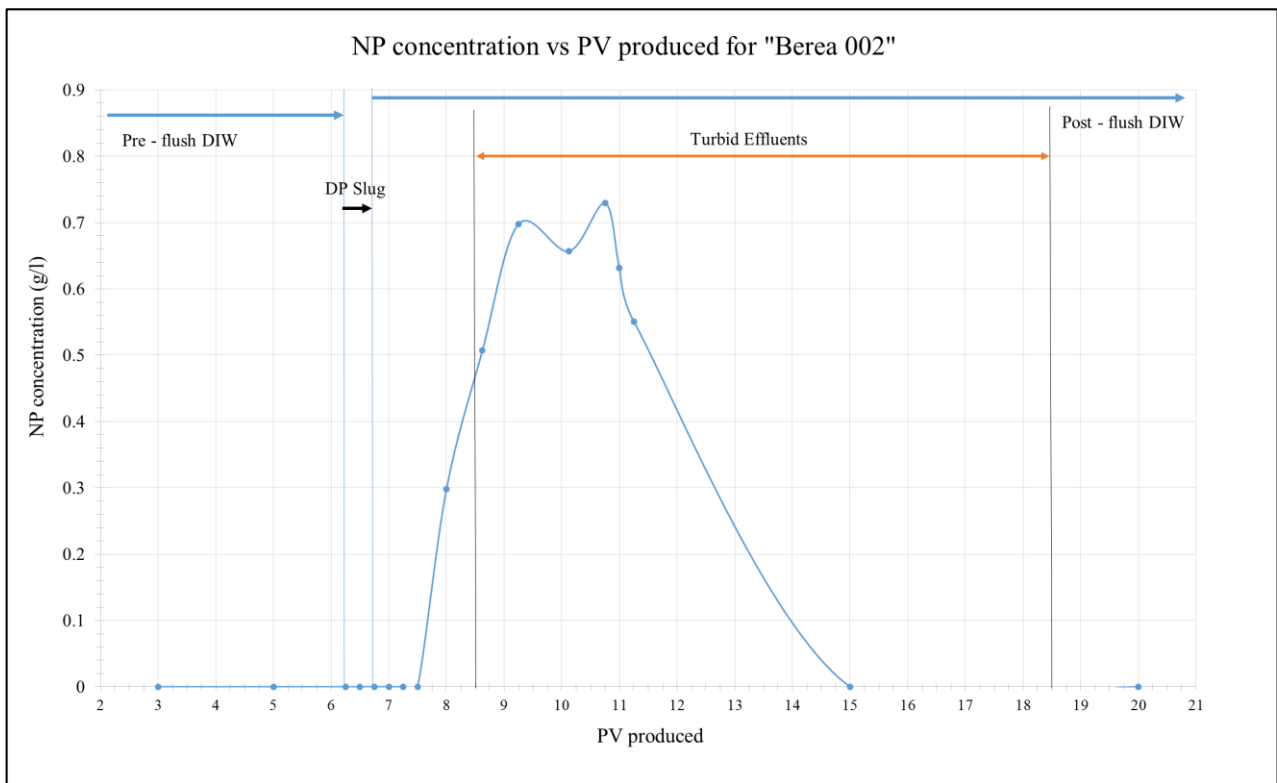


Figure 5.24 – NP concentration vs PV produced for “Berea 002”

According to calculations given in Table 5.9, 44 % of injected NP were produced and the rest 56 % of the initially injected amount was adsorbed / retained in the core. It may indicate that adsorption happening in Berea sandstone is not strong since only half of injected NP left inside the core. These calculations were performed with an assumption that baseline can be artificially unified for all flooding stages and the contribution of fine particles to absorbance readings can be at some degree equalized.

Considering that the post – flush was continued for 13.5 PV and the amount of NP retained in the core was 56 % indicates that the desorption process is very limited.

Effluent samples of “Berea 002” core flood were used for ion chromatography analysis to evaluate the presence of different ions. Cations detected for “Berea 002” are Li^+ , Na^+ , K^+ , Mg^{2+} , Ca^{2+} . Anions detected in effluent are SO_4^{2-} and Cl^- . Ions concentrations were plotted together with pH measurements. The following Figure 5.25 presents only Li^+ ion which is of higher importance for analysis. The rest ions were not representative or detected at extremely low concentrations in some samples and were either ignored or attributed to errors and disregarded due to possible contamination during samples preparation for IC measurements. Nevertheless, all the plots for detected ions can be found in Appendix A.

Concentrations of Li^+ (mol/l) and NP (g/l) in effluent vs PV produced are presented in Figure 5.25.

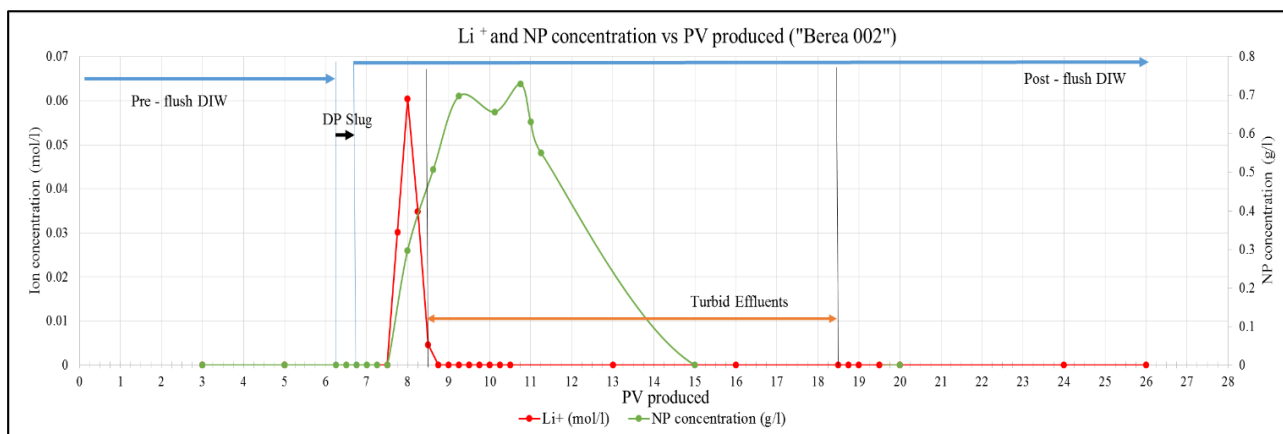


Figure 5.25 – Li^+ ion and NP concentrations in effluent from “Berea 002” experiment

Comparing curves for NP and Li^+ ion from tracer shows later breakthrough of nanofluid. This demonstrates enhanced interaction of the NP in the core. However, the big “tail” of the curve characterizing NP concentration in the effluent indicates the following:

- 1) Reversible adsorption;
- 2) Desorption occurrence as the post – flush continues;
- 3) Redistribution of NP within the core.

With the processes of redistribution and desorption, however, ΔP remains flat. Therefore, nanofluid does not hinder the flow in the core.

It can be concluded DP NP used in this study are good candidates for in-situ surface modification in Berea sandstone which can be associated with sweep efficiency. The effect of this in-situ surface modification of the sandstone rock and other mechanisms that lead to EOR are investigated in the following sections.

5.5.3 Core flood with “Berea 003”

Flooding of the core “Berea 003” was conducted as a repetition of “Berea 002” experiment at the same injection rate of 10 pore volumes per day (pump rate 0.144 ml / min), with confinement pressure of 30 bars and back-pressure close to 10 bars. This time the volume of the injected DP slug was increased up to 1.5 PV of the core, but the concentration of nanofluid was reduced down to 1 g/l.

Deionized water was injected during the pre - flush period of 6.5 PV. Then a nanofluid slug with lower concentration and tracing chemical (1 g/l DP + 0.1M LiCl in DIW) was introduced in a total volume of 1.5 PV. The slug was followed by the post - flush with DIW injection for 18 PV. Injection stages are presented in Figure 5.26.

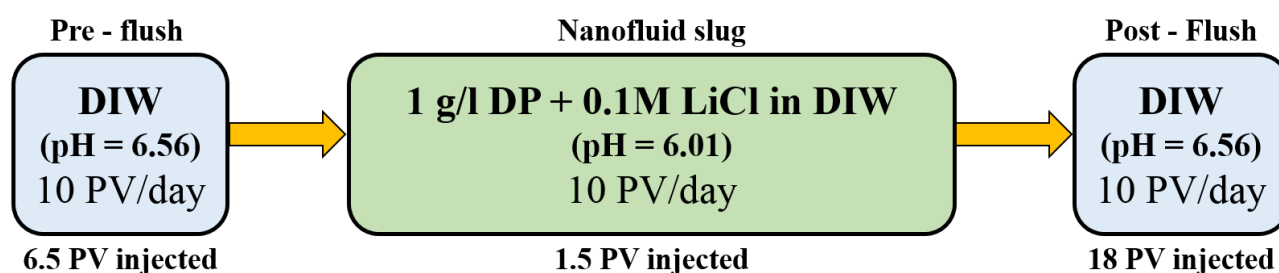


Figure 5.26 – Injection sequence for “Berea 003”

Figure 5.27 shows pH values for effluent samples, measured after the core flood was finished, averaged within each PV and plotted against PV produced.

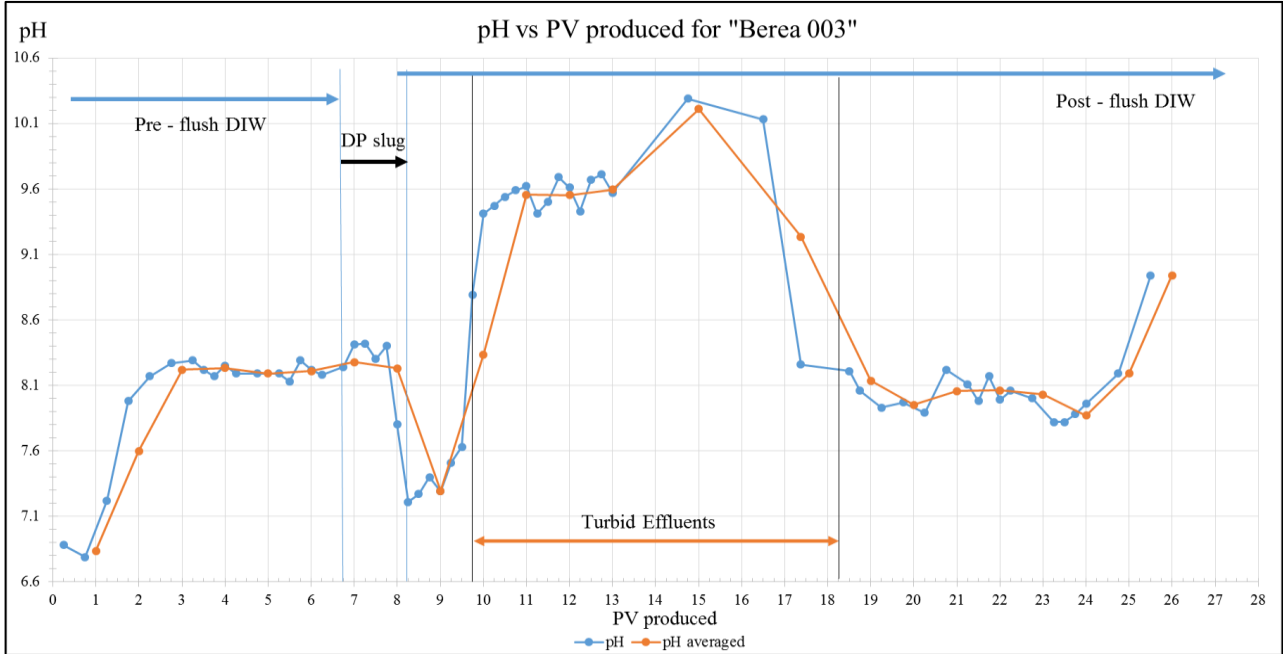


Figure 5.27 – pH values for “Berea 003”

This experiment behavior replicated two previous ones in a way that turbid effluent was also produced 1.5 PV after the end of nanofluid slug injection. During the pre – flush period and DP slug pH values are relatively constant in a range 8.2 – 8.4 units. Then it decreases down to 7.21 and again starts to rise significantly after PV 9 up to 10.29 units. At late post – flush, when effluent samples are becoming less turbid (PV 18) pH decreases down to 8 units.

Readings of pressure difference in the core were taken during the flood and recorded data were plotted in Figure 5.28.

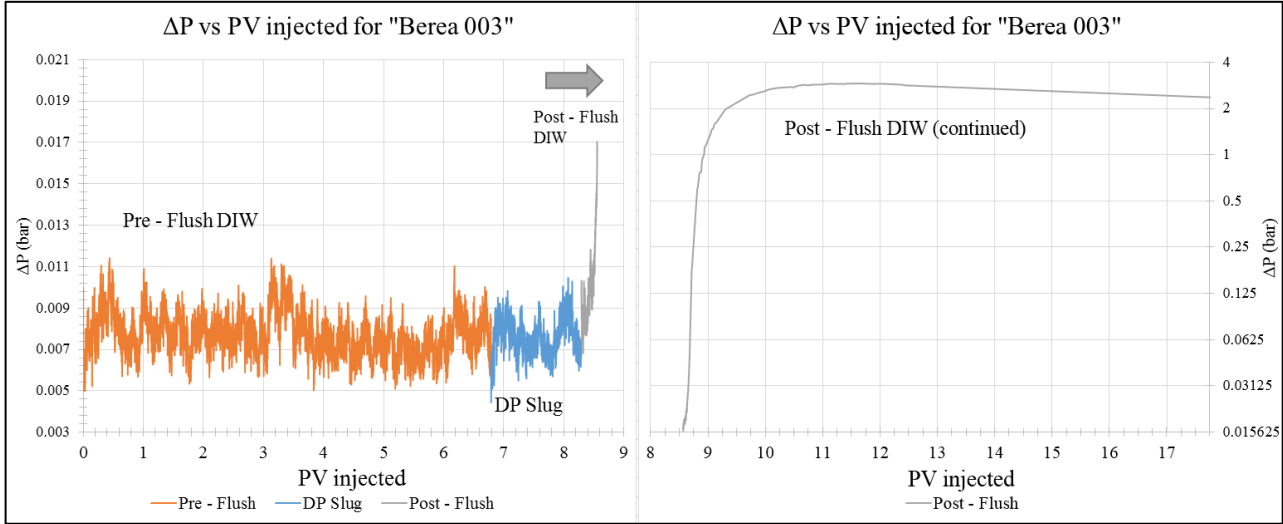


Figure 5.28 – ΔP vs PV injected for “Berea 003”

From Figure 5.28 we can see that DIW pre – flush and nanofluid slug stages demonstrated comparatively constant pressure drop of a range 0.005 – 0.011 bar between inlet and outlet of the core, but at post – flush pressure difference rose extremely and reached 2.9 bars which may indicate a serious blockage of the pore throats in the core. In order to determine whether this increase of pressure drop was caused by nanofluid the following flood was conducted (“Berea 004”).

The presence of different ions in the effluent was evaluated by “Dionex Ics-5000+ DP” ion chromatograph. SSW and low salinity calibration fluid were used as references to calculate concentrations of cations and anions in samples. Cations detected for “Berea 003” are Li^+ , Na^+ , K^+ , Mg^{2+} , Ca^{2+} . Anions detected in effluent are SO_4^{2-} , CO_3^{2-} and Cl^- . The following Figure 5.29 presents only results for Li^+ ion which was more important for analysis. Its concentration was plotted together with pH values. Some ions were detected at extremely low concentrations in effluent and were either ignored or attributed to errors and disregarded due to possible contamination during samples preparation for IC. The rest of ion concentrations are also plotted against PV produced and can be found in Appendix A.

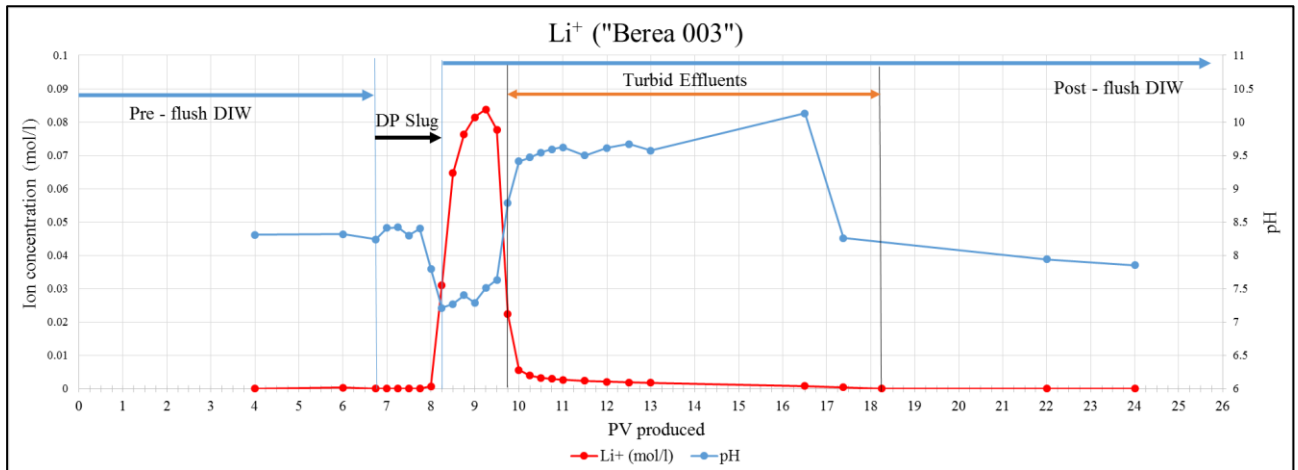


Figure 5.29 – Li^+ ion concentration in effluent and pH values for “Berea 003”

Figure 5.29 demonstrates that tracer was mostly produced in a period from PV 7.75 to PV 10. Like in the previous case with “Berea 002” the NP production is expected to occur with some delay, most likely together with the production of kaolinite mineral (region of “turbid effluents” in the plot).

5.5.4 Core flood with “Berea 004”

Core flood “Berea 004” was conducted at the same injection rate of 10 pore volumes per day (pump rate 0.145 ml / min), confinement pressure of 30 bars and back pressure close to 10 bars. But this time instead of nanofluid injection, DIW with adjusted pH was used to mimic DP slug that was used in “Berea 002” core flood. Hence, pH was controlled by adding HCl acid to an originally used fluid with tracing chemical without adding nanoparticles (0.1M LiCl in DIW + 90 μl of 0.1M HCl). The aim of this low pH DIW injection experiment was to check possible pore throat blockage and production of the turbid effluent in the post - flush period.

Deionized water (DIW) was injected during the pre - flush period of 6 PV. Then DIW with tracing chemical and adjusted pH slug was introduced in a total volume of 0.5 PV. The slug was followed by the post - flush with DIW injection for 18.5 PV. Injection stages are presented in Figure 5.30.

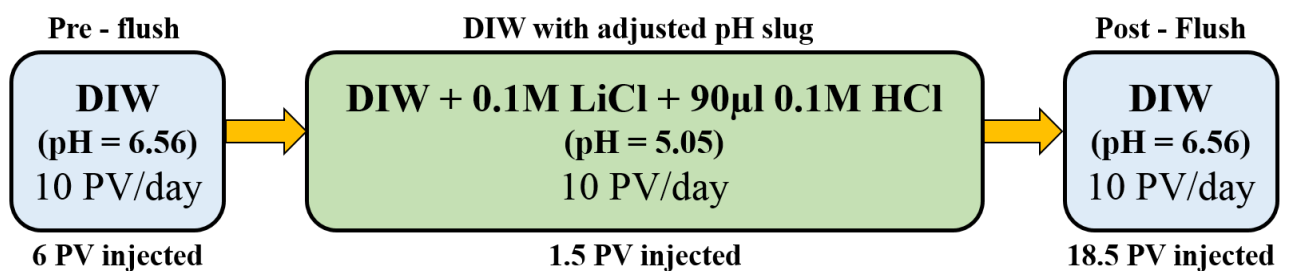


Figure 5.30 – Injection sequence for “Berea 004”

During the experiment the expected production of turbid effluent was observed at post – flush stage. It turned out that possible blockage of pore throats in the core and further production of detached fine particles was probably triggered by the “water shock” and pH difference between fluids used at different stages of the flood.

The plot with pH values of the effluent samples against PV produced is presented in Figure 5.31.

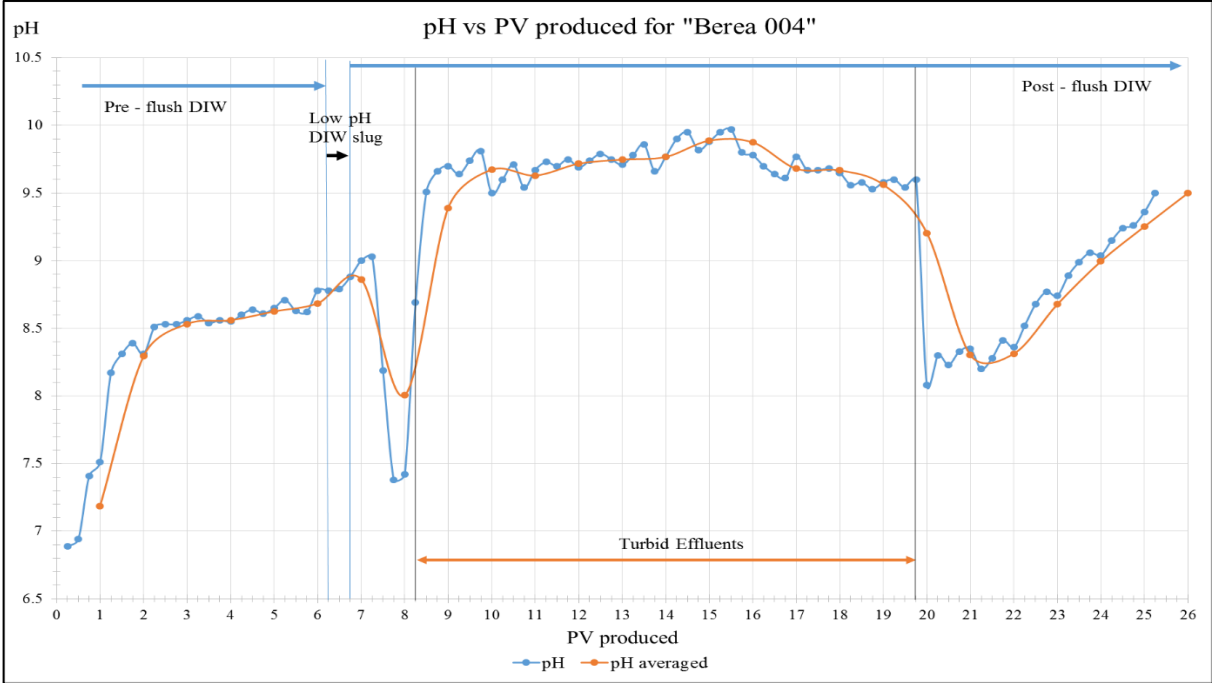


Figure 5.31 – pH values for “Berea 004”

Figure 5.31 shows a pH curve that has a familiar shape which was observed in the previous experiments. But in the latest post – flush period we observe a gradual increase in pH after the production of turbid effluent is stopped at PV 19.75 (from 8.08 to 9.5 units at PV 25 produced). Figure 5.32 shows a comparison of pH measurements for core floods “Berea 004” and “Berea 002”.

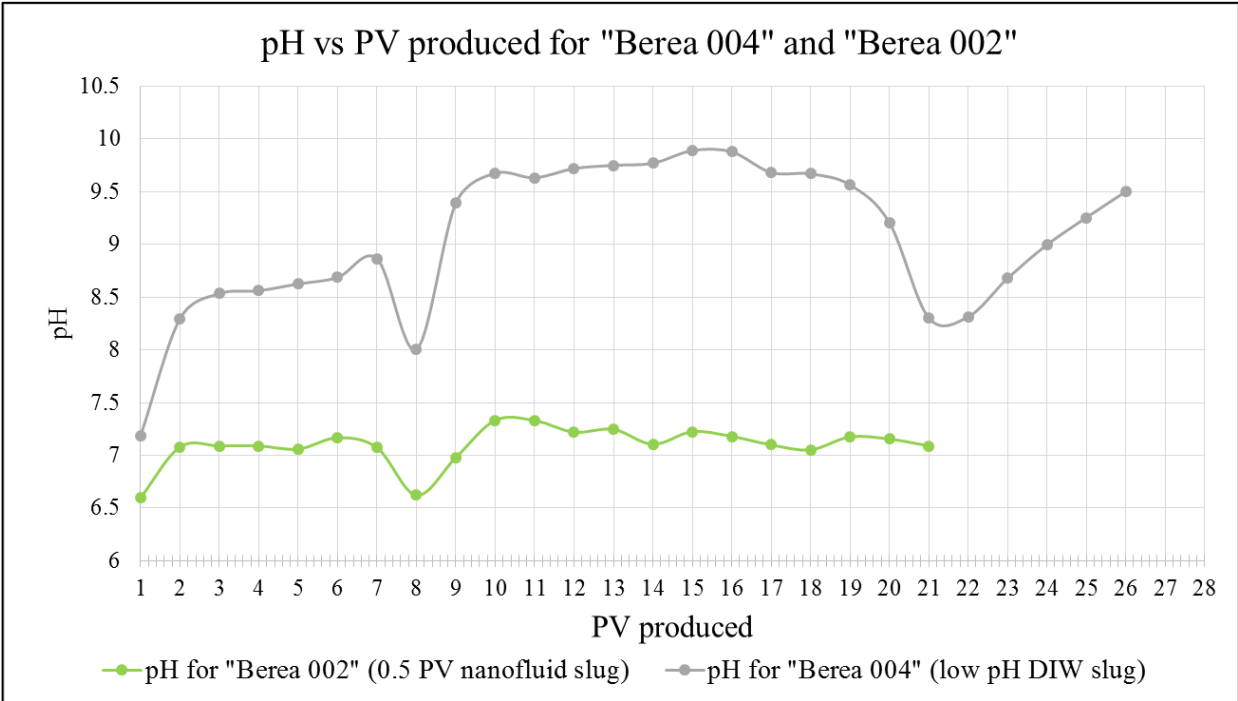


Figure 5.32 – Comparison of pH readings for “Berea 002” and “Berea 004”

As we can see from Figure 5.32 pH curves of “Berea 004” and “Berea 002”, have similar shapes but the different magnitude and “Berea 004” has much higher readings of pH at all flood stages.

The pressure difference across the core was recorded at all three stages. ΔP values were plotted against PV injected (Figure 5.33).

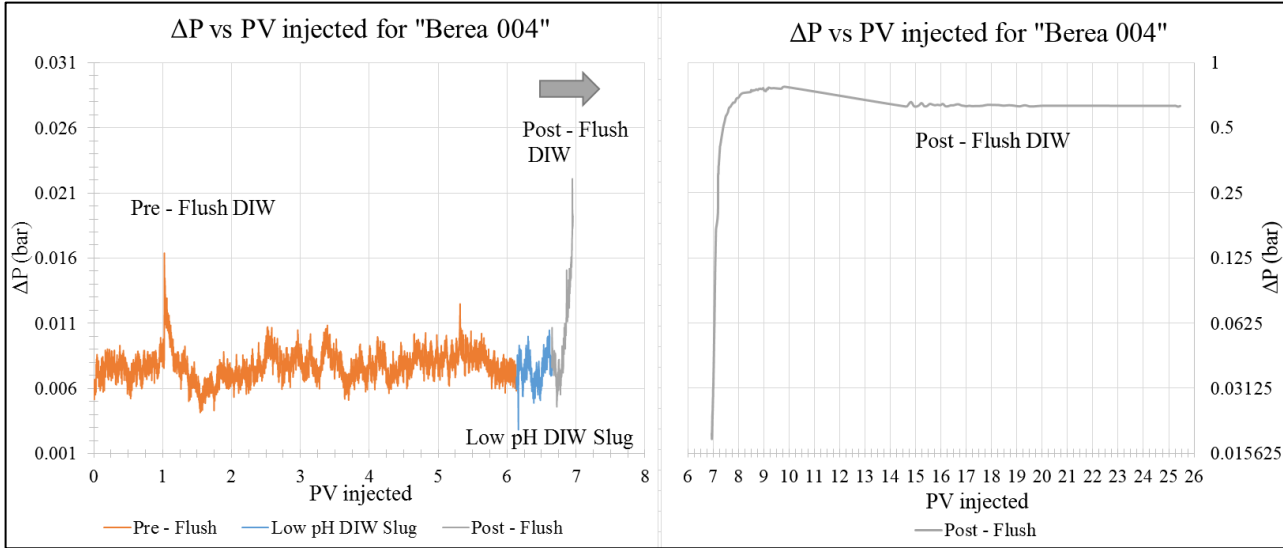


Figure 5.33 – ΔP vs PV injected for “Berea 004”

Figure 5.33 demonstrates that at the beginning of the post – flush period after low pH DIW slug is introduced differential pressure rises fast up to 0.77 bars and keeps at a high level for the whole post – flush stage. Compared to ΔP values of the “Berea 002” core flood, in this case, there probably happened more serious blockage in the core throats due to fine detachment and migration, and it caused a pressure increase. On the contrary, when we had a small nanofluid slug (0.5 PV) in “Berea 002” injected NP probably interacted with the rock surfaces and therefore mitigated fines migration. Pore throat blockage and intense release of kaolinite were observed during core flood “Berea 003”. Therefore, this increase in ΔP happened probably due to “water shock” from introducing DIW and low pH in the core, but not an exclusive effect of NP.

Absorbance curve was acquired for “Berea 004” after representative samples were diluted in a ratio 1:1 with DIW and measured in “UV-1700 spectrophotometer”. Acquired values were plotted against PV produced along with corresponding pH readings (Figure 5.34).

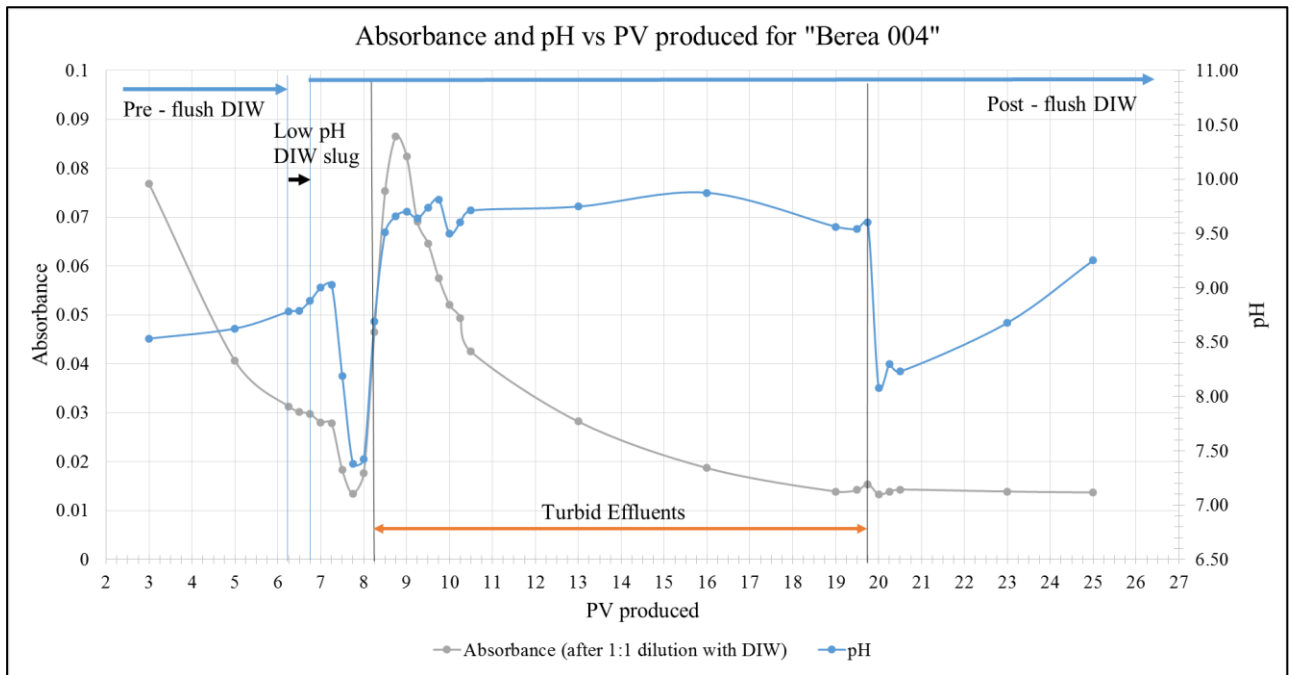


Figure 5.34 – Absorbance and pH values for “Berea 004”

Figure 5.35 shows the comparison of absorbance curves for effluents of “Berea 004” and “Berea 002” core floods.

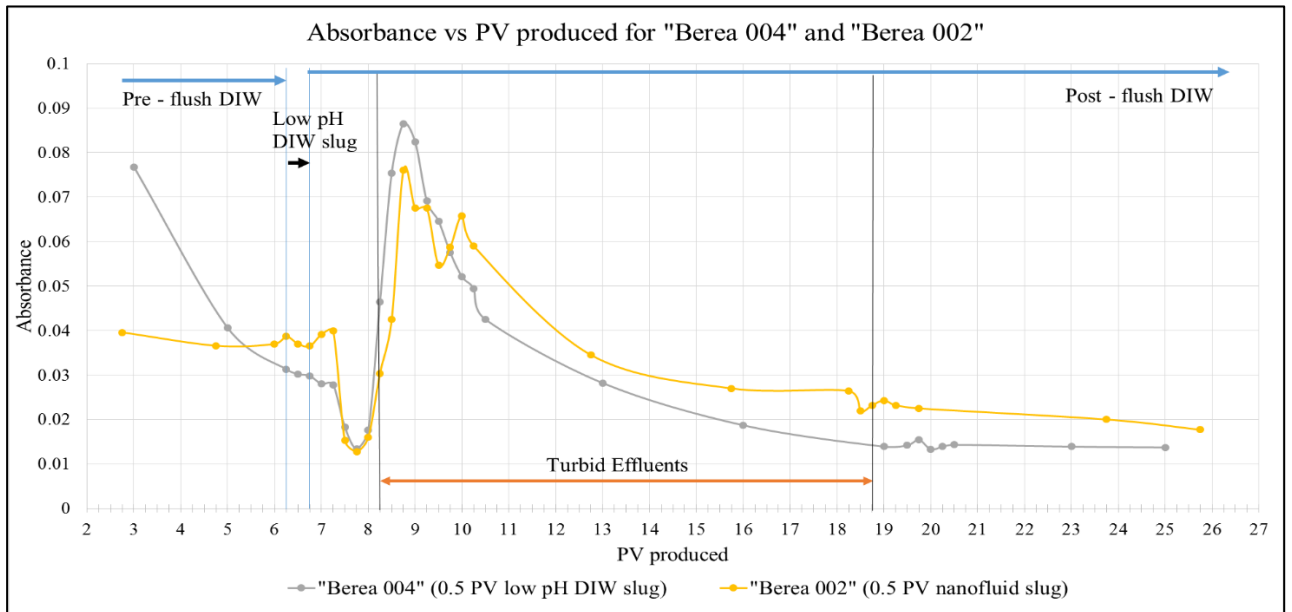


Figure 5.35 – Comparison of absorbance readings for “Berea 002” and “Berea 004”

As we can see from Figure 5.35 absorbance curves for “Berea 004” and “Berea 002” experiments are very close to each other with some differences, especially at the pre – flush period. At the beginning of the post – flush stage when a significant drop in absorption values is observed, the trends for two experiments are overlapping. But from PV 8.25 to PV 9.75 absorbance curve for “Berea 002” is lower than that for “Berea 004”. It may be an indication, that after the nanofluid was injected and NP adsorbed in the core, they contributed to mitigation in fines migration and the fewer amounts of fine particles were eventually produced in the effluent. Without NP injection we could probably expect a high single peak for absorption curve of “Berea 002” as we got for “Berea 004” experiment. Starting from PV 10 where we have the second peak, the original trend was probably continued with gradual decrease contribution from fines present in the effluent.

5.5.5 SEM imaging of Berea core and effluent

Berea sandstone core without any treatment was subjected to analysis with scanning electron microscope. Figure 5.36 shows SEM image of Berea sandstone rock sample.

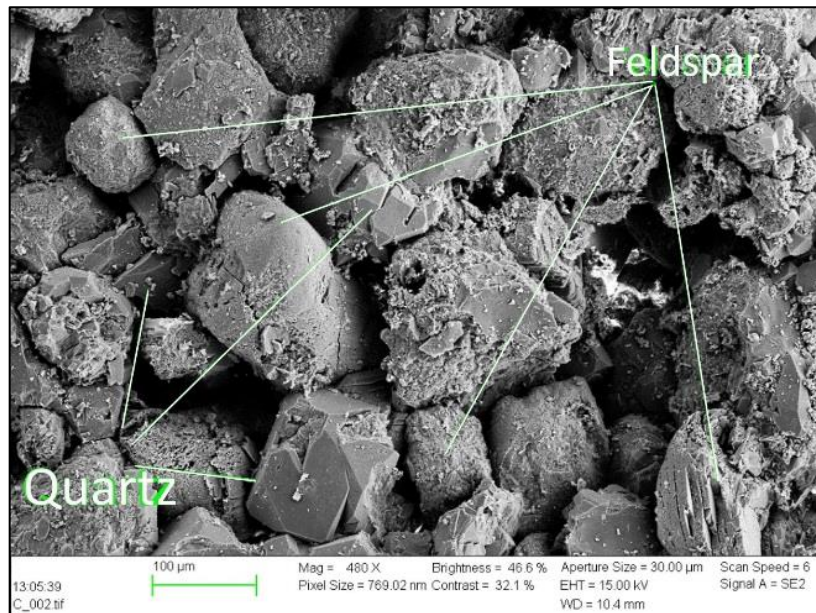


Figure 5.36 – SEM image of Berea sandstone rock sample

As we can see from Figure 5.36 sandstone consists mostly of quartz with some amount of feldspar (kaolinite) mineral sheets. This rock has well defined grains and a pore throat sizes with the order of micrometers (μm).

Further increase in scale of the SEM instrument allowed to have a more detailed look on kaolinite mineral. In Berea sandstone kaolinite appears in a form of sheets and flakes which is clearly demonstrated in Figure 5.37.

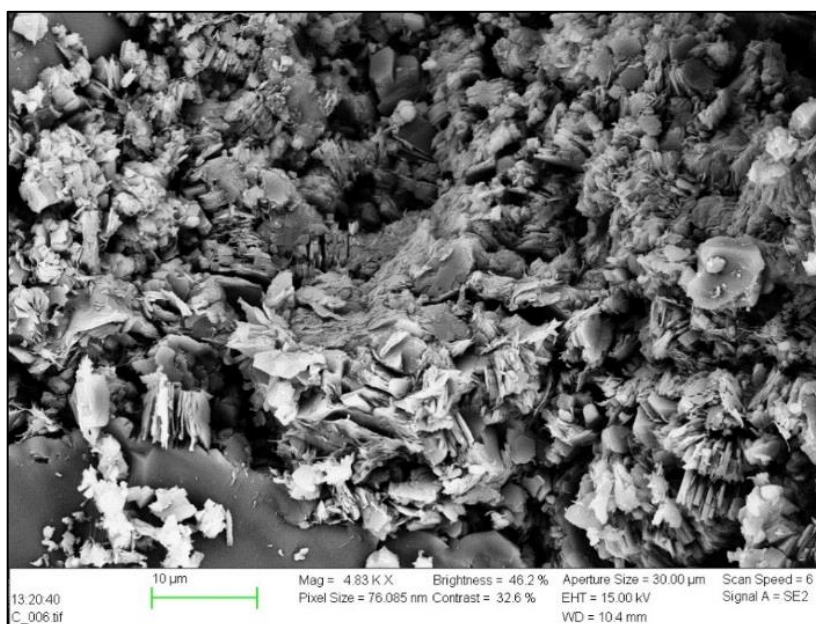


Figure 5.37 – SEM image of Kaolinite mineral in Berea sandstone

SEM technique was also utilized to analyze a Berea sandstone core sample saturated for 24 hours with nanofluid of 1 g/l concentration. Acquired image of the rock under magnification of 1 μm level and down to nano dimension is presented in Figure 5.38.

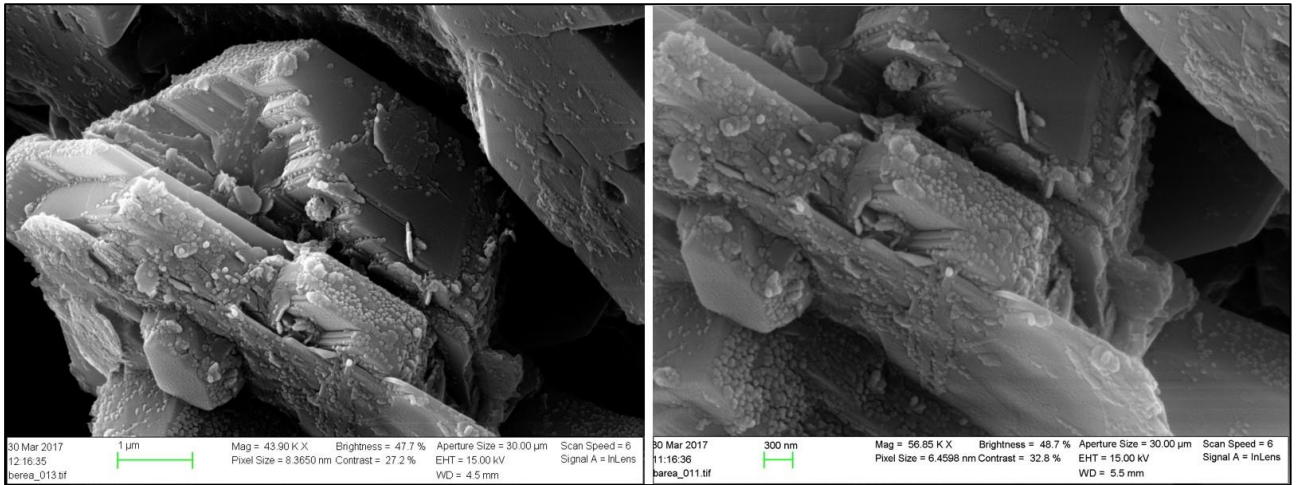


Figure 5.38 – SEM image of Berea sandstone rock sample pretreated with nanofluid

Spherical form of the nanoparticles adhered onto the rock surface can be identified in Figure 5.38. Performed X-ray spectroscopy spot analysis confirmed that these small spheres are silica nanoparticles. More than that, it should be noted that adhesion of the nanoparticles is observed preferentially on flat surfaces of quartz mineral. Herewith, NP are distributed separately from each other without in-situ aggregation.

Finally, the turbid effluent produced during “Berea 003” core flood experiment was prepared for SEM study and investigated. Taken image of the sample and the result of the X-ray spectroscopy spot analysis are presented in Figure 5.39.

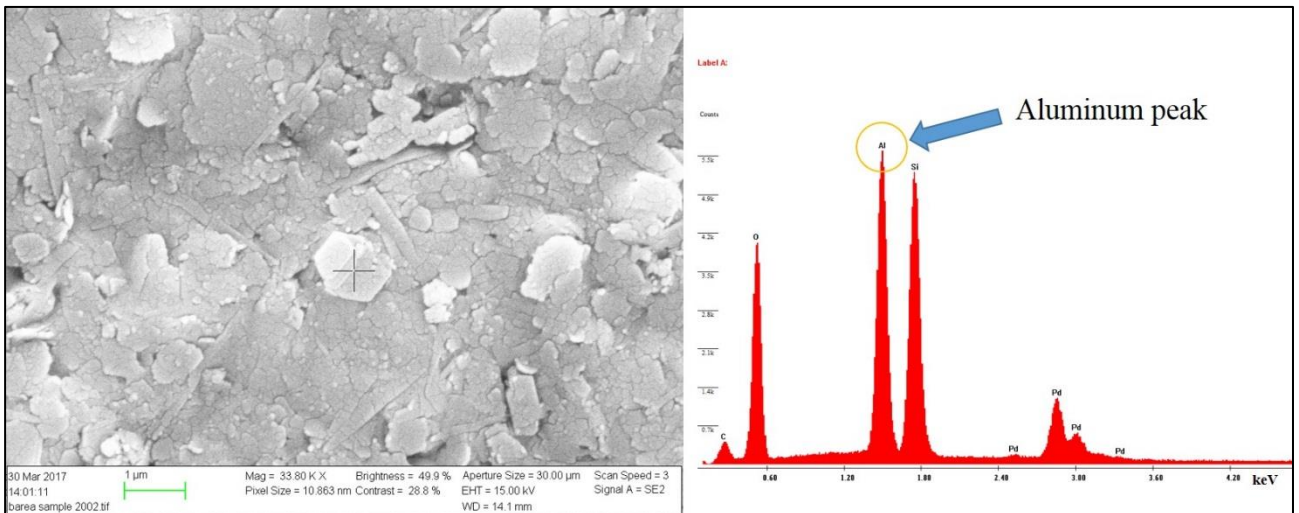


Figure 5.39 – SEM image and spot analysis of turbid effluent produced during the core flood with “Berea 003”

According to X-ray spectroscopy test aluminum was detected as expected among chemical components in the analyzed sample. Aluminum peak serves as a good confirmation that turbid effluent produced during the flooding experiments is kaolinite mineral that was flushed out from the Berea sandstone cores.

5.6 Enhanced oil recovery (EOR) experiments

5.6.1 Core floods with “Berea 005”

“Berea 005” was used firstly for drainage flood to establish irreducible water saturation S_{wirr} by flooding preliminary 100 % saturated with SSW core with model oil (n-Decane + 0.01M NN-DMDA) at flow rates from 0.01 ml/min to 3 ml/min until no more water production was possible. Flood was carried out at ambient temperature (25 °C) and confinement pressure of 25 bars was used to avoid cross-flow in the core with the pore volume equal to 20.46 cm³.

The primary core flood experiment resulted in the cumulative production of 12.4 ml of SSW from the core. Irreducible water saturation $S_{wirr} = 0.394$ was calculated by using Equation 5.1.

$$S_{wirr} = \frac{PV - V_{w.p.}}{PV}, \quad (5.1)$$

where PV – pore volume of the core (cm³);

$V_{w.p.}$ – total volume of water produced from the core during drainage (cm³).

After irreducible water saturation was established, the core was aged in an aging cell for three weeks at a constant temperature of 50 °C before further use in the secondary flooding.

Secondary flooding (oil recovery flood) was conducted on aged core according to the following steps: LSW injection at low flow rate (4PV/day), LSW injection at high rate (16 PV/day), injection of nanofluid suspension prepared in LSW at low flow rate (4 PV/day) and the same nanofluid injection at high flow rate (16 PV/day). Increasing the flow rate for every injected fluid is done to account for possible capillary end effects in the core. The flood was run at 70°C temperature with back-pressure of 10 bar, confinement pressure was kept at 25 bar to mimic conditions in a reservoir. Figure 5.40 shows injection sequence for oil recovery flood with “Berea 005” core.

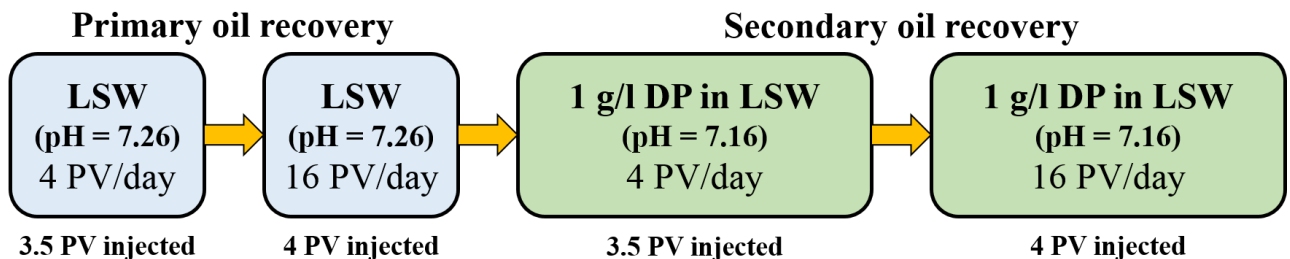


Figure 5.40 – Injection sequence for oil recovery flood with “Berea 005”

Inlet pressure and ΔP between inlet and outlet of the core were recorded during all stages and plotted in Figure 5.41.

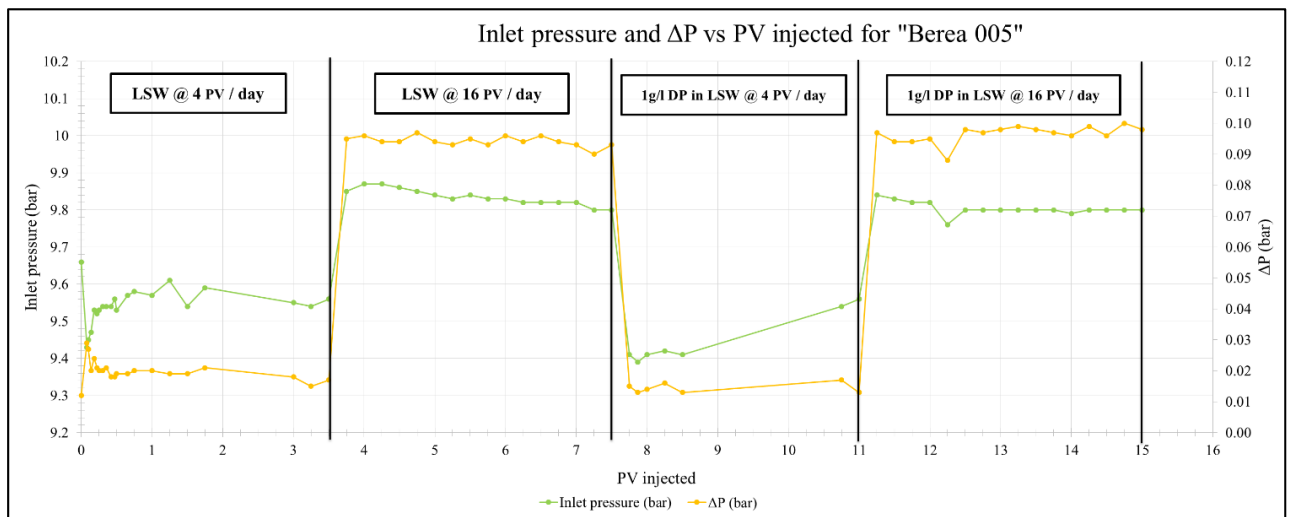


Figure 5.41 – EOR experiment with “Berea 005”: Inlet pressure and ΔP vs PV injected

Comparing injection stages at 4 PV/day flow rate with and without the presence of nanofluid one can notice that both pressure drop and inlet pressure are slightly lower at a period of nanofluid injection. This may be a good indication of injectivity enhancement caused by NP interactions with the rock. By comparing two stages at 16 PV/day it can be observed, that inlet pressure is slightly lower at the stage with nanofluid injection, while pressure drop for nanofluid injection period is slightly higher.

During the primary recovery flood with LSW when the rate of injection was changed from 4 PV/day to 16 PV/day increase in ΔP was around 0.078 bars. Concerning to secondary recovery with nanofluid, this change of pressure drop related to increasing of injection flow rate was around 0.084 bar. This difference may indicate that injection of NP improves sweep efficiency which is similar to observations made in single phase transport behavior flood (“Berea 002”).

Readings of pH were taken for all collected effluent water samples (each quarter of PV injected). Cumulative oil recovery and pH values were plotted against PV injected and presented in Figure 5.42.

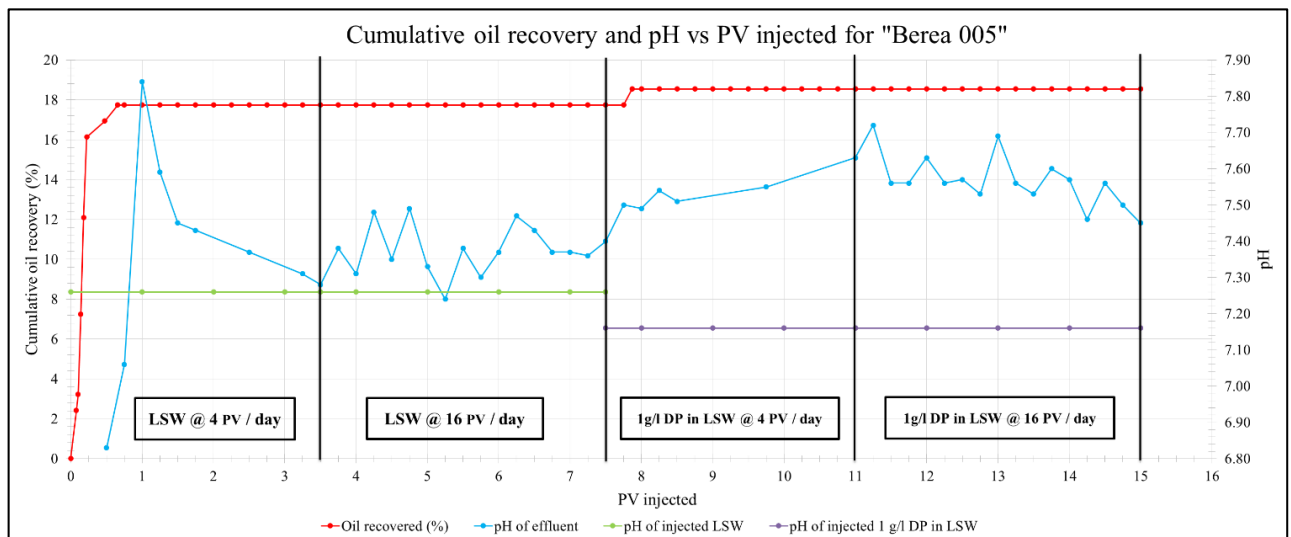


Figure 5.42 – EOR experiment with “Berea 005”: Cumulative oil recovery and pH vs PV injected

Major amount of oil was produced within first pore volume injected during the primary recovery with LSW at a rate 4 PV/day. LSW injection stage at 16 PV/day did not show any additional oil extraction and cumulative recovery by the end of this period was equal to 17.74 %. After flood was shifted to nanofluid injection at 4 PV/day there appeared an increment of 0.81 % in oil production (PV injected 7.75 in Figure 5.42). When the nanofluid injection rate was increased up to 16 PV/day no more

additional oil production was observed till the end of the experiment which was stopped after total injection of 15 PV of fluids. Therefore, total oil production from the core was 2.3 ml out of 12.40 ml oil initially in place (OIIP), hence ultimate oil recovery constituted 18.55 %.

Readings of pH for collected effluent remain higher than pH values of injected fluids during the whole experiment. A slight increase in pH is observed during nanofluid injection at 4 PV/day compared to primary recovery with LSW. After shifting to nanofluid injection at 16 PV/day pH curve show a slight decrease trend with minor fluctuations.

Produced water effluent was further used for characterization with UV. The absorbance curve for “Berea 005” was acquired and plotted together with pH readings in Figure 5.43.

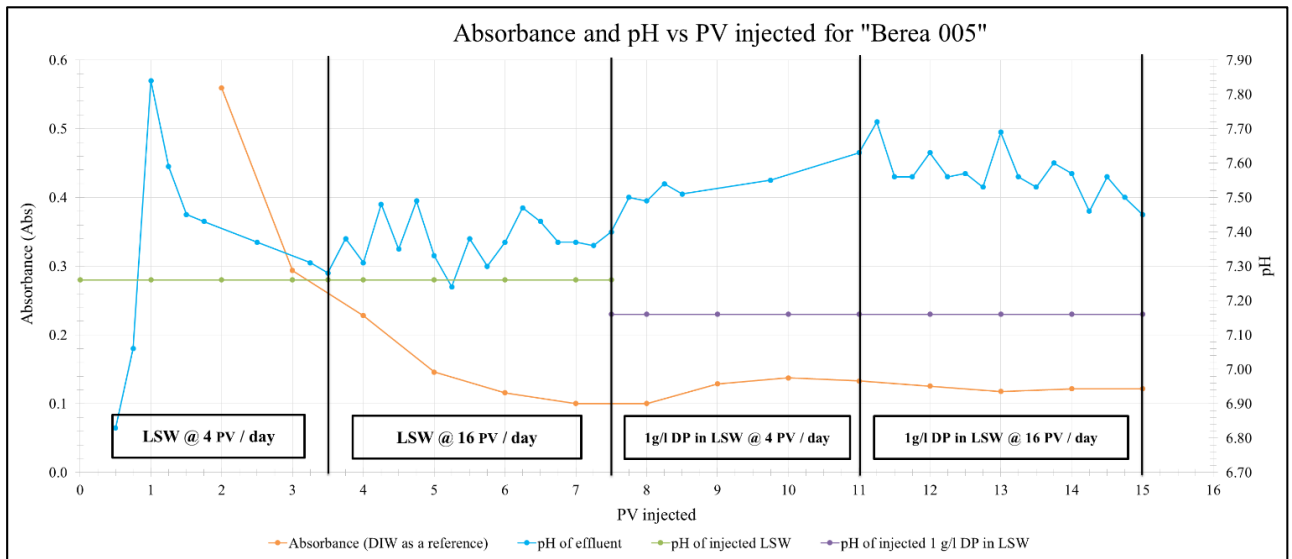


Figure 5.43 – EOR experiment with “Berea 005”: Absorbance curve and pH vs PV injected

Samples from the earliest period of the flood showed extremely high values of absorbance due to the fact that collected water was colored. This yellow color could not be removed in a centrifuge, so it was not just a turbidity due to the presence of produced fines as was observed in single phase flood experiments. It is interesting that absorbance curve becomes flat at the end of LSW injection stage (PV 7) and has the same magnitude at the beginning of nanofluid injection (PV 8). Therefore, Abs values from PV 2 to PV 6 were disregarded in order to look attentively at nanofluid injection stages (Figure 5.44).

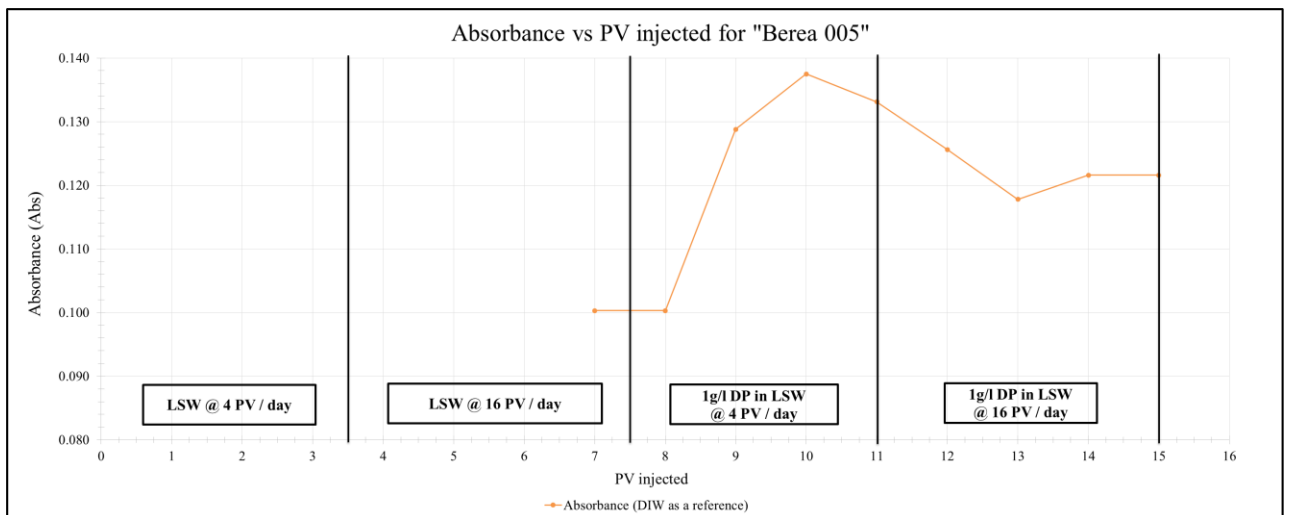


Figure 5.44 – EOR experiment with “Berea 005”: Absorbance curve for nanofluid injection stages

As we can see from Figure 5.44 when the nanofluid is introduced at an injection rate of 4 PV/day absorbance values started to increase until reaching the maximum at PV 10. It may indicate that at PV 8 there happened a breakthrough of nanofluid in the core and NP become to be present in the effluent. When the rate was increased four times up to 16 PV/day Abs values lowered which may say about decreasing concentration of nanofluid produced in the effluent. Hence, at a higher flow rate of nanofluid injection at the same concentration there is a possibility for more interaction between NP and rock grains, thereby adsorption process is enhanced.

Absorbance values were utilized further for evaluation of concentration of produced NP. For this purpose calibration line was built for nanofluid in LSW (Figure 5.45) and Abs readings 0.1003 units for PV 7 and PV 8 were utilized as a baseline correction for all the samples from later PV.

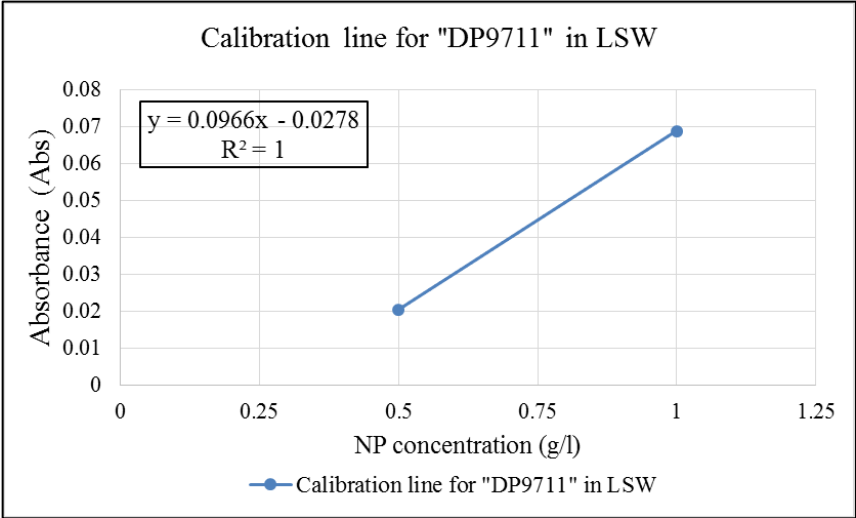


Figure 5.45 – Calibration line for “DP9711” nanofluid prepared in LSW

NP concentration plot vs. PV injected for “Berea 005” is presented in Figure 5.46.

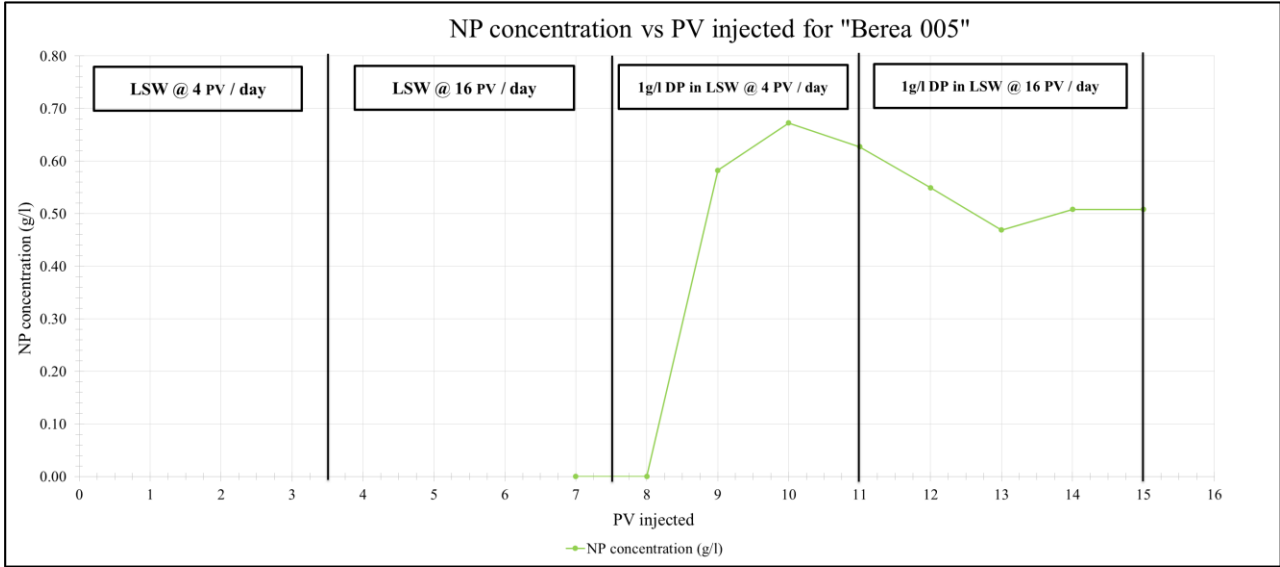


Figure 5.46 – EOR experiment with “Berea 005”: NP concentration vs. PV injected

Mass balance calculations were performed to evaluate the amount of NP produced and adsorbed / retained. Table 5.10 presents the results of mass balance calculations for “Berea 005”. The total volume of injected nanofluid at concentration 1 g/l constitutes 7.5 PV of the core. Each PV collected in effluent equals to 20 ml of water and the NP concentration in the volume of a certain sample is assumed to be representative for the whole corresponding PV produced.

Table 5.10 – NP mass balance calculations for “Berea 005”

PV injected	Absorbance (DIW as a reference)	Absorbance corrected	NP concentration (g/l)	Sample volume (l)	NP amount (g)
7	0.1003	0	0	0.02	0
8	0.1003	0	0	0.02	0
9	0.1288	0.0285	0.582815735	0.02	0.011656315
10	0.1375	0.0372	0.672877847	0.02	0.013457557
11	0.1331	0.0328	0.627329193	0.02	0.012546584
12	0.1256	0.0253	0.549689441	0.02	0.010993789
13	0.1178	0.0175	0.468944099	0.02	0.009378882
14	0.1216	0.0213	0.508281573	0.02	0.010165631
15	0.1216	0.0213	0.508281573	0.02	0.010165631
Baseline correction	NP concentration			Total amount NP produced (g)	0.078364389
				Total amount NP injected (g)	0.15345
0.1003	NP conc = (Abs + 0.0278)/0.0966			Percent of NP produced (%)	51.07
				Percent of NP adsorbed / retained (%)	48.93

As we can see from Table 5.10, mass balance calculations resulted in 51.07 % production of the total amount of NP injected while 48.93 % of them was attributed to adsorption / retention in the core. This ratio is very close to the ratio observed earlier in mass balance calculations for single phase flood experiment “Berea 002”.

In order to investigate further the interactions occurring within the core, ion tracking was performed using Ion Chromatograph. The following figures demonstrate detected ions in the effluent. Ion concentration profiles which were not discussed here can be found in Appendix A.

Potassium ion concentration is presented in Figure 5.47.

During the first stage of injection LSW (4PV/day) there is an instability of pH readings and this period is considered not representative for all ion concentrations due to the presence of salts from SSW, which was used to saturate the core before establishing irreducible water saturation S_{wirr} by model oil injection.

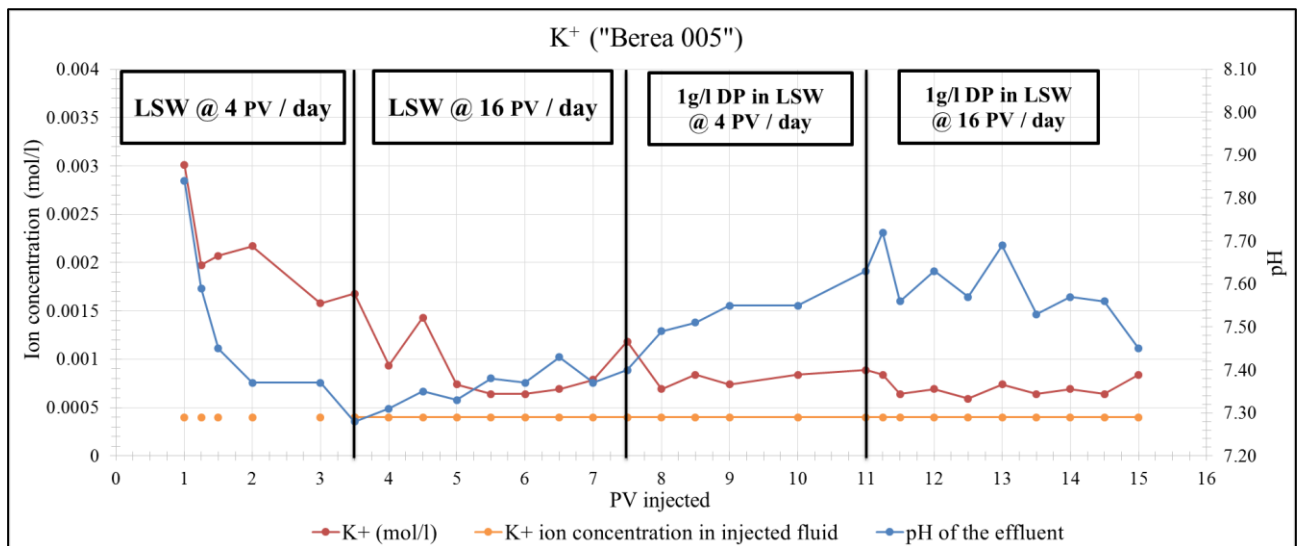


Figure 5.47 – K^+ ion concentration in effluent and pH values for “Berea 005”

After the initial period, potassium ion concentration detected in the effluent is consistently higher than its concentration in the injected fluid. When the flooding rate of LSW was increased to 16 PV/day, the potassium ion concentration stabilizes around 0.0008 mol/l at PV 5. After that, it remains relatively constant during nanofluid injection stage at 4 PV/day. After switching to a higher flow rate of 16 PV/day, the presence of potassium in effluent decreases slightly down to concentration 0.0006 mol/l. This decrease may be explained by enhanced adsorption of NP on the minerals during this period causing reduced interaction between water and rock that leads to release of potassium.

Magnesium ion concentration is presented in Figure 5.48.

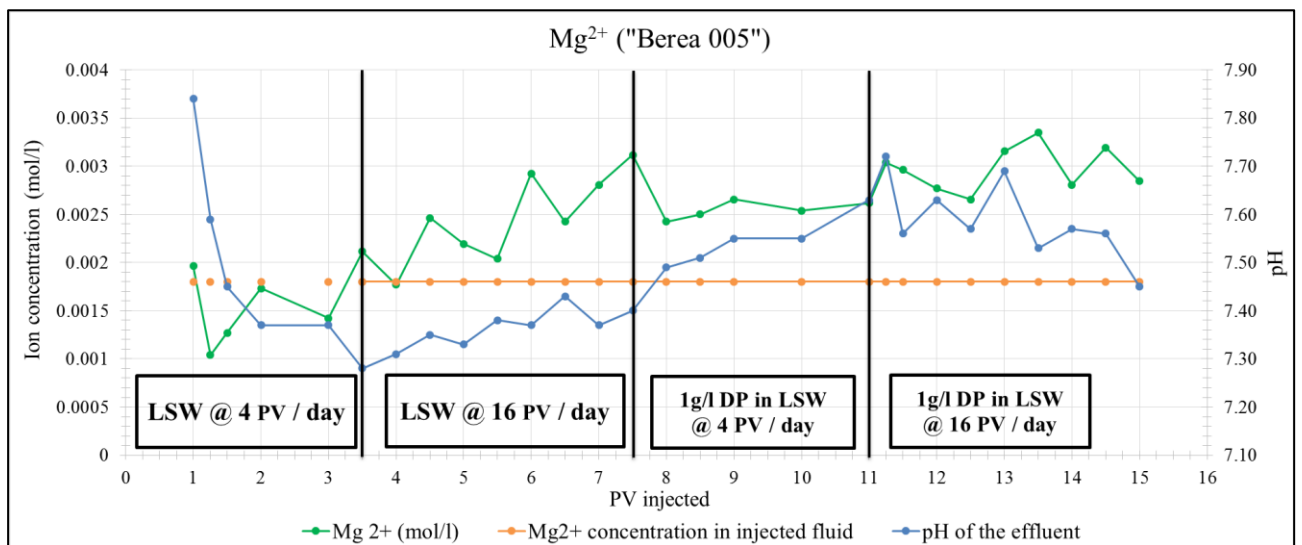


Figure 5.48 – Mg^{2+} ion concentration in effluent and pH values for “Berea 005”

The concentration of magnesium ion detected in effluent remains higher than that in injected fluid during primary recovery with LSW at 16 PV/day showing an increase in steps from 0.0021 mol/l (PV 3.5) up to 0.0031 mol/l (PV 7.5). When nanofluid is introduced the concentration of Mg^{2+} stabilizes at 0.0025 mol/l for the period of injection at 4 PV/day. Then at 16 PV/day, it rises slightly and can be averaged within 0.003 mol/l.

Calcium ion concentration is presented in Figure 5.49.

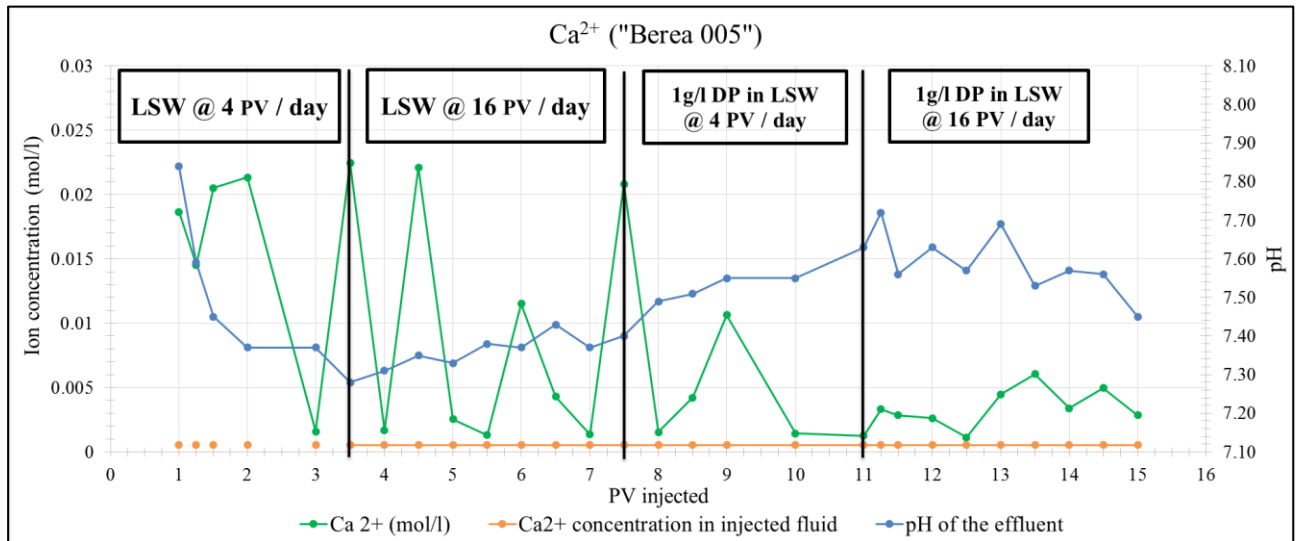


Figure 5.49 – Ca²⁺ ion concentration in effluent and pH values for “Berea 005”

Calcium ion concentration fluctuates during the primary oil recovery period with LSW within the range from 0.0014 mol/l to 0.022 mol/l. At nanofluid injection stage, the magnitude of fluctuations decreases but the concentration values remain higher than the concentration in the injected fluid.

Some connections between Mg²⁺ and Ca²⁺ ion trends can be noticed. The expected behavior of mutual exchange of these ions that was investigated in the previous work in our lab and reported by A. A. Hamouda and O. M. Valderhaug [34] was not clearly observed. In this experiment, the concentration peaks of Mg²⁺ ion correspond to that for Ca²⁺, which may indicate that the mechanism of ion interactions does not clearly include the exchange of these two ions. In this case contribution from interacting minerals is more active and different. Magnesium may be produced from illite or chlorite minerals that are present in the core, and the mechanisms of their dissolution are also different.

At the same time pH is not increasing with a high magnitude as was observed by A. A. Hamouda and O. M. Valderhaug, so pH increase was probably hindered by NP adsorption occurring in the core. It is in accordance with Figure 5.44 indicating that adsorption of NP was enhanced with the increase of injection flow rate. NP presence may affect interactions between injected water and the rock leading to decrease in the production of potassium as a contributor to pH increase with associated chemical reaction.

Also, from Figure 5.49 one can observe that the production of Ca²⁺ ion fluctuates within quite a high range during primary recovery with LSW injection which suggests that the active process of calcium dissolution may take place in the core. However, when the flood is shifted to nanofluid, the concentration of Ca²⁺ ion falls drastically which may be connected with a decrease in the dissolution of calcium. This can be supported by our investigations from static adsorption experiment, which showed that adsorption on calcite mineral was the highest. Hence, preferential adsorption of NP on calcite favors reduction of its dissolution.

5.6.2 Core floods with “Berea 006”

Irreducible water saturation $S_{wirr} = 0.539$ was established at the beginning of the experiment with “Berea 006” core. Then it was aged in an aging cell for 4 months at a constant temperature of 50 °C before utilizing in the secondary flooding.

After aging, imbibition (oil recovery flood) was conducted on aged core according to the following steps: SSW injection at low flow rate (4PV/day), SSW injection at high rate (16 PV/day), injection of nanofluid suspension prepared in LSW at low flow rate (4 PV/day) and the same nanofluid injection at high flow rate (16 PV/day). Increasing the flow rate for every injected fluid is done to account for possible capillary end effects. In order to mimic conditions in a reservoir, the flood was run at 70° C temperature with back-pressure of 10 bar and confinement pressure of 25 bar. Figure 5.50 shows injection sequence for imbibition oil recovery flood with “Berea 006” core.

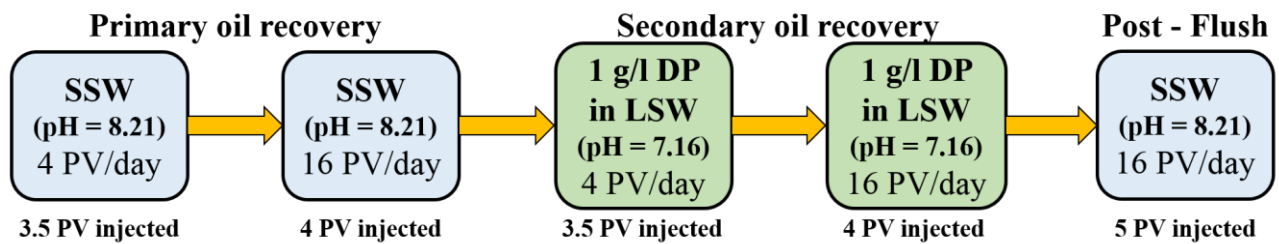


Figure 5.50 – Injection sequence for oil recovery flood with “Berea 006”

Inlet pressure and pressure drop along the core were recorded during the experiment (Figure 5.51).

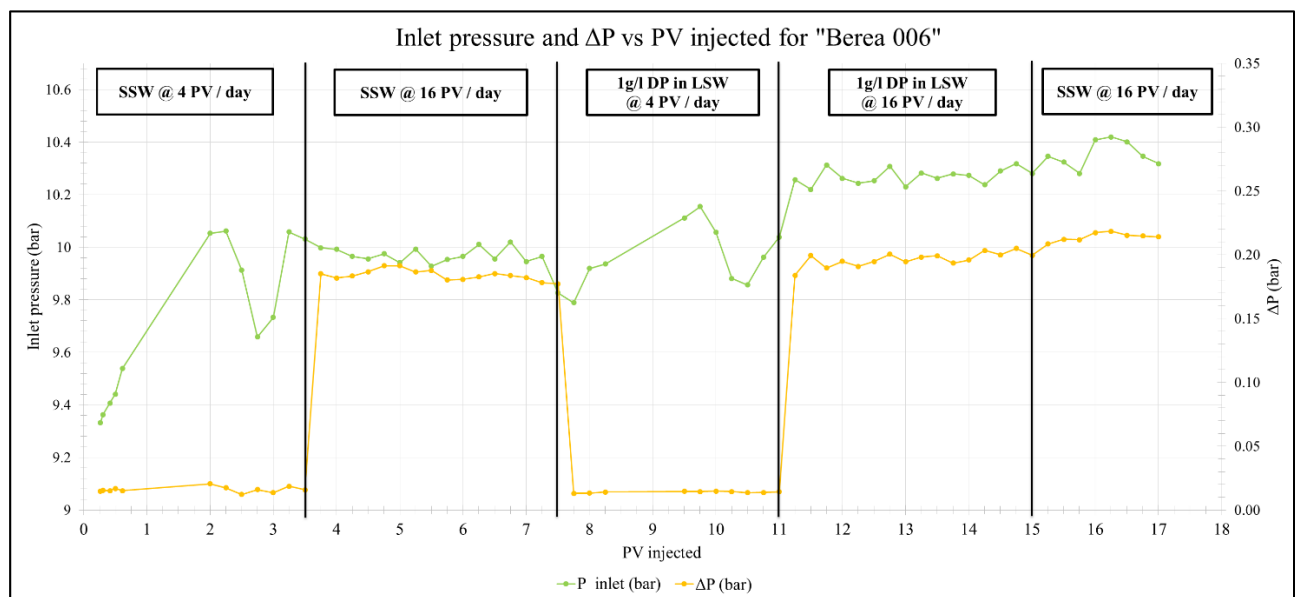


Figure 5.51 – EOR experiment with “Berea 006”: Inlet pressure and ΔP vs PV injected

During the primary recovery flood with SSW when the rate of injection was changed from 4 PV/day to 16 PV/day increase in ΔP was around 0.169 bars. Concerning to secondary recovery with nanofluid, this change of pressure drop related to increasing of injection flow rate was around 0.175 bar. This difference may indicate that injection of NP improves sweep efficiency which is similar to observations made in single phase transport behavior flood (“Berea 002”).

Cumulative oil recovery and measured pH were plotted vs. PV injected and presented in Figure 5.52.

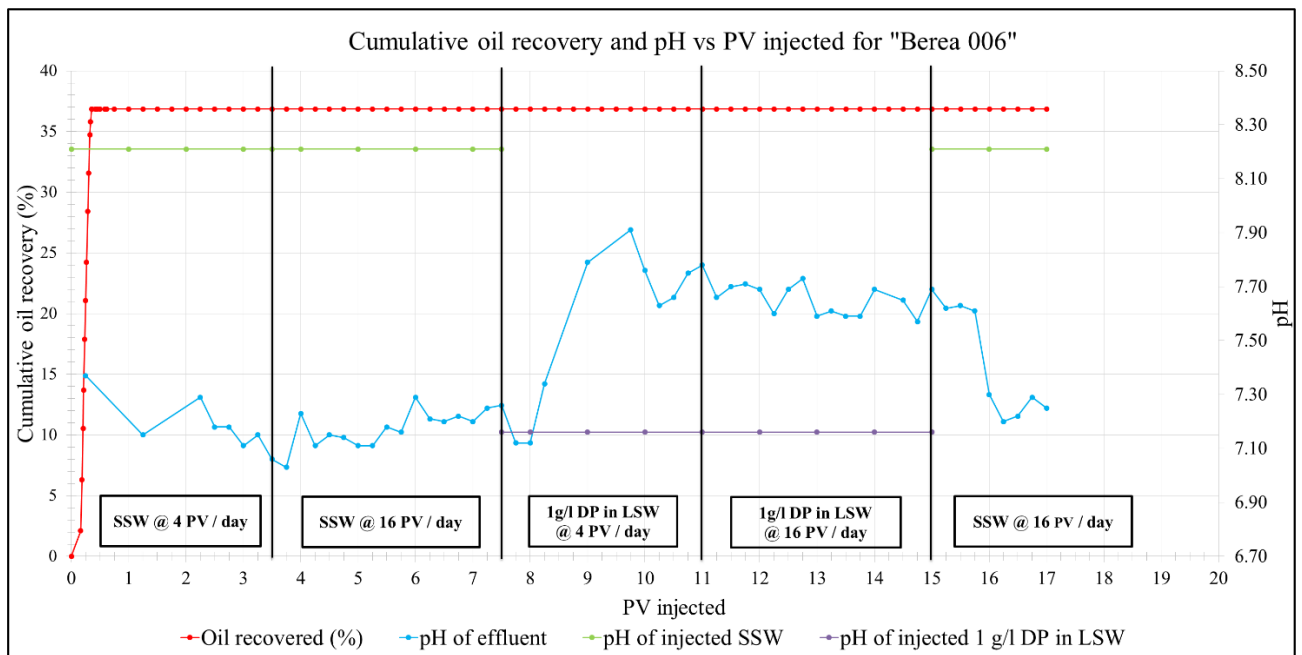


Figure 5.52 – EOR experiment with “Berea 006”: Cumulative oil recovery and pH vs PV injected

In the period of primary recovery with SSW, pH values are close to 7.15 units and keep relatively constant for both injection rates of 4 PV/day and 16 PV/day. After the nanofluid is introduced there happens an escalation of pH up to 7.9 units, and after that it starts to decrease gradually with minor fluctuations during nanofluid injection stages. Post – flush with SSW injection makes pH decrease down to the values close to that during primary recovery flood with SSW.

Concerning to oil recovery, all possible production of oil from the core occurred at the beginning of the first stage of SSW injection. No additional oil extraction was observed at the latter stages of SSW injection at 16 PV/day and subsequent secondary recovery flood with nanofluid injection. Therefore, the experiment resulted in ultimate oil recovery of 36.86 %.

The effluent of “Berea 006” EOR flood was characterized with UV by measuring the absorbance of mixture of produced water samples that represent each injected PV. Absorbance values were plotted together with pH readings and presented in Figure 5.53.

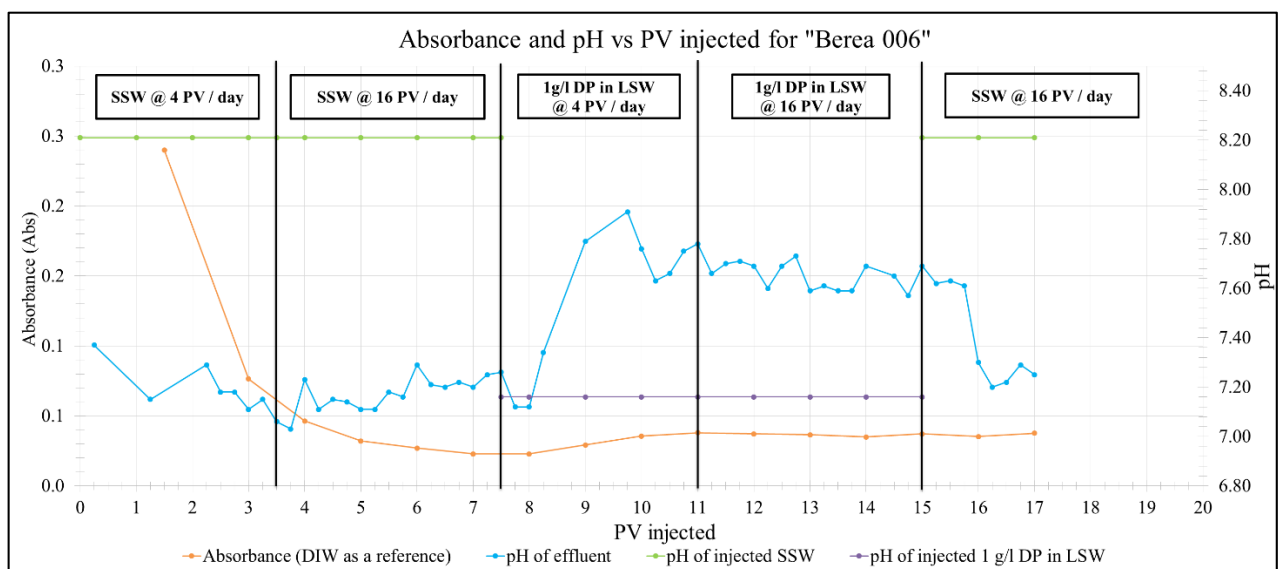


Figure 5.53 – EOR experiment with “Berea 006”: Absorbance curve and pH vs PV injected

Because of the colored effluent, Abs values are comparatively high for samples from the earliest stages of injection. During the primary recovery injection with SSW at 4 PV/day and 16 PV/day the values decrease gradually and stabilize before injection of the nanofluid (PV 7 – PV 8). If the absorbance curve is analyzed for periods of injection of 1 g/l DP in LSW and post – flush with SSW, the plot will look as presented in Figure 5.54.

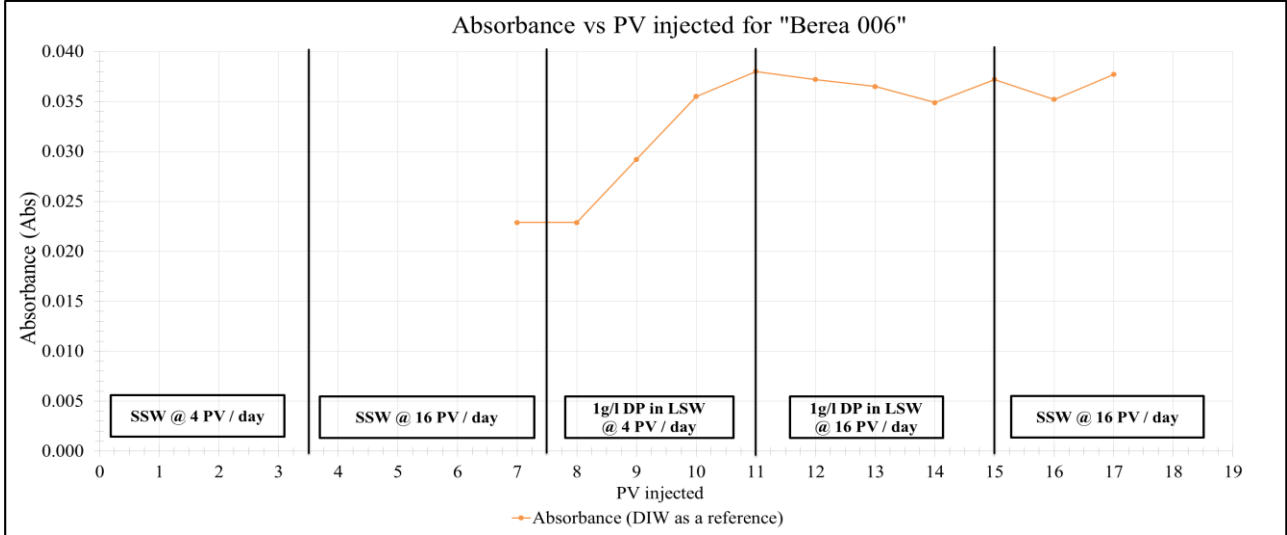


Figure 5.54 – EOR experiment with “Berea 006”: Absorbance curve for nanofluid injection and post-flush stages

From Figure 5.54 it can be noticed that at a higher flow rate on nanofluid injection absorbance readings tend to decrease slowly. Nevertheless, the rapid drawdown as was mentioned for “Berea 005” at this period is not observed.

Calibration line for nanofluid prepared in LSW (Figure 5.45) and absorbance readings helped to acquire the plot of NP concentration vs. PV injected which is presented in Figure 5.55.

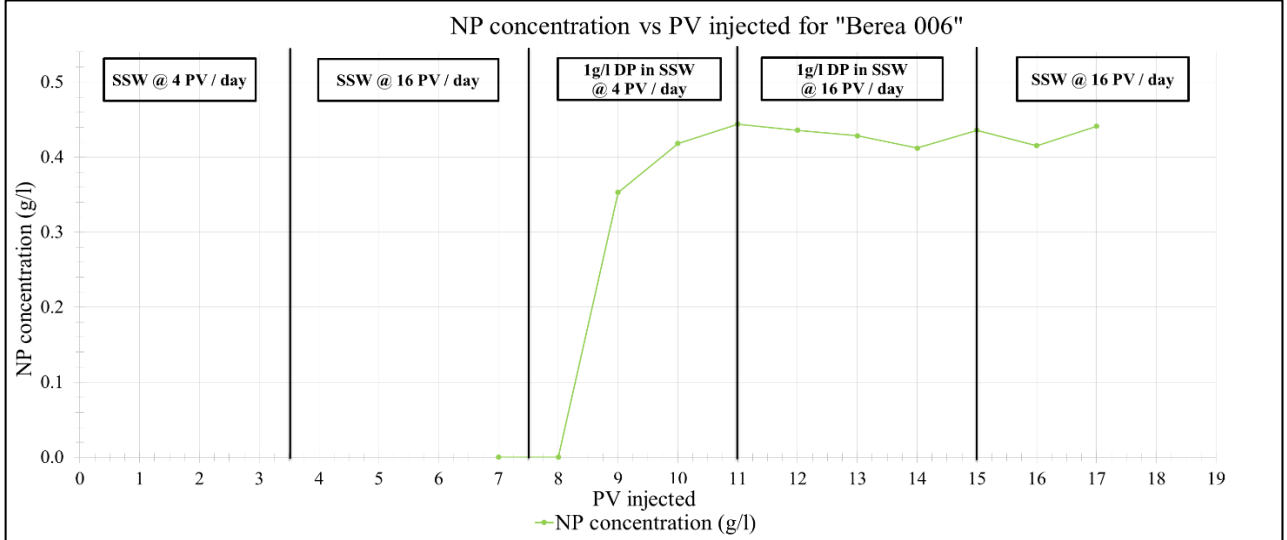


Figure 5.55 – EOR experiment with “Berea 006”: NP concentration vs PV injected

Produced and adsorbed / retained NP were evaluated by applying the mass balance calculations. The results are shown in Table 5.11. The total volume of injected nanofluid at concentration 1 g/l constitutes 7.5 core PV. Each PV collected in effluent equals to 20 ml of water and the NP concentration in the volume of a certain sample is assumed to be representative for the whole corresponding PV produced. In order to compare this mass balance of produced and adsorbed / retained NP with the results from the previous core flood (“Berea 005”), the calculations are made only for the period of the secondary oil recovery with nanofluid injection (PV 7.5 – PV 15).

Table 5.11 – NP mass balance calculations for “Berea 006”

PV injected	Absorbance (DIW as a reference)	Absorbance corrected	NP concentration (g/l)	Sample volume (l)	NP amount (g)
7	0.0229	0	0	0.02	0
8	0.0229	0	0	0.02	0
9	0.0292	0.0063	0.35300207	0.02	0.007060041
10	0.0355	0.0126	0.418219462	0.02	0.008364389
11	0.038	0.0151	0.444099379	0.02	0.008881988
12	0.0372	0.0143	0.435817805	0.02	0.008716356
13	0.0365	0.0136	0.428571429	0.02	0.008571429
14	0.0349	0.012	0.412008282	0.02	0.008240166
15	0.0372	0.0143	0.435817805	0.02	0.008716356
Baseline correction	NP concentration	Total amount NP produced (g)			0.058550725
		Total amount NP injected (g)			0.1545
0.0229	NP conc = (Abs + 0.0278)/0.0966	Percent of NP produced (%)			37.90
		Percent of NP adsorbed / retained (%)			62.10

Mass balance calculations show that only 37.90 % of NP injected during secondary recovery flood was produced in the effluent. The rest amount of 62.10 % is considered to be adsorbed / retained in the core. Comparing acquired ratio with the previous experiment “Berea 005” (51.07% NP production, 48.93 % adsorption / retention) one can notice, that the current experiment with SSW injection during primary recovery stage results in less NP production. It may be an indication that adsorption is enhanced by the presence of high salinity environment which was confirmed by our previous investigations (static adsorption experiment).

Ion concentration profiles for this EOR experiment are not included in the project. Analysis of ion interactions for this core “Berea 006” with detailed interpretation of the results is a subject of further investigation.

6 Conclusions

In this study, the potential for application of silica nanofluid for EOR was systematically examined. Based on the experimental investigation, the following conclusions may be stated:

- 1 Silica nanofluid “DP 9711” is stable under conditions of elevated salinity and temperature which makes it relevant for use in field applications.
- 2 Nanoparticles have strongly negative values of zeta-potential when dispersed in DIW. The reduction of zeta-potential with an increase in salinity due to shrinkage of the double layer was observed.
- 3 Among the three minerals (quartz, kaolinite, calcite) the greatest affinity for NP adsorption was observed for calcite. At the same time adsorption on quartz mineral is higher than that on kaolinite. Besides, it was noted that adsorption of NP on all minerals was enhanced in high salinity environment.
- 4 Single phase core flood experiments with nanofluid suggested significant irreversible adsorption of NP and major amount of injected NP were retained in the core. This can lead to in-situ surface modification of the rock since NP used in experiments are highly hydrophilic.
- 5 The associated increase in sweep efficiency observed during nanofluid injection indicates that “DP 9711” nanofluid has good potential for EOR applications.
- 6 SEM imaging of the core saturated with nanofluid confirms observations made during static adsorption experiment that adsorption preferentially occurs on quartz as compared to kaolinite mineral. Visual evidence also suggests that silica NP do not aggregate in-situ and are well distributed on the rock surface.
- 7 Primary recovery by LSW followed by secondary recovery by “DP 9711” nanofluid prepared in LSW led to incremental oil of about 0.81%.
- 8 Preparation of nanofluid in SSW led to higher adsorption / retention in Berea sandstone. This was confirmed by static adsorption experiments, i.e. salinity enhances adsorption / retention of nanoparticles in Berea sandstone.
- 9 Injection of the nanofluid led to increasing sweep efficiency. Injection at higher rate led to higher adsorption / retention of nanoparticles in Berea sandstone.
- 10 pH of effluents and ion concentration profiles of potassium may suggest that injection of nanoparticles suppresses the rise of K^+ ion and pH compared to that in the case of LSW flooding.
- 11 Ion concentration profile of calcium in the effluent may suggest that dissolution of $CaCO_3$ (as cementing mineral) was reduced by injection of nanofluid. Higher adsorption of silica nanoparticles on calcite observed during static adsorption experiment might hinder the dissolution of calcium in Berea sandstone. Mutual exchange of Ca^{2+} and Mg^{2+} ions was not clear, and the production of magnesium may suggest a possible contribution from chlorite / illite. This needs to be further investigated.

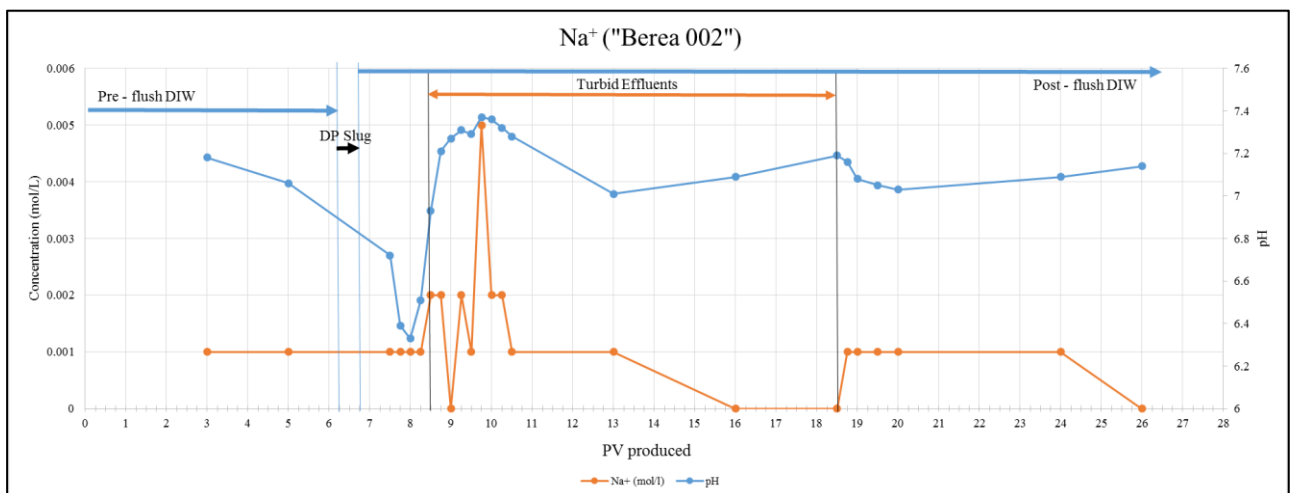
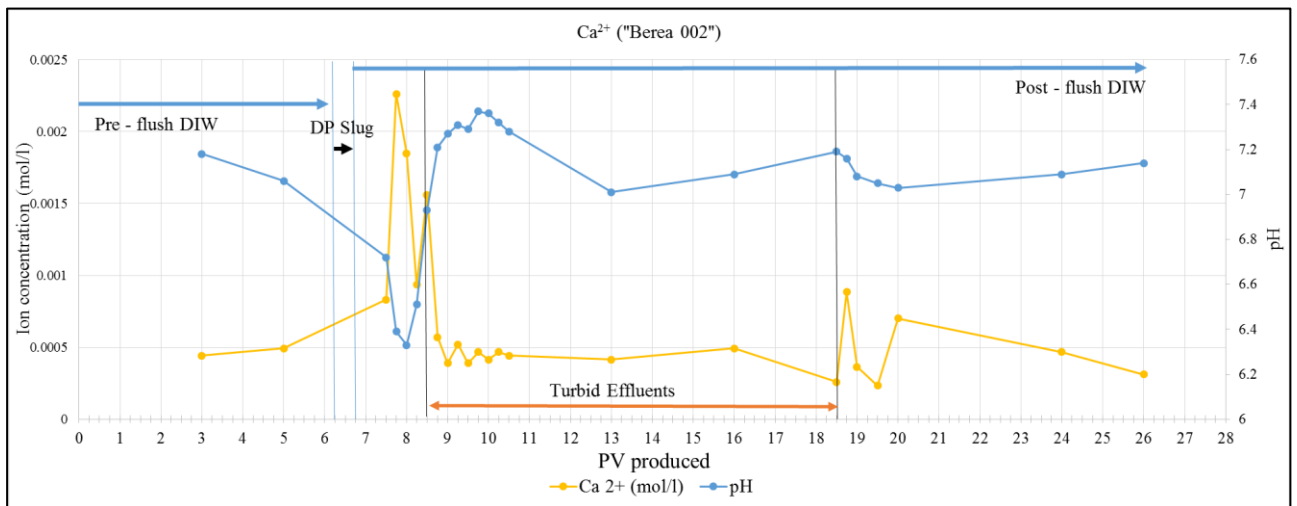
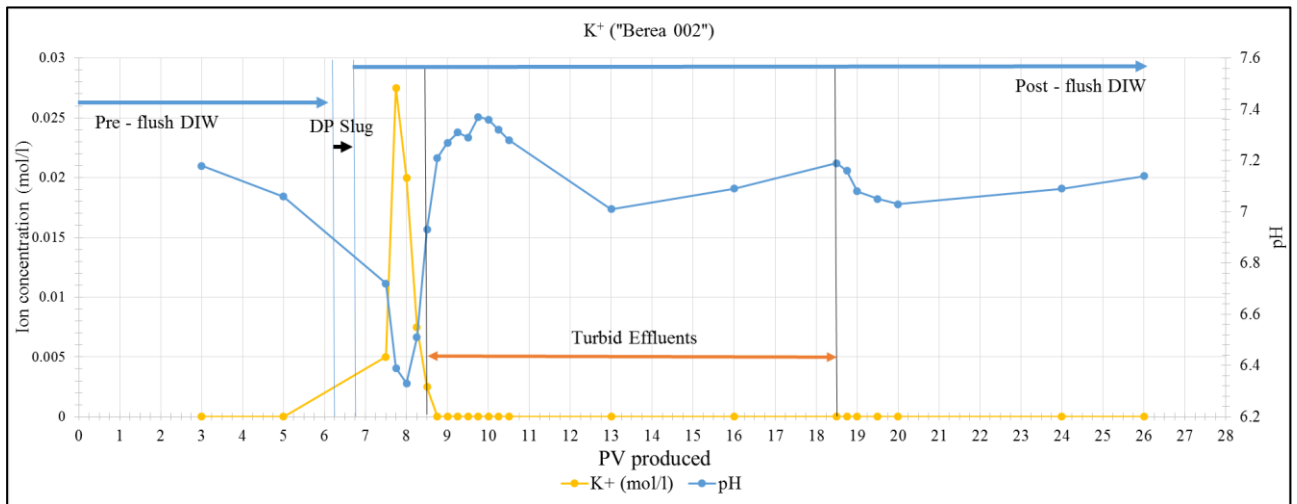
7 References

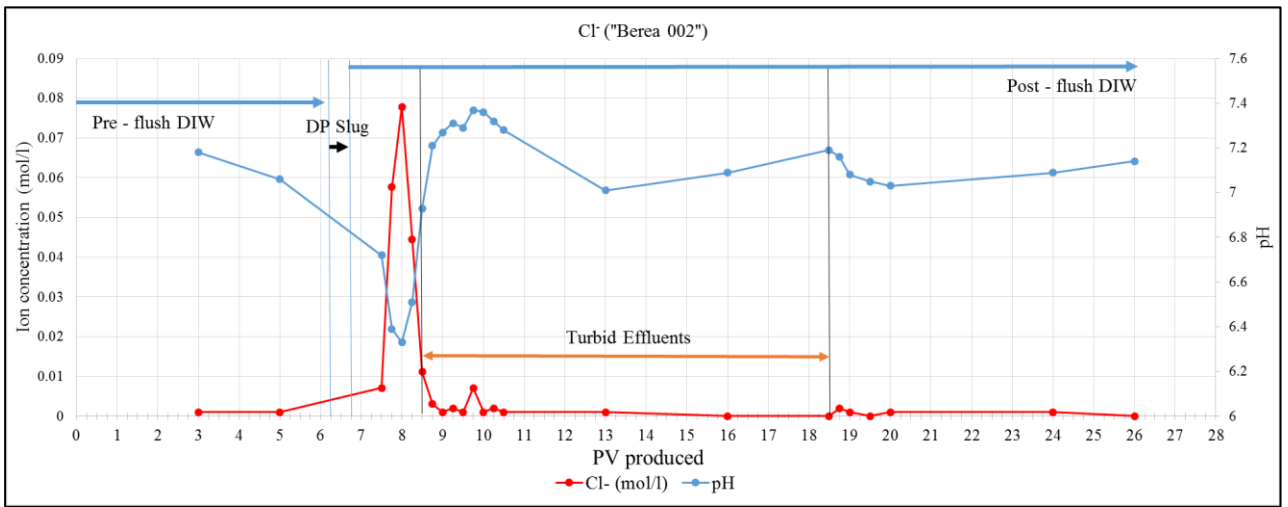
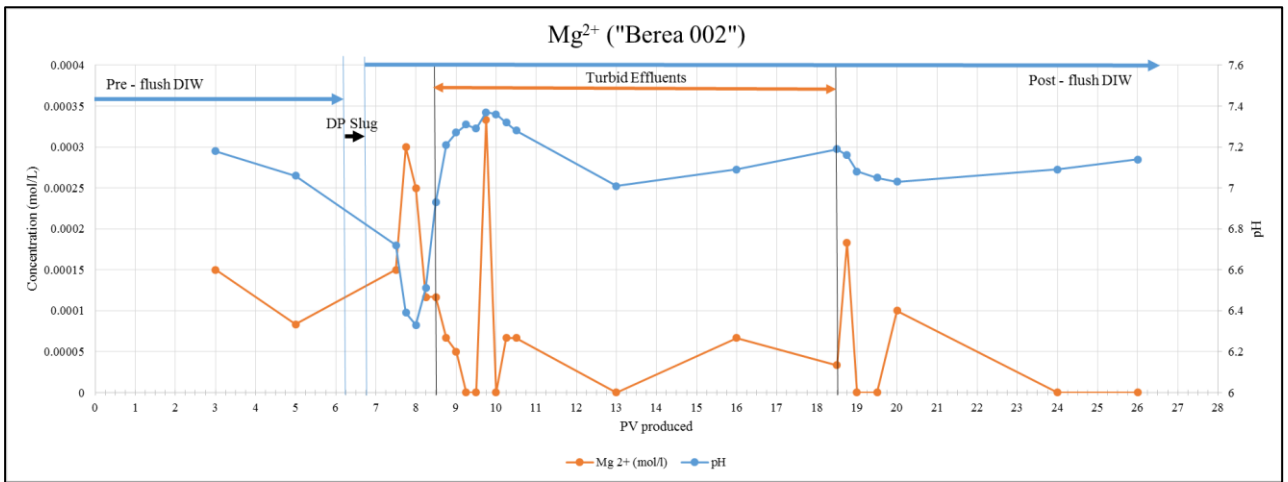
1. Kong, X. and M. Ohadi. *Applications of micro and nano technologies in the oil and gas industry-overview of the recent progress*. in *Abu Dhabi international petroleum exhibition and conference*. 2010. Society of Petroleum Engineers.
2. Li, S. and O. Torsæter. *Experimental investigation of the influence of nanoparticles adsorption and transport on wettability alteration for oil wet Berea sandstone*. in *SPE Middle East Oil & Gas Show and Conference*. 2015. Society of Petroleum Engineers.
3. Metin, C.O., J.R. Baran, and Q.P. Nguyen, *Adsorption of surface functionalized silica nanoparticles onto mineral surfaces and decane/water interface*. *Journal of Nanoparticle Research*, 2012. **14**(11): p. 1246.
4. Arab, D. and P. Pourafshary, *Nanoparticles-assisted surface charge modification of the porous medium to treat colloidal particles migration induced by low salinity water flooding*. *Colloids and Surfaces A: Physicochemical and Engineering Aspects*, 2013. **436**: p. 803-814.
5. Yuan, B., R.G. Moghanloo, and D. Zheng, *Analytical evaluation of nanoparticle application to mitigate fines migration in porous media*. *SPE Journal*, 2016.
6. Wasan, D.T. and A.D. Nikolov, *Spreading of nanofluids on solids*. *Nature*, 2003. **423**(6936): p. 156.
7. Zhang, H., A. Nikolov, and D. Wasan, *Enhanced Oil Recovery (EOR) Using Nanoparticle Dispersions: Underlying Mechanism and Imbibition Experiments*. *Energy & Fuels*, 2014. **28**(5): p. 3002-3009.
8. Ashraf, A., et al. *Laboratory investigation of low salinity waterflooding as secondary recovery process: effect of wettability*. in *SPE Oil and Gas India Conference and Exhibition*. 2010. Society of Petroleum Engineers.
9. Hassenkam, T., et al., *The low salinity effect observed on sandstone model surfaces*. *Colloids and Surfaces A: Physicochemical and Engineering Aspects*, 2012. **403**: p. 79-86.
10. Rivet, S., L.W. Lake, and G.A. Pope. *A coreflood investigation of low-salinity enhanced oil recovery*. in *SPE Annual Technical Conference and Exhibition*. 2010. Society of Petroleum Engineers.
11. Berg, S., et al., *Direct experimental evidence of wettability modification by low salinity*. *Petrophysics*, 2010. **51**(05).
12. Yuan, H. and A.A. Shapiro, *Induced migration of fines during waterflooding in communicating layer-cake reservoirs*. *Journal of Petroleum Science and Engineering*, 2011. **78**(3): p. 618-626.
13. Almada, P., et al. *Experimental investigation on the effects of very low salinity on Middle Eastern sandstone corefloods*. in *SPE European Formation Damage Conference & Exhibition*. 2013. Society of Petroleum Engineers.
14. Stoll, M., et al. *Alkaline-surfactant-polymer Flood—From the Laboratory to the Field*. in *IOR 2011-16th European Symposium on Improved Oil Recovery*. 2011.
15. Assef, Y., D. Arab, and P. Pourafshary, *Application of nanofluid to control fines migration to improve the performance of low salinity water flooding and alkaline flooding*. *Journal of Petroleum Science and Engineering*, 2014. **124**: p. 331-340.
16. Krumrine, P., E. Mayer, and G. Brock, *Scale formation during alkaline flooding*. *Journal of Petroleum Technology*, 1985. **37**(08): p. 1,466-1,474.
17. Wang, W., et al. *Nanoparticles Adsorption, Straining and Detachment Behavior and its Effects on Permeability of Berea Cores: Analytical Model and Lab Experiments*. in *SPE Annual Technical Conference and Exhibition*. 2016. Society of Petroleum Engineers.
18. Yuan, B. and K. Wang. *Injectivity Improvement by Nanofluid Preflush During Low Salinity Water Flooding*. in *International Petroleum Technology Conference*. 2016. International Petroleum Technology Conference.
19. Maghzi, A., et al., *Monitoring wettability alteration by silica nanoparticles during water flooding to heavy oils in five-spot systems: A pore-level investigation*. *Experimental Thermal and Fluid Science*, 2012. **40**: p. 168-176.
20. Huang, T., J.B. Crews, and J.R. Willingham. *Using nanoparticle technology to control fine migration*. in *SPE Annual Technical Conference and Exhibition*. 2008. Society of Petroleum Engineers.
21. Ahmadi, M., et al. *Zeta potential investigation and mathematical modeling of nanoparticles deposited on the rock surface to reduce fine migration*. in *SPE Middle East Oil and Gas Show and Conference*. 2011. Society of Petroleum Engineers.

22. Hendraningrat, L., S. Li, and O. Torsæter, *A coreflood investigation of nanofluid enhanced oil recovery*. Journal of Petroleum Science and Engineering, 2013. **111**: p. 128-138.
23. Buckley, J.S. and T. Fan, *Crude oil/brine interfacial tensions I*. Petrophysics, 2007. **48**(03).
24. Hendraningrat, L. and O. Torsæter, *Metal oxide-based nanoparticles: revealing their potential to enhance oil recovery in different wettability systems*. Applied Nanoscience, 2014. **5**(2): p. 181-199.
25. Ehtesabi, H., et al., *Enhanced heavy oil recovery in sandstone cores using tio2 nanofluids*. Energy & Fuels, 2013. **28**(1): p. 423-430.
26. Zhang, T., et al., *Investigation of nanoparticle adsorption during transport in porous media*. SPE Journal, 2014.
27. Dunphy Guzman, K.A., M.P. Finnegan, and J.F. Banfield, *Influence of surface potential on aggregation and transport of titania nanoparticles*. Environmental Science & Technology, 2006. **40**(24): p. 7688-7693.
28. Burdick, G., N. Berman, and S. Beaudoin, *Describing hydrodynamic particle removal from surfaces using the particle Reynolds number*. Journal of Nanoparticle research, 2001. **3**(5): p. 453-465.
29. Colloidal Dynamics. *The Zeta Potential*. Electroacoustics Tutorials 1999 06.06.2017]; Available from: <http://www.colloidal-dynamics.com/docs/CDEITut1.pdf>.
30. Wikipedia the free encyclopedia. *Zeta Potential*. 2017 29.05.2017]; Available from: https://en.wikipedia.org/wiki/Zeta_potential.
31. Helmenstine, A.M. *Definition of Zeta Potential*. Science 2017 01.06.2017]; Available from: <https://www.thoughtco.com/g00/definition-of-zeta-potential-605810?i10c.referrer=https%3A%2F%2Fwww.google.com%2F>.
32. Particulate Systems. *Principle of Zeta Potential Measurement*. NanoPlus DLS 2016 02.06.2017]; Available from: <http://particulatesystems.com/Products/NanoPlus-DLS-/Principle-of-Zeta-Potential-Measurement.aspx>.
33. NYACOL NANOTECHNOLOGIES. *DP9711 Colloidal Silica Surface Modified*. 15.04.2017]; Data sheet]. Available from: <http://www.nyacol.com/app/uploads/2015/04/DP9711-Data-Sheet-20130812.pdf>.
34. Hamouda, A.A. and O.M. Valderhaug, *Investigating Enhanced Oil Recovery from Sandstone by Low-Salinity Water and Fluid/Rock Interaction*. Energy & Fuels, 2014. **28**(2): p. 898-908.
35. Hamouda, A., et al. *Possible Mechanisms for Oil Recovery from Chalk and Sandstone Rocks by Low Salinity Water (LSW)*. in *SPE Improved Oil Recovery Symposium*. 2014. Society of Petroleum Engineers.
36. Tabrizy, V.A., R. Denoyel, and A. Hamouda, *Characterization of wettability alteration of calcite, quartz and kaolinite: Surface energy analysis*. Colloids and Surfaces A: Physicochemical and Engineering Aspects, 2011. **384**(1): p. 98-108.
37. Colloidal Dynamics. *AcoustoSizer II-M Particle Size and Zeta Potential Analysis System*. 11.05.2017]; Product Data Sheet]. Available from: <http://www.pragolab.cz/documents/AcoustoSizer%20II-M.pdf>.
38. Malvern Instruments. *Zetasizer Nano Series user manual*. 2013 30.04.2017]; Zetasizer technical brochure].
39. Malvern Instruments. *Dynamic light scattering: An introduction in 30 Minutes*. Technical Note 2012 15.04.2017]; Available from: <http://www.malvern.com/en/support/product-support/zetasizer-range/zetasizer-nano-range/zetasizer-nano-zsp/default.aspx>.
40. Shimadzu Corporation. *The Structure of a Spectrophotometer* Fundamentals of UV-Vis-NIR Spectroscopy 2017 27.03.2017]; An overview of the structure of UV-VIS spectrophotometers]. Available from: <http://www.shimadzu.com/an/uv/support/fundamentals/structure.html>.
41. Dario, C. *UV-1700 Spectrophotometer From Shimadzu*. Product reviews, 2007.
42. Minde, M.W., *Micro-and nano-applications to monitor the rock-fluid interaction in fractured chalk*. 2015, University of Stavanger, Norway.
43. Caldelas, F.M., et al. *Factors governing distance of nanoparticle propagation in porous media*. in *SPE Production and Operations Symposium*. 2011. Society of Petroleum Engineers.

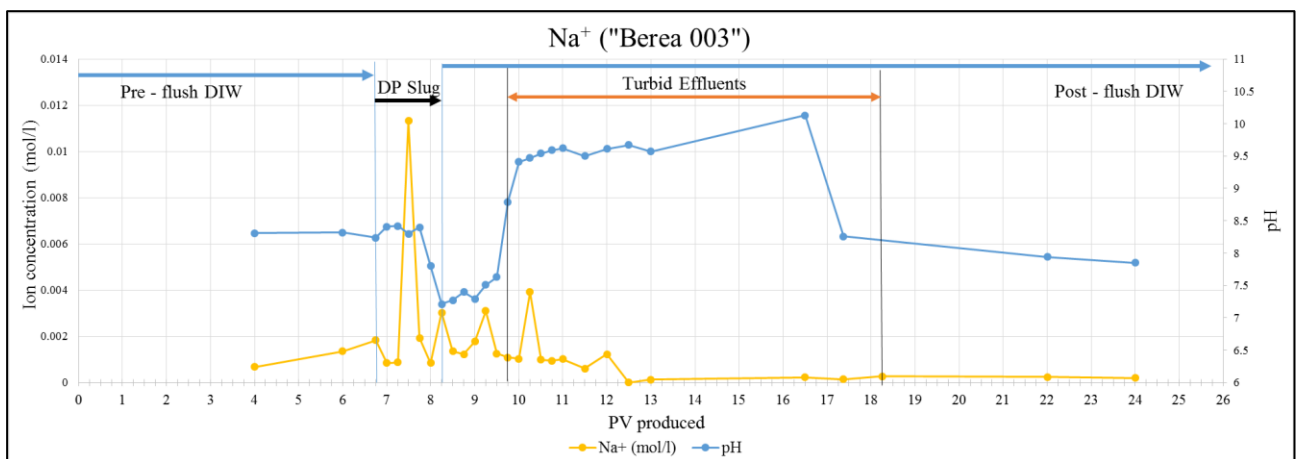
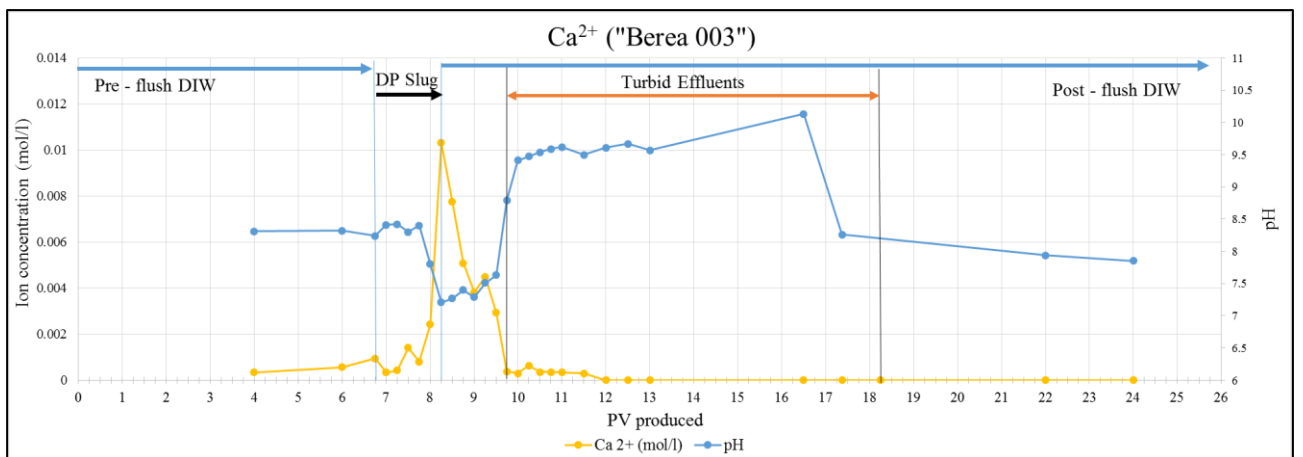
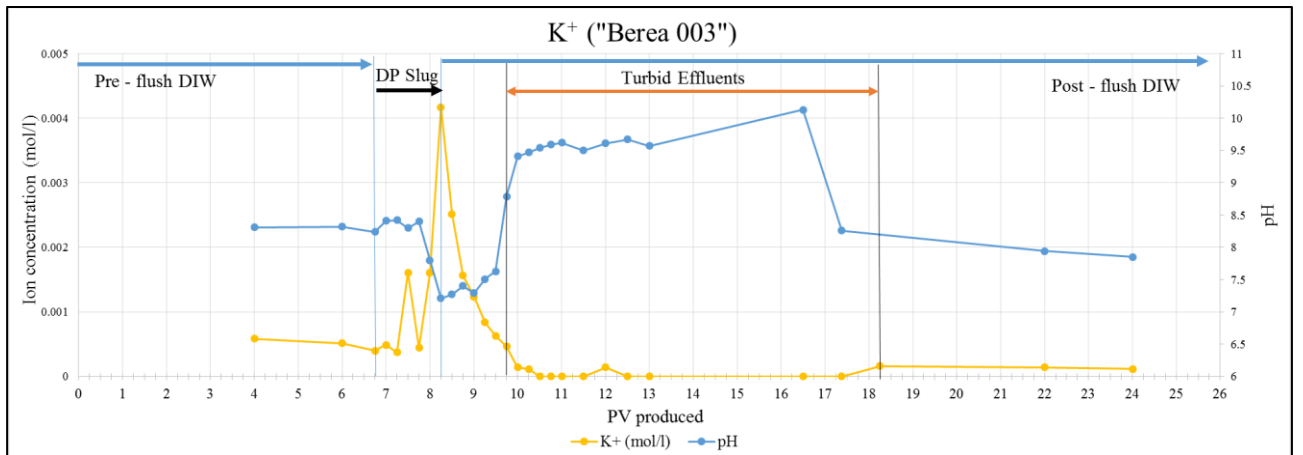
Appendix A

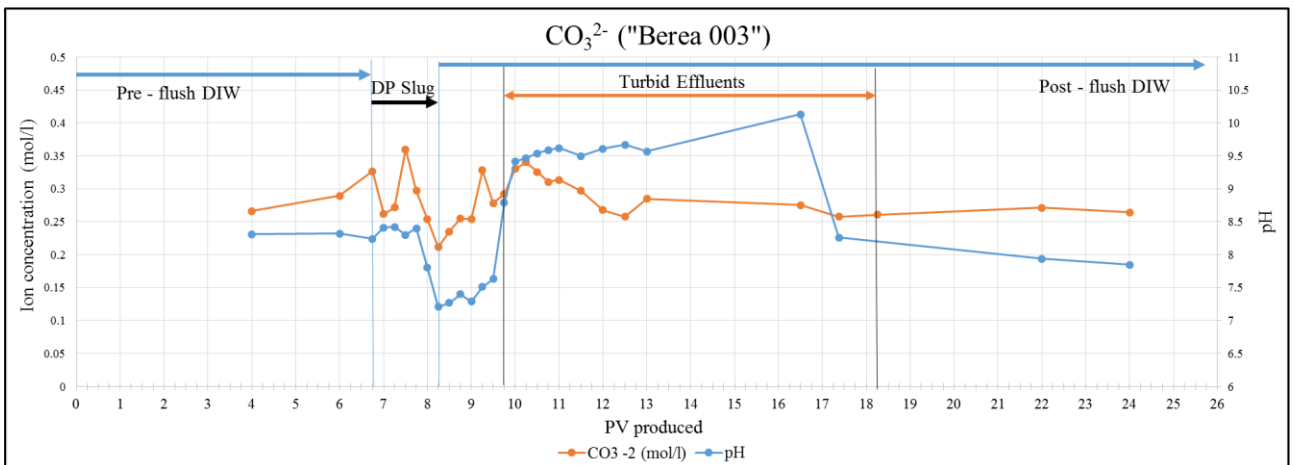
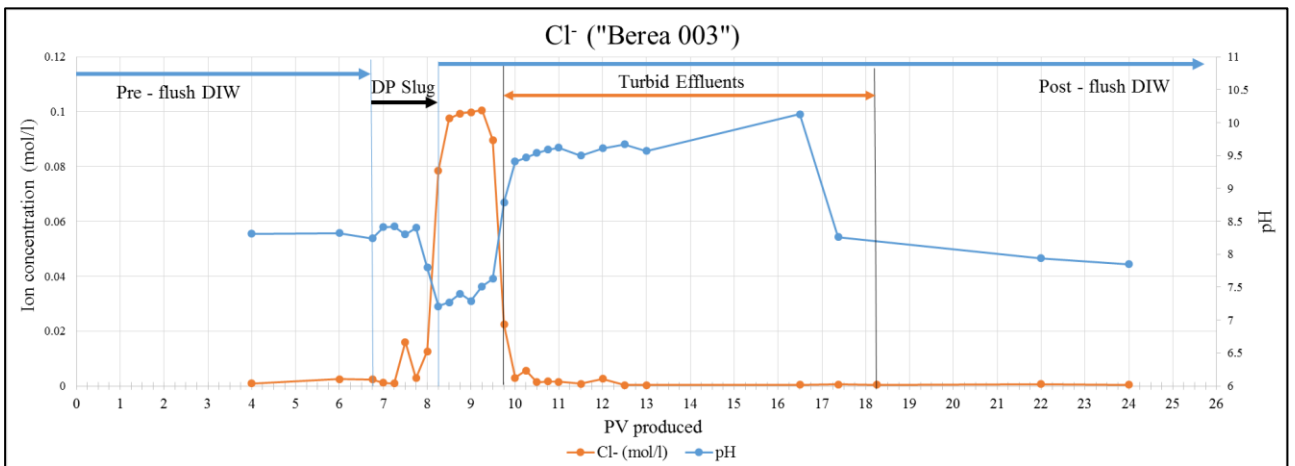
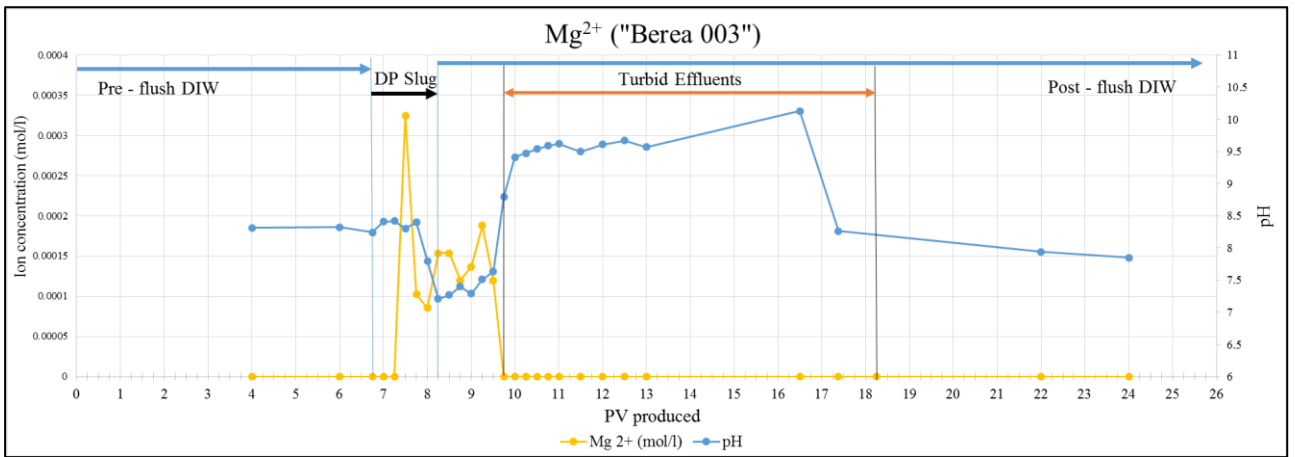
IC results for "Berea 002" effluent





IC results for "Berea 003" effluent





IC results for "Berea 005" effluent

